SPECTRUM SYNTHESIS OF EVOLVED STARS

Peter Cottrell

1978

A thesis submitted for the degree of
Doctor of Philosophy
to the Australian National University
Canberra

To Dee

The work described in this thesis is that of the candidate alone, except for Chapter 2 and a small portion of Chapter 6. Chapter 2 was a joint publication with Dr. J. Norris, whose contributions were the acquisition of the DDO photometry and the interpretation of the weak-G-band phenomenon. In Chapter 6, §IV*(a)* was a joint paper with Drs. D. T. Wickramasinghe and M. S. Bessell, in which Dr. Wickramasinghe assisted in the discussion of the object under investigation.

....

June, 1978

A C K N O W L E D G E M E N T S

I would like to thank my supervisors, Drs. John Norris and Mike Bessell, for their help in guiding my post-graduate research, as without their support and constructive criticism this thesis would not have been possible. In addition, I am most grateful for many useful discussions with Dr. Dayal Wickramasinghe, and to all the staff and students at Mount Stromlo for their help during the tenure of my scholarship.

During the last four years the Observatory Council has been most generous in allocating telescope time, which has enabled many of my research activities to come to fruition.

I extend my deepest thanks to my wife Deirdre, who has been most patient, and shown great understanding, during these last few years.

Finally, I acknowledge the financial support of an Australian National University Post-graduate Award.

ABSTRACT

Spectrum synthesis techniques have been employed to derive abundances in giants, dwarfs and white dwarfs.

For the giants (a weak-G-band star, a carbon-rich Cepheid, and a number of extremely metal-weak stars) carbon, nitrogen, and in one instance oxygen abundances have been determined using molecular bands of CH, CN, and NH.

(i) The weak-G-band star HD 91805 was examined, and found to be extremely underabundant in carbon, and slightly (but significantly) overabundant in nitrogen. The metal and oxygen abundances were essentially solar. From a photometric analysis, the group of weak-G-band stars are in the core-helium burning phase of their evolution. On the basis of the present data, the peculiar carbon and nitrogen abundances are possibly a combined result of mass loss and meridional circulation.

(ii) High dispersion spectra of the carbon-rich Cepheid V553 Centauri were acquired, from which a curve-of-growth analysis gave a near-solar iron abundance. The subsequent spectrum synthesis revealed both carbon and nitrogen enrichments relative to the metals. For carbon to be enriched in the surface layers as a result of evolutionary processes, the star must have mixed sometime after the He-core flash stage, possibly during helium-shell flashing. The star could possibly be a loop Cepheid, evolving through the instability strip. Significant mass loss is required to produce a loop Cepheid at the luminosity of this object.

(iii) For the extremely metal-poor giants, carbon and nitrogen abundances have been determined. The carbon to nitrogen ratio for the objects studied is shown to obey the following least squares relation, $[C/N] = 0.5(\log g) - 1.3$. There also appears to be a slight enhancement of nitrogen with increasing luminosity. The luminosities derived for

some of these objects are less than that required for helium-shell flashing, and therefore, these peculiar abundances are possibly produced during a star's first ascent of the giant branch. Thus the above abundances could be attained by a combination of mass loss and a number of hydrogen-shell instabilities, which mix material, processed by the CNO cycle, into the surface layers.

In addition, two grids of model atmospheres have been constructed. One grid of cool dwarf and subdwarf models has been used to compute synthetic G-bands and MgH features. At certain effective temperatures, and as the metal abundance is lowered, both these bands are shown to remain stronger than neighbouring pure atomic-line regions. This result adequately interprets the "CH" and "MgH" classifications of Greenstein, without having to invoke any peculiar abundances for carbon or magnesium. The strengthening of these features with decreasing metal abundance means that CH and MgH are abundance discriminants in subdwarf stars with effective temperatures $\lesssim$ 5500 K and $\lesssim$ 4000 K, respectively.

For the other grid, cool H- and He-rich white dwarf models have been constructed. Molecular hydrogen (H_2) determined the atmospheric structure of the H-rich models, by altering the adiabatic temperature gradient such that the conditions for convection became more favourable. A number of synthetic spectra were computed for both the hydrogen- and helium-rich models, which demonstrated that the heavily blanketed white dwarf LP701-29 was a H-rich star, with a T_{eff} = 4000 K, log g = 8.0, and a metal abundance, [M/H] ~ -3.

TABLE OF CONTENTS

CHAPTER 1

INTRODUCTION

In this thesis a spectrum synthesis technique is employed to derive abundances in the atmospheres of evolved stars which have a wide range of luminosities. Both the technique and its application to the various types of objects will be discussed here.

I. SPECTRUM SYNTHESIS

The spectrum synthesis technique has become a standard tool for interpreting photometric data and determining stellar abundances. There are a number of researchers who have developed synthesis programs, which have been used in the analysis of widely varying types of data (e.g., Bell 1970*a*,*b*; Sneden 1974*a*; Wehrse 1975, 1977). All have a basic model atmosphere program with additional subroutines to include the atomic and molecular line contributions in the total opacity. Using this opacity, the emergent flux can be calculated over a specified wavelength interval. Bell's line-list consists of many thousands of lines, and he has the facility to compute synthetic spectra between $\lambda\lambda$~3000 and ~12000Å. These spectra have then been matched directly with spectroscopic observations (e.g., Bell and Dickens 1974; Dickens and Bell 1976), or convolved with the response function of a particular photometric system (DDO, Strömgren, or UBV), and compared with photometric colours (Bell and Gustafsson 1975; Bell 1976). Sneden (1973, 1974*a*,*b*), on the other hand, synthesised restricted wavelength intervals ($\Delta\lambda$~40Å), which were sensitive to variations in the CNO abundances. High dispersion observational data were then required, because continuum placement can be difficult when only such a limited spectral region is computed. Many other authors have used the synthesis techniques, and some of these will now be discussed briefly to indicate this method's diversity.

Deming (1978) has developed a synthesis program to compute the DDO index δCN. This program was broadly based on that of Bell (see above), and used Bell's list of atomic and molecular lines. For the determination of δCN, Deming required a detailed fit of the wavelength interval λλ~4100 to ~4300Å. Mould (1978) constructed synthetic spectra near the Mg *b* lines at λ~5200Å, using routines supplied to him by Dr. R. L. Kurucz. Using integrated galaxy light Mould has shown that the Mg line region can be used as a metallicity indicator. Mallia (1977) in his survey of abundances in a number of globular clusters, computed synthetic spectra in three wavelength intervals, from which he deduced carbon and overall metal abundances. Scalo and Ross (1976) have computed representative bandheads for a number of diatomic molecules. They adopted a theoretical approach, and computed their spectra for very cool (T_{eff} < 3000K) red giant model atmospheres, without any reference to specific stellar objects.

All of the above work has involved the interpretation of giant or dwarf star spectra. By computing synthetic spectra of white dwarf stars (Wehrse 1975, 1977), it has been shown that the synthesis technique can be applied to all luminosity classes. It is particularly useful in spectral regions where unblended lines cannot be measured. Abundance analysis using equivalent width measurements of isolated features have been described most recently by Hearnshaw (1974), Paradijs and Kester (1976), Lambert and Ries 1977). Precise abundances can be obtained using the above method, but very high resolution and high dispersion data are required, so that one is sure that there is not severe blending of the lines being measured. (For some molecular features, a blend of two lines of the same species was acceptable.) This is only possible for bright stars and isolated features, and so far most objects and crowded spectral regions, spectrum synthesis enables abundances to be derived from blended features.

Most of the observations described in this thesis were made by the author, excepting in Chapters 5 and 6 where the synthetic spectra have been compared with existing data. Chapters 2 to 6 of this thesis can be divided into a study of three groups of evolved objects, all of which have effective temperatures (T_{eff}) $\lesssim$ 7000 K (a) Giant/supergiant stars (Chapters 2, 3, 4), (b) Dwarf/subdwarf stars (Chapter 5), and (c) H- and the He-rich white dwarf stars (Chapter 6). The significance of applying spectrum synthesis techniques to each group of objects will only be discussed briefly in the following pages, since each of the chapters contains its own introduction. However a general outline of the research that is to be undertaken will be given here.

II. STUDIES OF EVOLVED STARS

(a) Mixing in giant stars

There is an ever-increasing amount of observational evidence which suggests that in giant stars there has been mixing between nuclear-processed material and the surface layers. These data exist for both clusters of stars, particularly the globular clusters (e.g., Zinn 1973, 1977; Bell and Dickens 1974; Dickens and Bell 1976; Norris and Zinn 1977; Bessell and Norris 1976; Norris and Bessell 1977; McClure and Norris 1977; Mallia 1977), and field stars (e.g., Sneden 1973, 1974*a*,*b*; Bond 1974; Dearborn, Lambert, and Tomkin 1975; Sneden and Bond 1976; Sneden, Lambert, Tomkin, and Peterson 1978). All of the objects discussed above are in a wide variety of evolutionary stages, from subgiant stars to luminous giants, the latter nearing the end of their nuclear-burning evolution.

There are a number of phases in a star's main-sequence and post-main-sequence evolution during which mixing could occur. These are (a) the main sequence, (b) the first ascent of the red giant branch, when a star is burning hydrogen in a shell, (c) the He-core flash at the tip of the giant branch, (d) He-core burning on either a horizontal branch or in a "clump" near the giant branch, its exact position depending on both the stellar composition and the amount of mass exterior to star's core, and (e) during double-shell-source burning on the second ascent of the giant branch. Each of the above will be considered as a possible source of mixing.

During the main-sequence phase a composition gradient is produced between the surface layers and regions in which CNO processing has occurred (see Figures 1 and 2 of Dearborn, Eggleton, and Schramm 1976). Paczyński (1973) demonstrated that meridional circulation in rapidly rotating stars in the mass range 3-10$M_\odot$ could result in this abundance gradient being smoothed out, and thus the outer layers of the star would be enriched with CNO-processed material (low $^{12}C/^{13}C$ and high N/C ratios).

As a star evolves off the main sequence, there is a deepening surface convection zone which enables the mixing of the products of the core H-burning phase into the surface layers (see Iben 1967; Faulkner and Iben 1967; Dearborn *et al.* 1976). At its deepest penetration, significant amounts of ^{13}C and ^{14}N could be mixed up into the atmospheric layers. The growth of this convection zone, and hence the end of this mixing phase, is halted by the outward movement of the hydrogen-burning shell.

Bolton and Eggleton (1973) and Dearborn, Bolton, and Eggleton (1974) have considered a possible process by which material may be mixed into the surface layers during H-shell burning. This is not a once-only process, but a series of mixing events due to instabilities in the hydrogen burning shell. Thus small amounts of CNO-processed material could contaminate the outer envelope during each instability, successively lowering the $^{12}C/^{13}C$ and

C/N ratios.

In stars with $M \lesssim 2.5M_{\odot}$, Iben (1967) has shown that they will undergo an explosive He-core flash in an effort to eliminate an electron degeneracy, which has been established in the core (see also Schwarzschild and Härm 1962). Following the flash there is a large core convection zone which has been shown by Härm and Schwarzschild (1964, 1966) to almost reach the hydrogen-rich surface layers. Thomas (1967) and Demarque and Mengel (1971) concluded similarly. Paczyński and Tremaine (1977) considered that neutrino cooling in the central portions produced an off-centre He flash (similar to the work of Thomas 1967), and their subsequent evolution could give some mixing, but only by allowing the position of the "flash" to be their free parameter. However the general consensus (see Iben 1974, and references therein) is that it is unlikely that any mixing takes place at or immediately following the He-core flash.

Similarly no mixing has been predicted during the quiescent phase of core-He burning (Iben 1974), and thus we now consider the evolution on the second ascent of the giant branch.

Since Schwarzschild and Härm (1965) first produced thermal instabilities in the helium-burning shell of a $1M_{\odot}$ Population II model, many workers have reproduced their results for a wide range of masses and compositions (Iben 1974, and references therein; Mengel 1972; Gingold 1974). Calculations involving these instabilities (e.g., Gingold 1974) have shown that only a small amount of processed material may reach the outer layers following each of these flashes. Specifically Gingold determined a nitrogen enrichment factor of only 1.6 after 14 relaxation oscillations, which is not sufficient to interpret most of the peculiarities mentioned earlier in this section. Thus a number of more exotic schemes (e.g., the deep mixing mechanism of Sackmann, Smith, and Despain 1974, and plume mixing of Ulrich and Scalo 1972, 1973) have been described which have endeavoured to produce some of these peculiarities, including the extreme case of the CH and carbon stars, in which C/O > 1.

The above processes illustrate the evolutionary phases at which mixing could occur, but mass loss from the envelope is a mechanism which can enhance the effects of any mixing. Mass loss prior to the mixing event will produce more significant results for the same amount of mixed material, since the dilution factor is smaller. Thus mass loss must, and has throughout this thesis, always been considered in conjunction with any of the above processes.

In the present research, mixing at any one of the above evolutionary phases has been considered in the interpretation of a number of peculiar objects. In Chapter 2, the weak-G-band stars are investigated, and both spectroscopic and photometric data have been obtained in an effort to understand these objects. A carbon and nitrogen abundance analysis of both the carbon-rich Cepheid V553 Centauri, and a number of extremely metal-poor giants are described in Chapters 3 and 4 respectively. The mixing mechanisms discussed in this section have been used to provide a possible interpretation of the derived abundances.

(b) Abundances in subdwarfs

Subdwarfs, metal-deficient main-sequence stars, are most likely objects which were formed during the very early evolution of the Galaxy. In these early phases there has been little, if any contamination from previous generations of stars. Abundance analyses of these stars could therefore provide additional constraints on the formation of the heavy elements during this early evolution. Eggen and Greenstein have found many apparent subdwarfs ("red subluminous stars") in their efforts to extend the degenerate sequence to cooler temperatures (Eggen and Greenstein 1965; Greenstein 1969, 1971).

For some of these subdwarfs they indicated any spectroscopically peculiar features, the most frequent referring to the strength of the CH or MgH bands. Greenstein (1969) suggested that the strong CH objects could possibly be overabundant in carbon.

Bidelman and Smethells (1976) have indicated in a recent abstract that the CaH bands at $\lambda \sim 6385$ Å are an abundance discriminant. Mould (1976*a*,*b*) constructed CaH band spectra using cool ($T_{eff} \lesssim 3500$ K) dwarf model atmospheres, which showed that these bands remained stronger than neighbouring features, particularly the TiO bands, as the metal abundance was lowered.

In Chapter 5, CH and MgH bands have been constructed using spectrum synthesis techniques. These spectra, together with a detailed discussion of the molecular equilibria are used to explain Eggen and Greenstein's "strong CH" and "strong MgH" classifications. In addition, the use of these features as abundance discriminants is also discussed.

(c) Characteristics of cool white dwarfs

Recently there has been much research devoted to the modelling of both cool ($T_{eff} \lesssim 7000$ K) hydrogen- and helium-rich white dwarf atmospheres (Wehrse 1975, 1977; Shipman 1977; Böhm, Carson, Fontaine, and van Horn 1977). Many of these are a result of new observations (Hintzen and Strittmatter 1974; Greenstein 1976), which have shown that there are many cool degenerates, contrary to an earlier suggestion (Greenstein 1971). The new models have enabled workers to predict the characteristics of cool white dwarfs.

The spectral uniqueness of cool DA white dwarfs was questioned by Hintzen and Strittmatter (1975). They computed Hγ and various metal-line profiles for a number of cool subdwarf and white dwarf model atmospheres, and concluded that there could well be a significant number of white dwarfs masquerading as subdwarfs. More recent computations by Wickramasinghe, Bessell, and Cottrell (1977) have shown that it is very unlikely that this spectroscopic confusion could occur, since at a given effective temperature the subdwarfs would have many more visible lines of the Balmer series.

Other spectroscopic properties have been described by Wehrse (1975, 1977), particularly in the later paper, where he constructed synthetic spectra by including up to 850 metal lines in the interval between λλ2400 and 8000Å. These illustrated graphically (in particular see Figures 5, 6 and 7 of Wehrse 1977), the changing appearance of white dwarf spectra as the effective temperature, metal abundance, and hydrogen to helium ratio were altered.

Chapter 6 of this thesis describes in detail the atmospheric characteristics of cool H- and He- rich white dwarf models, with particular emphasis on the importance of H_2 molecule formation. In the latter portions of this chapter, a number of synthetic spectra were constructed using some of the models computed for this study. These were used in the interpretation of a heavily line-blanketed white dwarf, LP701-29 which has been identified by Dahn *et al.* (1978).

The spectrum synthesis technique used in this thesis has been developed by the author and is described in Chapters 2 and 5. The giant star model atmospheres used in Chapters 2, 3, and 4 have been taken from Bell *et al.*'s (1976) grid of models, while the atomic-line list has been constructed from the line data of Kurucz and Peytremann (1975). The model atmospheres discussed in Chapters 5 and 6, were converged using the program ATLAS5, originally compiled by Kurucz (1970), but which has undergone many modifications, principally made by Dr. J. R. Mould.

REFERENCES

Bell, R. A. 1970*a*, *M.N.R.A.S.*, 148, 25.

———. 1970*b*, *M.N.R.A.S.*, 149, 176.

———. 1976, in *IAU Symposium No. 72, Abundance Effects in Classification*, ed. B. Hauck and P. C. Keenan (Dordrecht: Reidel), p. 49.

Bell, R. A., and Dickens, R. J. 1974, *M.N.R.A.S.*, 166, 89.

Bell, R. A., and Gustafsson, B. 1975, Albany Conference on *Multicolor Photometry and the Theoretical H-R diagram*, ed. A. G. Davis Philip (Dudley Obs. Rept., 9, 319).

Bell, R. A., Eriksson, K., Gustafsson, B., and Nördlund, Å. 1976, *Astr. Ap. Suppl.*, 23, 37.

Bessell, M. S., and Norris, J. 1976, *Ap.J. (Letters)*, 208, 369.

Bidelman, W. P., and Smethells, W. G. 1976, in *IAU Symposium No. 72, Abundance Effects in Classification*, ed. B. Hauck and P. C. Keenan (Dordrecht: Reidel), p. 205.

Böhm, K.-H., Carson, T. R., Fontaine, G., and van Horn, H. M. 1977, *Ap. J.*, 217, 521.

Bolton, A. J. C., and Eggleton, P. P. 1973, *Astr. Ap.*, 24, 429.

Bond, H. E. 1974, *Ap. J.*, 194, 95.

Dahn, C. C., Hintzen, P. M., Liebert, J. W., Stockman, H. S., and Spinrad, H. 1978, *Ap. J.*, 219, 979.

Dearborn, D. S. P., Bolton, A. J. C., and Eggleton, P. P. 1975, *M.N.R.A.S.*, 170, 7P.

Dearborn, D. S. P., Lambert, D. L., and Tomkin, J. 1975, *Ap. J.*, 200, 675.

Dearborn, D. S. P., Eggleton, P. P., and Schramm, D. N. 1976, *Ap. J.*, 203, 455.

Demarque, P., and Mengel, J. G. 1971, *Ap. J.*, 164, 317.

Deming, D. 1978, *Ap. J.*, 222, 246.

Dickens, R. J., and Bell, R. A. 1976, *Ap. J.*, 207, 506.

Eggen, O. J., and Greenstein, J. L. 1965, *Ap. J.*, 142, 925.

Faulkner, J., and Iben, I. Jr. 1967, *Nature*, 215, 46.

Gingold, R. A. 1974, *Ap. J.*, 193, 177.

Greenstein, J. L. 1969, in *Low Luminosity Stars*, ed. S. Kumar (New York: Gordon and Breach), p. 281.

————. 1971, in *IAU Symposium No. 42, White Dwarfs*, ed. W. J. Luyten (Dordrecht: Reidel), p. 46.

————. 1976, *A. J.*, 81, 323.

Härm, R., and Schwarzschild, M. 1964, *Ap. J.*, 139, 594.

————. 1966, *Ap. J.*, 145, 496.

Hearnshaw, J. B. 1974, *Astr. Ap.*, 34, 263.

Hintzen, P. M., and Strittmatter, P. A. 1974, *Ap.J. (Letters)*, 193, L111.

————. 1975, *Ap.J. (Letters)*, 201, L37.

Iben, I. Jr. 1967, *Ann. Rev. Astr. Ap.*, 5, 571.

————. 1974, *Ann. Rev. Astr. Ap.*, 12, 215.

Kurucz, R. L. 1970, *SAO Spec. Rept.*, No. 309.

Kurucz, R. L., and Peytremann, E. 1975, *SAO Spec. Rept.*, No. 362.

Lambert, D. L., and Ries, L. M. 1977, *Ap. J.*, 217, 508.

Mallia, E. A. 1977, *Astr. Ap.*, 60, 195.

McClure, R. D., and Norris, J. 1977, *Ap.J. (Letters)*, 217, L101.

Mengel, J. G. 1972, Ph.D Thesis, Yale University.

Mould, J. R. 1976*a*, *Ap. J.*, 207, 535.

————. 1976*b*, *Astr. Ap.*, 48, 443.

————. 1978, *Ap. J.*, 220, 434.

Norris, J., and Bessell, M. S. 1977, *Ap.J. (Letters)*, 211, L91.

Norris, J., and Zinn, R. 1977, *Ap. J.*, 215, 74.

Paczyński, B. 1973, *Acta Astr.*, 23, 191.

Paczyński, B., and Tremaine, S. D. 1977, *Ap. J.*, 216, 57.

Paradijs, J. van, and Kester, D. 1976, *Astr. Ap.*, 53, 1.

Sackmann, I.-J., Smith, R. L., Despain, K. H. 1974, *Ap. J.*, 187, 555.

Scalo, J. M., and Ross, J. E. 1976, *Astr. Ap.*, 48, 219.

Schwarzschild, M., and Härm, R. 1962, *Ap. J.*, 136, 158.

———. 1965, *Ap. J.*, 142, 855.

Shipman, H. L. 1977, *Ap. J.*, 213, 138.

Sneden, C. 1973, *Ap. J.*, 184, 839.

———. 1974*a*, Ph.D Thesis, University of Texas at Austin.

———. 1974*b*, *Ap. J.*, 189, 493.

Sneden, C., and Bond, H. E. 1976, *Ap. J.*, 204, 810.

Sneden, C., Lambert, D. L., Tomkin, J., and Peterson, R. C. 1978, *Ap. J.*, 222, 585.

Thomas, H. C. 1967, *Z. Astr.*, 67, 420.

Ulrich, R. H., and Scalo, J. M. 1972, *Ap. J.*, 176, L37.

———. 1973, *Ap. J.*, 183, 151.

Wehrse, R. 1975, *Astr. Ap.*, 39, 169.

———. 1977, *Mem. Soc. Astr. It.*, 48, 13.

Wickramasinghe, D. T., Bessell, M. S., and Cottrell, P. L. 1977, *Ap.J. (Letters)*, 217, L65.

Zinn, R. 1973, *Ap. J.*, 182, 183.

———. 1977, *Ap. J.*, 218, 96.

CHAPTER 2

HD 91805 AND THE NATURE OF THE BIDELMAN-MACCONNELL WEAK-G-BAND STARS

P. L. Cottrell and J. E. Norris

ABSTRACT

High dispersion spectra of the weak-G-band star HD 91805, and DDO intermediate band photometry of a number of the weak-G-band stars of Bidelman and MacConnell have been analyzed, and lead to the following results: (i) For HD 91805 [Fe/H] ~ 0.0, [C/H] ~ -1.4, [N/H] ~ +0.6, [O/H] ~ +0.1. The simplest explanation of these abundance ratios is that material processed in the CN cycle (but not the NO cycle) has been introduced into the surface layers. (ii) The majority of the Bidelman-MacConnell objects are in the same phase of evolution as the Hyades clump stars. They are probably core helium burning objects, subsequent to the helium flash. (iii) Consideration of several mechanisms (the helium core flash, mass loss, thermal instability of hydrogen burning shells, the Paczyński mechanism of N/C enhancement by meridional circulation) suggests that the Paczyński mechanism coupled with moderate mass loss alone invokes no radical postulates and violates none of the observational constraints.

I. INTRODUCTION

Stars possessing anomalously weak CH bands (the weak-G-band stars) appear to exist in all populations. The peculiarity was first recognized by Cannon (1912) and Bidelman (1951) in HR 885, the Population I prototype. Eggen (1971) places HD 191046, another member of the class (Greenstein and Keenan 1958), in the Arcturus group. The existence of weak-G-band stars in the halo was first recognized by Zinn (1973), who discovered them in M92; his result appears to extend to all metal-poor globular clusters ([Fe/H] $\lesssim$ -1.0) (*cf.* Mallia 1975; Norris and Bessell 1977; Norris and Zinn 1977; Zinn 1977).

While no field halo stars are yet available for detailed (i.e. high dispersion) analysis, more progress can be made in the younger populations. Hopefully this will throw light on the phenomenon in Population II. Greenstein and Keenan (1958) first demonstrated that HR 885 is deficient in CH and CN by factors of ~30 and ~100, respectively. Following the survey work of Bidelman and MacConnell (1973), some 40 weak-G-band stars are now recognized amongst field stars brighter than tenth magnitude. One of these, HR 6766, has recently been analyzed by Dean, Lee, and O'Brien (1977) and by Sneden and Peterson (1977). The latter authors find [Fe/H] ~ -0.25, [C/Fe] ~ -1.3, [N/Fe] ~ +0.8, and [O/Fe] ~ -0.1.

There is a growing consensus that the weak-G-band phenomenon in all populations results from the mixing of CNO processed material to the surface of these stars (Butler, Carbon, and Kraft 1975; Norris and Zinn 1977; Dean *et al.* 1977; Sneden and Peterson 1977; Carbon *et al.* 1977). The site and details of the mixing process, however, are not yet clear. In an effort to provide more information on this problem we have obtained spectroscopic and photometric observations of the weak-G-band star HD 91805 together with intermediate band photometry of a number of the Bidelman-MacConnell objects

(§II). In particular, we have performed a curve-of-growth, and spectrum synthesis analysis of the weak-G-band star HD 91805 to obtain an insight into the products of mixing (§III); our results are very similar to those reported by Sneden and Peterson (1977) for HR 6766. In §IV we present evidence, based on DDO intermediate band photometry, that the majority of the Bidelman-MacConnell weak-G-band stars are burning helium in their cores subsequent to the helium core flash. In the final section we consider possible causes of the weak-G-band anomaly, subject to the constraints deduced in the earlier sections. Of the mechanisms considered, carbon depletion due to meridional circulation (*cf.* Paczyński 1973) requires the least radical departure from presently well-understood astrophysical processes.

II. OBSERVATIONS

(a) Spectra

The weak-G-band star HD 91805, together with two Hyades giants HD 28307 (cluster) and HD 100407 (group) were observed with a variety of gratings and cameras available on the coudé spectrograph of the 1.9m telescope at Mount Stromlo.

High dispersion spectra to be used in a curve-of-growth analysis were obtained by utilizing an échelle grating in combination with the 81cm camera and a 2-stage Carnegie image tube. The spectral range covered was from λλ5200Å to 5500Å with a reciprocal dispersion of ~1.5Åmm^{-1}, and a wavelength range of ~50Å per order. Good wavelength coverage was obtained for HD 91805 and HD 100407, but the data for HD 28307 were less extensive, and our method of analysis for this star will be discussed in §III(a). We also used the échelle grating to obtain spectra in the region of the [OI] line at 6300.3Å; the reciprocal dispersion was ~2.5Åmm^{-1}.

The échelle grating was not particularly useful in obtaining spectra of the blue molecular features. Not only is its response function curved along a given order, but there are few (if any) continuum points in each order, making any effort at continuum placement quite imprecise. Therefore the G-band and the CN molecular feature running blueward of λ4216Å were obtained directly (without image tube) using the B grating in the second order and the 81cm camera to give a reciprocal dispersion of $10\text{Å}mm^{-1}$. Direct plates were obtained for only HD 91805 and HD 28307. However, for HD 100407 an échelle spectrum, with reciprocal dispersion of $\sim 1\text{Å}mm^{-1}$, was obtained in the G-band region. This spectrum had a higher resolution, ~0.4Å, than that found for the direct plate spectra. For the latter, the resolution was ~0.6Å.

The CN feature near λ3883Å was acquired with the C grating in the third order in combination with the 81cm camera, and the image tube. The reciprocal dispersion of this combination was $\sim 7\text{Å}mm^{-1}$. 2mm of BG3 was used to remove overlapping orders.

Finally we obtained spectra of the NH features near λ3360 using the C grating in the fourth order, together with a Carnegie image tube attached to the 40cm camera. The reciprocal dispersion was $\sim 10\text{Å}mm^{-1}$. Overlapping orders were removed using 2mm of UG5, together with 5mm of a liquid $CuSO_4$ solution.

For these last two regions, we were able to obtain data for HD 91805, and only one of the Hyades giants, HD 100407.

All data were recorded on IIaO emulsion using various methods of sensitization. The direct plates were obtained on baked plates, the NH and CN features on nitrogen soaked plates, and the échelle plates on hydrogen sensitized emulsions. Intensity calibrations were taken on separate plates, except for the direct plate which carried its own calibration, and all were used to program the Göttingen microphotometer to give intensity tracings of the above spectra. Line strength measurements from these tracings, which form the basis of our curve-of-growth analysis, are given in the Appendix.

(b) Photometry

DDO intermediate band photometry has been obtained for 23 of the weak-G-band stars of Bidelman and MacConnell (1973). The observations were made with the 0.6m telescope on Siding Spring Mountain in February 1975 and January 1977. A 1P21 pulse counting photometer was employed, together with the equatorial standards of McClure (1976). The results are given in Table 1 where the columns are self-explanatory. In the final row of the table we list the mean standard errors of our colors, derived from those stars having multiple observations.

In view of the fact that several of the DDO bandpasses include features of the CN and CH molecule the data in Table 1 are difficult to interpret. We believe, however, that an important result can be distilled from the results in the [C(45-48), C(42-45)] - plane. We prefer to leave this discussion, however, until we have completed our abundance analysis of HD 91805, which we regard as a typical weak-G-band star.

III. ANALYSIS OF HD 91805 WITH RESPECT TO TWO HYADES GIANTS

Our analysis is divided into two sections; (a) a differential curve-of-growth analysis using Pagel's (1964) formulation as expressed by Griffin (1969) to determine the iron abundance and electron pressure of HD 91805, and (b) a detailed analysis of the following features: (1) the forbidden [OI] line at λ6300.3Å, (2) the G-band between $\lambda\lambda$4290Å and 4330Å, (3) the wavelength interval $\lambda\lambda$3870Å to 3885Å which is dominated by 2 bandheads of the blue CN system ($\Delta v=0$), (4) the section of spectrum from $\lambda\lambda$4192Å to 4217Å which contains 2 bandheads of the $\Delta v = -1$ blue CN system,

TABLE 1

DDO PHOTOMETRY OF 23 WEAK-G-BAND STARS

HD	C(45-48)	C(42-45)	C(41-42)	C(38-42)	n
18636	1.130	0.676	0.135	-0.385	1
21018	1.109	0.640	0.133	-0.516	1
BD+5°593	1.286	0.774	0.141	-0.281	3
26575	1.205	0.833	0.250	-0.209	3
28932	1.169	0.723	0.136	-0.406	3
BD-19°967	1.027	0.656	-0.019	-0.745	3
31274	1.184	0.720	0.133	-0.288	5
31869	1.164	0.695	0.101	-0.411	3
36552	1.144	0.662	0.130	-0.467	4
40402	1.150	0.701	0.105	-0.400	3
49960	1.202	0.737	0.144	-0.232	3
54627	1.170	0.739	0.156	-0.273	3
56438	1.197	0.741	0.124	-0.267	3
67728	1.262	0.841	0.258	-0.222	2
78146	1.235	0.846	0.218	-0.108	2
82595	1.184	0.774	0.148	-0.172	2
91805	1.168	0.692	0.132	-0.331	3
94956	1.182	0.715	0.122	-0.325	3
102851	1.208	0.766	0.124	-0.236	2
CD-37°7613	1.182	0.743	0.123	-0.308	2
105783	1.240	0.764	0.119	-0.257	3
120170	1.169	0.677	0.118	-0.399	1
120213	1.375	1.048	0.229	0.139	2
<s.e.>	.006	.010	.008	.010	

and (5) the region λλ3356Å to 3377Å which encompasses 2 bandheads of the NH triplet system (A $^3\Pi$ - X $^3\Sigma$). This approach yields C, N and O abundances in the atmosphere of the weak-G-band star, HD 91805.

(a) Curve-of-growth analysis

HD 91805 has been compared with two stars, HD 28307 and HD 100407. Both are members of the Hyades cluster or moving group according to Eggen (1972) and Boyle and McClure (1975). Recently, Eggen (1977) has shown that HD 100407 may not be a member of the group. This, however, does not affect our analysis, since we determine all our parameters relative to HD 28307, a confirmed cluster member. Photometric data for the three stars (Eggen, 1972) are given in Table 2, together with estimates of their atmospheric parameters, a discussion of which follows.

TABLE 2

PHOTOMETRIC AND ATMOSPHERIC DATA

HD (1)	V (2)	$(R-I)_K$ (3)	M_{bol} (4)	T_{eff} (5)	[Fe/H] (6)	log g_{group} (7)	log g_{sp} (8)
28307	3.83*	0.325*	0.60*	5000	0.1†	2.8	...
91805	6.10‡	0.35§	...	4850	0.0	...	2.0
100407	3.55*	0.35*	-0.05*	4850	0.0	2.5	2.2

* From Eggen (1972).

† From Griffin (1969).

‡ From Dean *et al.* (1977).

§ From Eggen (private communication) and the present authors.

In our curve-of-growth treatment we make the basic assumption, following Griffin (1969), that

$$\Delta\theta_{exc} \equiv \Delta\theta_{ion} \equiv \Delta\theta_{eff},$$

where the effective temperatures have been derived from the broadband color $(R-I)_K$, using the transformations of Eggen (1972) and Johnson (1966) and are given in column (5) of Table 2.

Pagel's (1964) formula for the differential horizontal shift, $[X_0]$ of neutral lines of a particular element, j, relates this quantity to the differential abundance, $[N_j/H]$, of that species relative to hydrogen, by

$$[X_0] = [\theta] + \Delta\theta(I_j - 0.74) + [N_j/H],$$

where I_j is the ionisation potential of the element, j. [...] refers to the logarithmic difference in each parameter.

The Arcturus curve-of-growth (van de Held's curve from Griffin and Griffin 1967) was fitted to all our curves, and is represented by the solid line in Figures 1 and 3.

The FeI curves of growth for HD 91805 and HD 100407 are illustrated in Figures 1a, b, respectively. No relative horizontal shift is seen in these figures, and coupled with the identical temperature derived for these 2 stars, one concludes that they have the same iron abundance. This will be shown below to be solar, to within ± 0.2 dex, the accuracy of the method.

Only limited spectroscopic data were obtained for HD 28307. The equivalent widths of all available lines on our plates are plotted in Figure 2 against the values given by Griffin (1969). The agreement is good, and attests to the reliability of our line strength measurements. We have accordingly constructed the FeI curve-of-growth for HD 28307 using Griffin's equivalent widths for the lines used previously in HD 91805 and HD 100407, and show the result in Figure 1c.

FIG. 1. - FeI Curves of growth. (a) HD 91805, (b) HD 100407, (c) HD 28307.

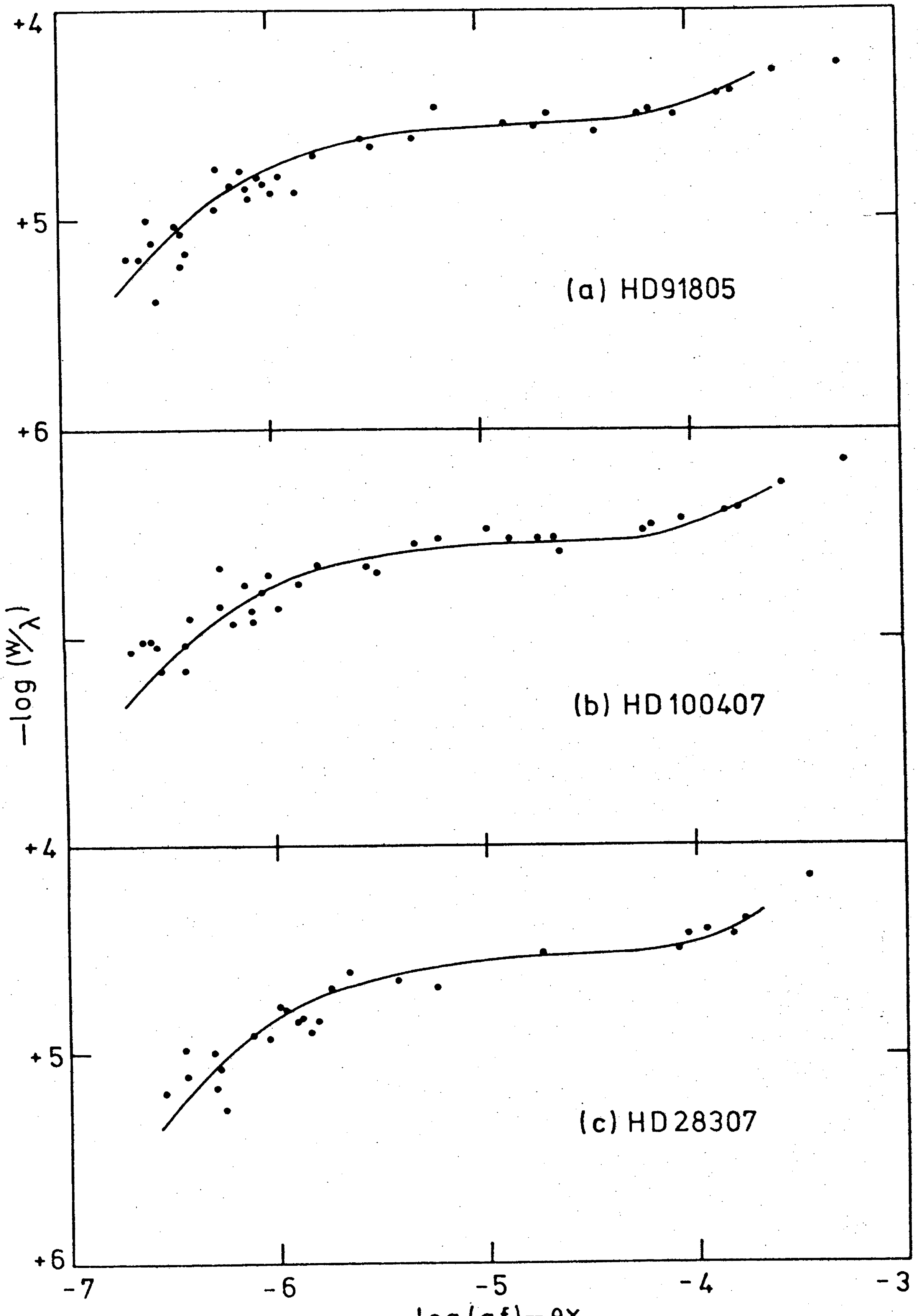

+4
+5
+6
(a) HD91805
(b) HD100407
+4
+5
+6
(c) HD28307
$-\log(W/\lambda)$
-7
-6
-5
-4
-3
log(gf) − θx

FIG. 2. - Comparison of equivalent widths for HD 28307. [CN] = Cottrell and Norris (this work); [Griffin] = Griffin (1969).

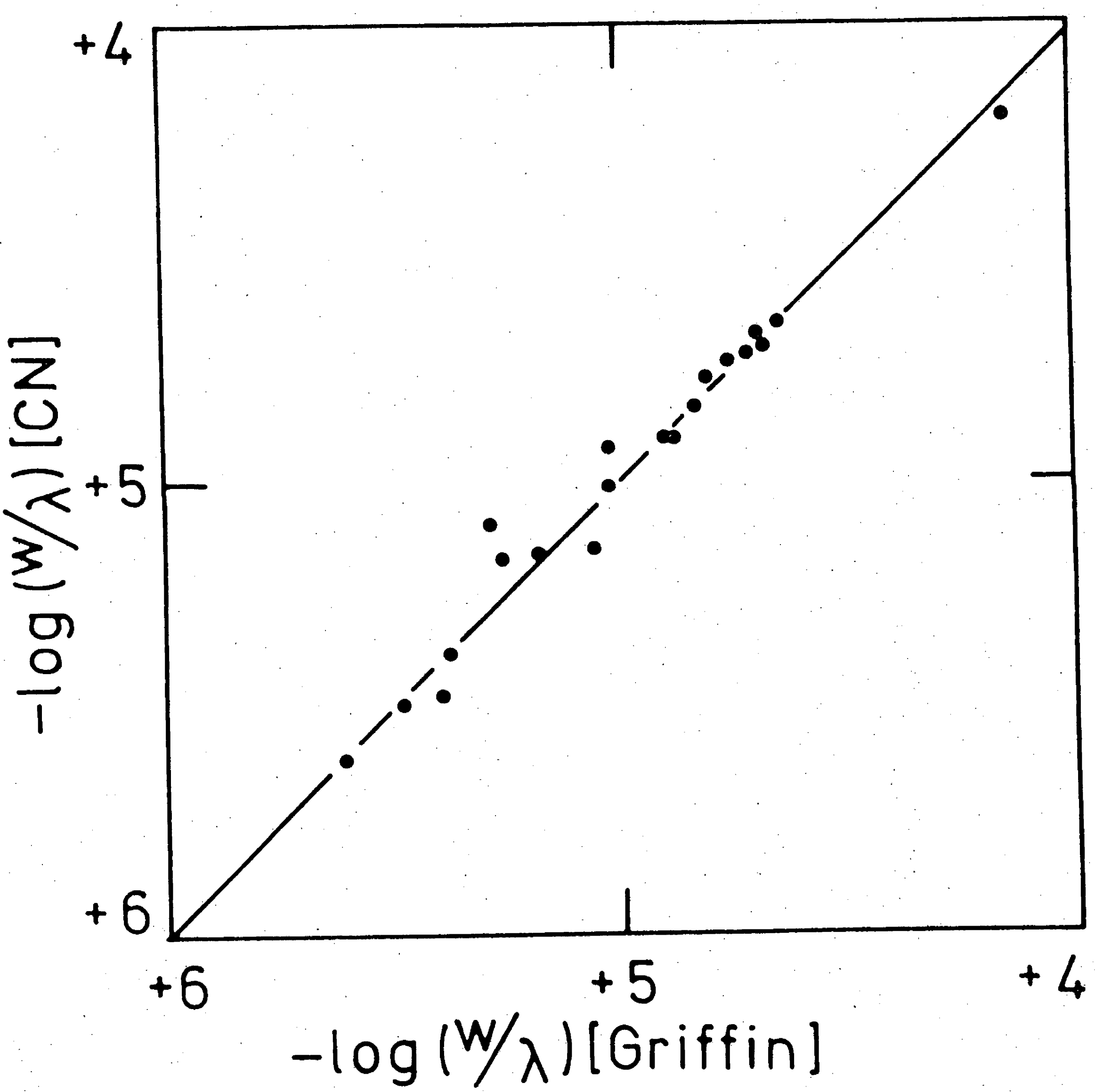
+4
+5
+6
-log (W/λ) [CN]
+6
+5
+4
-log (W/λ) [Griffin]

The available data were not of sufficient quality for differential vertical shift measurements to be made, so that a microturbulent velocity could not be inferred. This will be considered further when we discuss the model atmospheres. We assume here that the microturbulence is the same in all three stars.

We now determine the iron abundances in HD 91805 and HD 100407 relative to HD 28307. From Griffin (1969), the atmosphere of HD 28307 may be represented by the following parameters:

$$\theta = 1.02,\ \log P_e = 2.43 \text{ and } [Fe/H]_{(HD\ 28307\ -\ \odot)} = +0.1.$$

Considering the temperature difference between HD 28307 and both HD 91805 and HD 100407, the shift required to move the curves of growth of the latter 2 stars onto that of HD 28307 results in a differential iron abundance,

$$[Fe/H]_{\left(\begin{Bmatrix}HD100407\\HD\ 91805\end{Bmatrix} - HD\ 28307\right)} = -0.1,$$

and thus a solar iron abundance for the weak G-band star, HD 91805. The abundances for all 3 stars are given in column (6) of Table 2. In what follows we assume that this result applies to all elements in the atmosphere of HD 91805 with the important exceptions of carbon, nitrogen, and oxygen.

The differential electron pressure, $[P_e]$, between HD 28307, HD 91805 and HD 100407 was obtained by using the ionised lines of Ti and Cr. The horizontal shift, $[X_+]$ in the TiII and CrII curves of growth, Figures 3a, b, respectively, was interpreted using Pagel's (1964) relationship between this shift and $[P_e]$, $[N_j/H]$ and $[\theta]$, namely,

$$[X_+] = -1.5\ [\theta] + \Delta\theta(-0.74) - [P_e] + [N_j/H].$$

By applying $$[g] = 2[P_e] - [x_H + Ax_m] + 1.8\ \Delta\theta_{ion},$$

one can obtain the differential spectroscopic gravity, where A is the overall metal abundance and x_H and x_m are the mean degrees of ionisation of H and the

FIG. 3. - Curves of growth for ionised lines. (a) TiII, (b) CrII. Points for HD 28307 (●), HD 91805 (x), and HD 100407 (■) are shown. The curves are also identified.

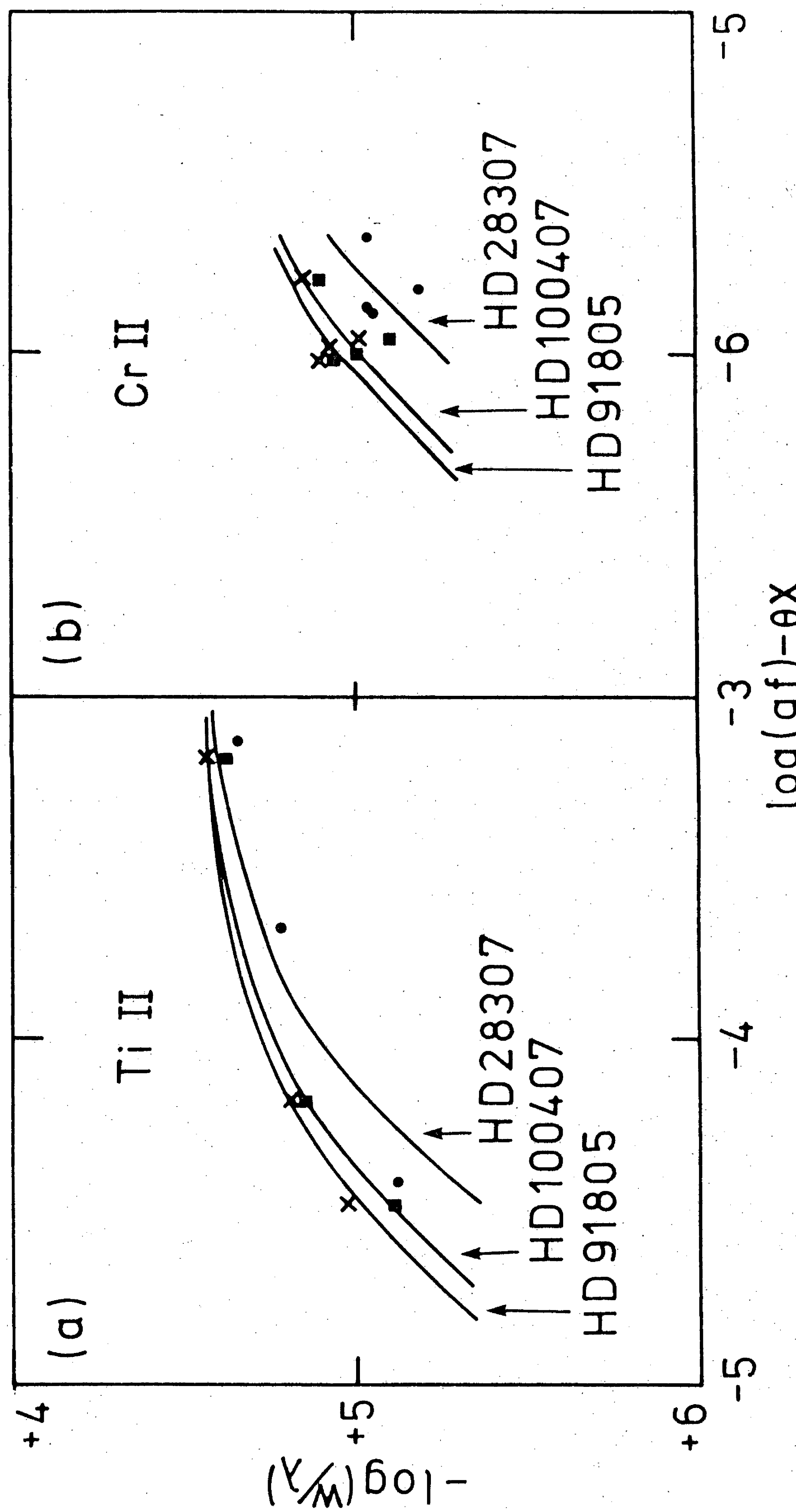
(a)
Ti II
HD28307
HD100407
HD91805
(b)
Cr II
HD28307
HD100407
HD91805
+4
+5
+6
$-\log(W/\lambda)$
−5
−4
−3
−6
−5
log(gf)−θX

metals. The line forming regions of the atmospheres considered in this analysis are sufficiently cool that all the hydrogen is neutral and all the electron contributing metals are singly ionised. This implies values of 0 and 1 for x_H and x_m respectively.

For HD 28307 and HD 100407 using bolometric magnitudes from Eggen (1972) and assuming masses of $\sim 2M_\odot$ for the Hyades giants, one obtains an estimate of the gravity, shown in column (7) of Table 2. Adopting HD 28307 as the primary standard, and using the above curve-of-growth analysis one determines spectroscopic gravities for HD 91805 and HD 100407 of 2.0 and 2.2, respectively. These are also listed in column (8) of Table 2. An error, ± 0.4 dex, in the spectroscopic gravity by this method provides satisfactory agreement between this and the group membership gravity for HD 100407.

(b) Spectrum synthesis of CH, CN and NH

Before proceeding to our CNO abundance analysis, the spectrum synthesis technique we employed will be described in detail.

(i) Technique

Molecular line lists have been constructed for the (A $^2\Delta$-X $^2\Pi$) electronic transition of CH and the blue system (B $^2\Sigma$-X $^2\Sigma$) of CN, by applying small perturbations to the formulations of Krupp (1974) and Herzberg (1955), respectively. The wavelength accuracy of all line lists, CH around λ4300Å, CN between λλ3860Å and 3883Å for $\Delta v = 0$, and also from λλ4180Å to 4216Å for $\Delta v = -1$, was better than .1Å. This gave an extremely good representation of the solar spectrum.

The line strengths were calculated in parallel with the wavelength determination. The total line strength, $f_{N'N''}$, of a particular transition is given by

$$f_{N'N''} = \frac{\lambda_{00}}{\lambda_{N'N''}} \cdot f_{el} \cdot q_{v'v''} \cdot \frac{[HL]_n}{2N'' + 1} ;$$

where N', N" are respectively the rotational quantum numbers of the upper and lower levels of the transition, λ_{00} is the band origin in Å, $\lambda_{N'N''}$ is the wavelength (Å) of the transition, f_{el} is the electronic oscillator strength, $q_{v'v''}$ is the Franck-Condon factor of the vibrational band, and $[HL]_n$ is the normalised Hönl-London factor of the individual rotational line. The sources, and in some cases the values of the individual components of the line strength are listed in Table 3.

TABLE 3

LINE STRENGTH DATA

Molecule	Electronic Oscillator Strength (f_{el})	Franck-Condon factors ($q_{v'v''}$)	Hönl-London factors ($[HL]_n$)
CH	Schadee (1964) 2.8×10^{-3}	Childs (1964)	Schadee (1964)
CN	Liszt and Hesser (1970) 3.95×10^{-2}	Spindler (1965)	Schadee (1964)

To the molecular line lists we added atomic lines from Kurucz and Peytremann (1975) dependent on the following selection criteria: (1) only lines of the elements calcium (Z = 20) through to nickel (Z = 28), and strontium (Z = 38) to ruthenium (Z = 44), excluding technetium (Z = 43) were included, (2) only neutral and singly ionised lines of the above elements were retained, (3) all lines which had low excitation potentials greater than 5ev were excluded, and (4) lines were included only if their line opacity, at a representative temperature of 5000°K in the Sun, was greater than that of a line whose measured equivalent width was 15mÅ (Moore, Minnaert, and Houtgast 1966).

Two additional line lists were constructed. The first covered the NH feature between λλ3355Å and 3380Å using data from Sneden (1974), while the second extended from λλ6295Å to 6305Å to encompass the [OI] line at λ6300.3Å.

These line lists were used in conjunction with the model atmosphere program, ATLAS, (Kurucz 1970) to produce synthetic stellar spectra. One notable change was the incorporation, in data block form, of the molecular partition functions for CH, CN, and NH from Tatum (1966). These are more explicit than those calculated in ATLAS.

The molecules, H_2, C_2, N_2, H_2O, CH, NH, OH, CO, NO, CN, were included in the equilibrium equations. These molecular species, with the exception of H_2, are competing for the available C, N, and O, and hence all number densities are intrinsically connected.

The continuous opacity sources included were absorption by HI, H^-, He^-, C^-, H_2^+, H_2^-, MgI, AlI, SiI, as well as Rayleigh scattering by H, He, and H_2, and electron scattering. Since the continuous opacity changes only slowly with wavelength, and we only compute fluxes over small wavelength intervals (<50Å), considerable saving in computer time was made by only determining this opacity every 25Å.

The emergent flux was calculated from the total opacity, line plus continuum, at equally spaced wavelength points over the interval requested. These fluxes were convolved with a Gaussian profile, whose width was determined by the instrument used to obtain the observational data, and with which the synthetic spectrum was compared.

Normalisation of all the spectral regions, except for the NH feature around 3360Å, was accomplished by taking the convolved fluxes and searching for the maximum value. All the other fluxes were then scaled accordingly. The continuum, or a point identified as a continuum point in the Arcturus Atlas (Griffin 1968), was reached in all bands when the raw fluxes were convolved with a Gaussian profile of full ½ width (full width at half maximum, FWHM) ≤ 0.6Å. In the region of the NH feature heavy line blanketing makes continuum placement impossible, and comparison between theory and observation extremely difficult. We shall return to this problem in the next section.

All the model atmospheres used in this analysis are those of Bell *et al.* (1976). Since, however, we are considering specific temperatures, gravities, and metal abundances, subsidiary programs were written to interpolate within this grid. At this stage we adopted a microturbulent velocity of 2 km s^{-1}, in line with the majority of the models constructed by Bell *et al.* The output from this process was in a form suitable for input into ATLAS, for construction of the synthetic spectra.

Some of the semi-empirical gf values of Kurucz and Peytremann (1975) varied from values tabulated by other authors, (Blackwell, Ibbertson, and Petford 1975; Bridges and Kornblith 1974; May, Ritcher, and Wichelmann 1974). Thus the gf values were revised until the synthetic solar spectrum fitted the Utrecht Solar Atlas (Minnaert, Mulders, and Houtgast 1940). As well as these adjustments to the atomic gf values the molecular bands had to be normalised, such that the solar spectrum was reproduced. These normalisation factors reflect the errors in the determination of the individual line strengths and the molecular partition functions.

(ii) C, N, and O abundance analysis

The above spectrum synthesis technique has been used to determine C, N and O abundances in the weak-G-band star, HD 91805, as well as the two Hyades giant stars, HD 28307 and HD 100407.

In late-type stars where CNO abundances are solar, or near solar, carbon and oxygen are intrinsically connected in equilibrium with CO. This situation pertains to the Hyades giants, but in the weak-G-band star we have a simplified situation. In the latter, because of the deficiency of carbon, which we initially estimate to be a factor of 10, C and O become decoupled. For example, changing the C abundance by a factor of 2, from one tenth to one twentieth normal, affects the [OI] line at λ6300.3Å by less than 1 percent.

We begin this analysis with our oxygen abundance determination, the results of which are tabulated in column (4) of Table 4. The [OI] line equivalent widths are given in the Appendix. All abundances in this table are logarithmic and relative to the Sun for which we adopted the values of Lambert (1968). For the Hyades cluster member, HD 28307, we have assumed [O/H] = [Fe/H] as the [OI] line in our spectrum was blended with a ScII line

TABLE 4

CNO ABUNDANCES

HD (1)	†[C/H] (2)	‡[N/H] (3)	[O/H] (4)
28307	+0.1 ± 0.2	-0.1 ± 0.3	+0.1*
91805	-1.4 ± 0.3	+0.6 ± 0.4	+0.1 ± 0.2
100407	-0.2 ± 0.3	-0.3 ± 0.4	-0.2 ± 0.2

* We assume [O/H] = [Fe/H] (see text).

† Errors in [C/H] determinations include uncertainty in the oxygen abundance, *plus* intrinsic errors associated with the fitting of the synthetic G-bands to the observational data.

‡ Errors in N/H include intrinsic errors due to the fitting of the synthetic spectra to the observations, as well as accumulated errors from the oxygen and carbon abundance determinations.

at $\lambda \sim 6300.7$Å. In the tracings of HD 91805 and HD 100407 this line was about the same strength as the measured [OI] line.

From the curve-of-growth analysis, the gravity produces the largest source of error, ±0.4 dex. We therefore investigated its effect on each of our C, N, and O abundance determinations. In the weak-G-band star model atmosphere, $\Delta \log g = 0.4$ has a 20 percent effect on the computed [OI] line strength, which transforms to an error in the O abundance of ±0.15 dex.

Thus, within the limits of the method, normal oxygen abundances were obtained for HD 100407 and, in particular, HD 91805, the weak-G-band star.

Next the C abundances were computed using CH lines within the G-band. For HD 91805 we estimate an abundance -1.4 dex relative to the Sun. That is, carbon in this weak-G-band star is underabundant by a factor of ~25. Figures 4a, b, and c show both the observed and synthetic G-bands for the C abundances chosen for HD 91805, HD 28307, and HD 100407, respectively. These abundances are shown quantitatively in column (2) of Table 4.

Assigning a C abundance to the weak-G-band star is made difficult by the weakness of the CH features. In Figure 4a we include a synthetic spectrum from which the contribution of the CH molecule has been removed. The arrows in this figure indicate the spectral regions which are most sensitive to changes in the abundance. Using these regions we estimate that [C/H] ~ -1.4 gives the best fit to the observations. Deriving the C abundance in HD 91805 involved an intrinsic fitting error which was larger than those involved in determining either the O or the N abundances. This error propagates into the uncertainty with which we can estimate the N abundance. However, it is important to note that our procedure produces good argument between theory and observation for both HD 28307 and HD 100407 for abundances very close to solar. Gravity variations, $\Delta \log g = 0.4$, have little effect, $<$ 1 percent, on the synthetic spectra, a result previously

FIG. 4. - Observed and synthetic spectra for the G-band. (a) HD 91805, additional line (dots) is synthetic spectrum with no CH lines, (b) HD 28307, (c) HD 100407. The fluxes in (a) and (b) were convolved with a Gaussian profile with FWHM = 0.6Å. For (c), a profile with FWHM = 0.4Å was used (see text §II).

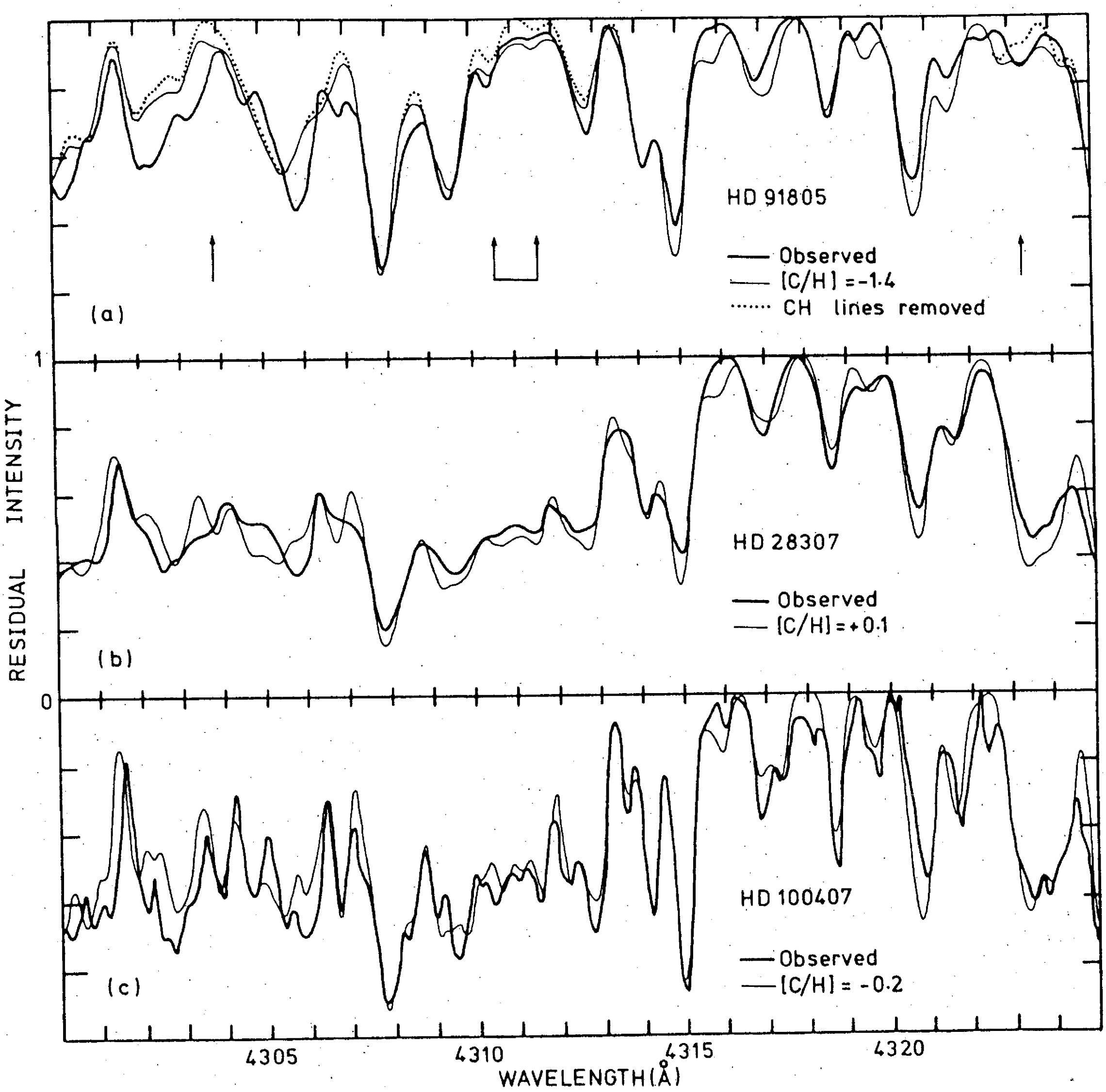
HD 91805
Observed
[C/H] =-1.4
CH lines removed
(a)
1
RESIDUAL INTENSITY
HD 28307
Observed
[C/H] = +0.1
(b)
0
HD 100407
Observed
[C/H] = -0.2
(c)
4305
4310
4315
4320
WAVELENGTH(Å)

obtained by Schadee (1968).

Having evaluated carbon and oxygen abundances for the three stars, we now proceed to our determination of the nitrogen abundances, using the CN features around λ4200Å (Δv = -1), and 3880Å (Δv = 0). With the abundances shown in column (3) of Table 4, Figures 5a, b give the regions around two bandheads of the Δv = -1 system for HD 91805 and HD 28307, respectively. To emphasize the weakness of these CN bands in HD 91805 we have also shown a synthetic spectrum from which the CN contribution has been omitted. Figures 6a, b illustrate our results for the spectral region from λλ3870Å to 3885Å for HD 91805 and HD 100407, respectively. Because of the greater intrinsic strengths of the Δv = 0 bands this region provides a better discriminant for determining the nitrogen abundance. From our analysis of these two regions we find that nitrogen is enhanced in HD 91805 by a factor ~4 relative to the Sun, whereas abundances obtained for the two comparison stars show no deviation from normality to within the errors estimated.

It should be noted that a change in gravity of 0.4 dex alters the above features by only about 2 percent. Over such a small range in gravity the luminosity effect exhibited by the CN molecule is not apparent. Hence since neither CH nor CN features are significantly affected by small changes in the gravity, once this parameter and an O abundance have been adopted, no additional errors are introduced from this source in determining the C and N abundances.

Finally, we discuss the NH feature in the near ultra-violet. N abundances were not determined directly from this region as not only was continuum placement hopeless, but also the blending of the features made identification of individual NH features impossible. Thus, this spectral region was used only as a check on the results obtained using the above

FIG. 5. - Blue CN band for $\Delta v = -1$ system. Observations and synthetic spectra, (a) HD 91805, with dotted line representing synthetic spectrum with all the CN lines removed, (b) HD 28307. Convolving profile had FWHM = 0.6Å.

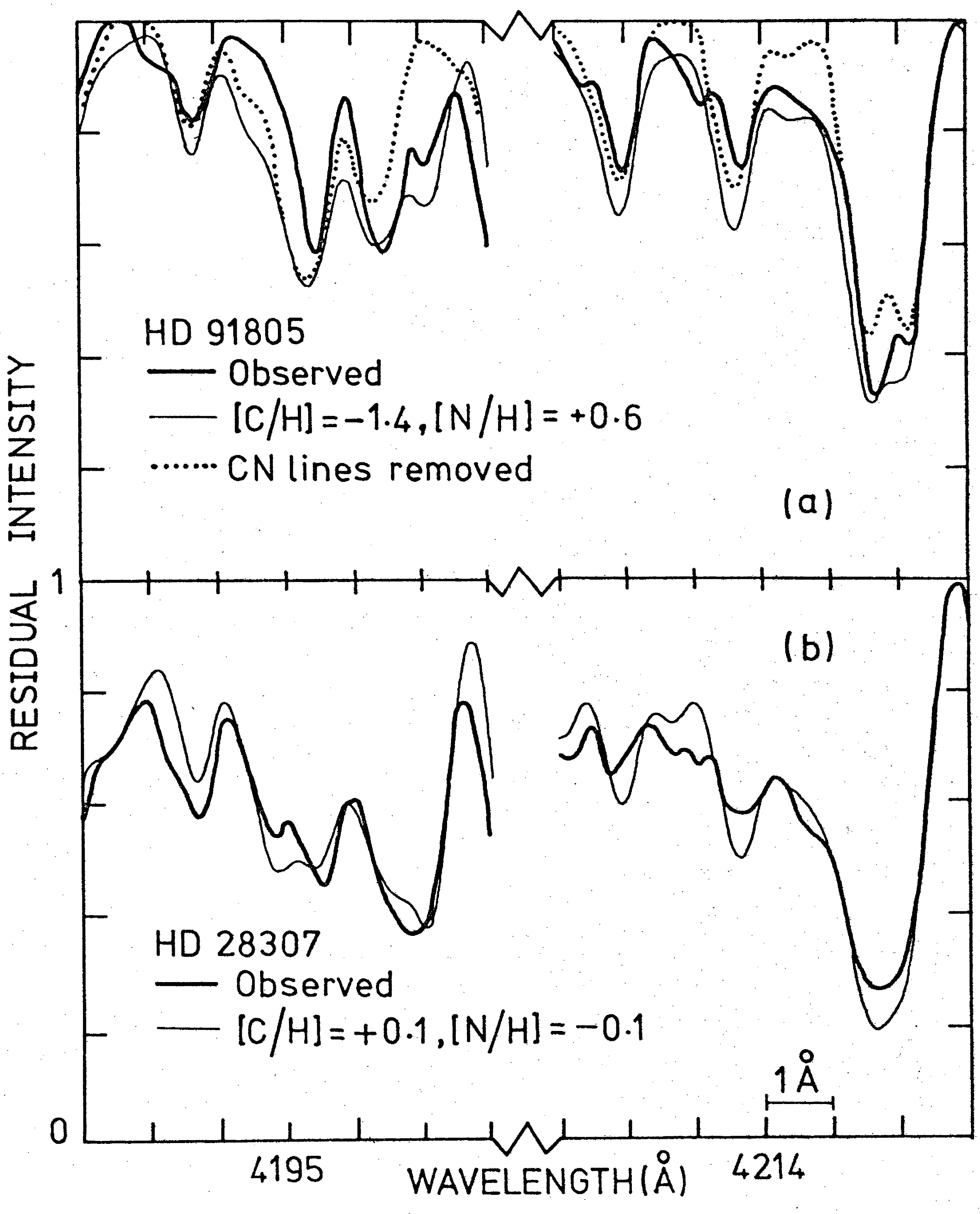
HD 91805
Observed
[C/H] = −1·4, [N/H] = +0·6
CN lines removed
(a)
(b)
HD 28307
Observed
[C/H] = +0·1, [N/H] = −0·1
1 Å
RESIDUAL INTENSITY
1
0
4195
4214
WAVELENGTH (Å)

FIG. 6. - Blue CN band for $\Delta v = 0$ for (a) HD 91805, (b) HD 100407. Convolving profile had FWHM = 0.6Å.

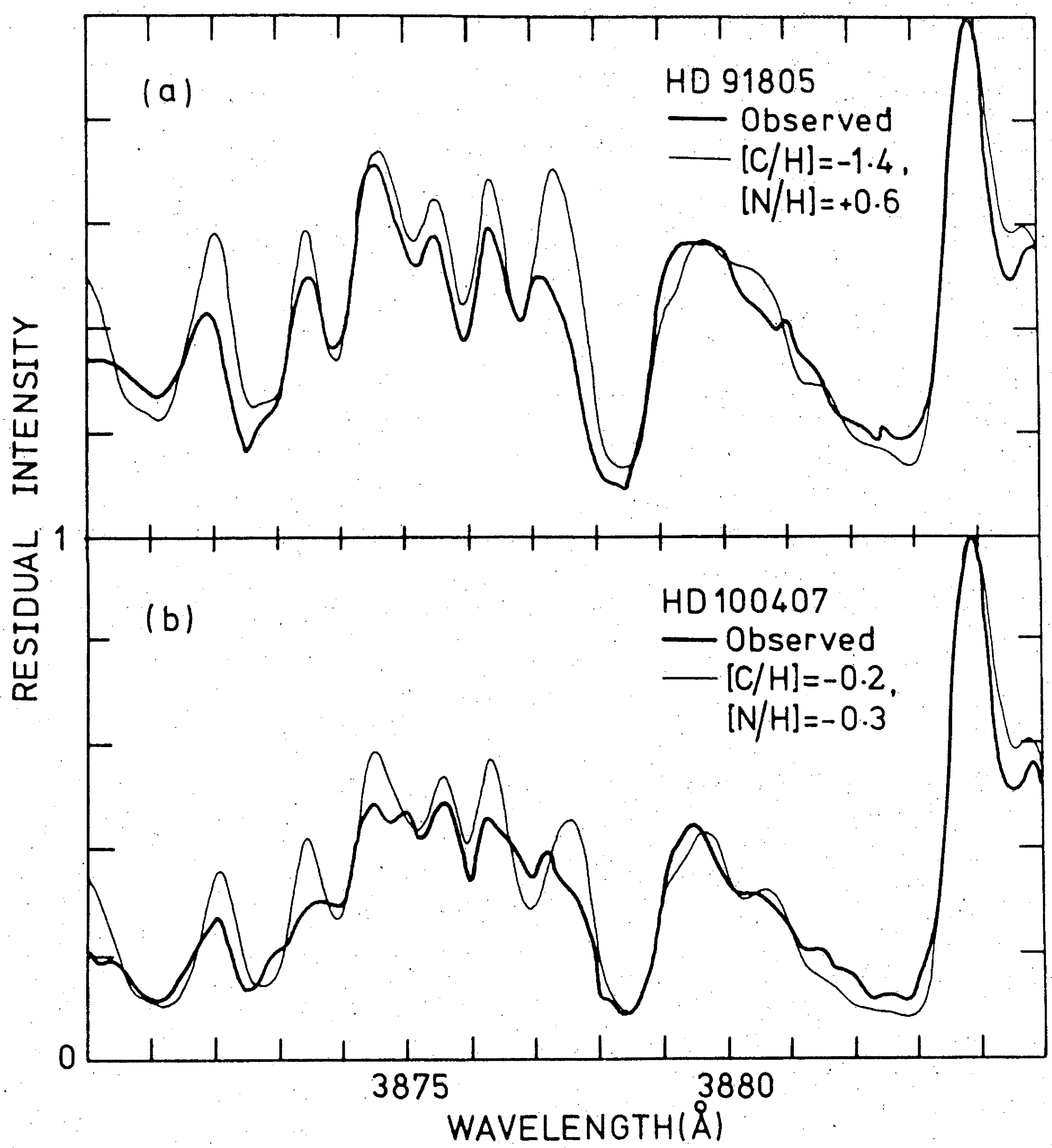
(a)
HD 91805
Observed
[C/H]=-1·4,
[N/H]=+0·6
(b)
HD 100407
Observed
[C/H]=-0·2,
[N/H]=-0·3
RESIDUAL INTENSITY
1
0
3875
3880
WAVELENGTH(Å)

CN features.

HD 91805 and HD 100407 have the same effective temperature and metal abundance, excluding C, N and O, and only $\Delta \log g = 0.2$, which has little effect on the NH feature. Thus, the observations of these two stars in this region can be compared directly, as shown in Figure 7. The enhanced N abundance in the weak-G-band star is apparent, but a quantitative estimate is difficult. The observed and synthetic spectra of these 2 stars with the nitrogen abundance adopted from the CN features are shown in Figures 8a, b, respectively. All the spectra shown in Figures 7 and 8, are normalised to the same point, $\lambda \sim 3356$Å. Although the continuum was not reached at this wavelength, normalisation at this point meant that we analysed all the data in a similar manner.

The discrepancy in Figure 8 could result from a number of effects. For the dispersions (10Å/mm) and resolutions (~1Å) which we obtained, individual NH lines were not isolated. The measurable features are at $\lambda \sim 3360$Å and $\lambda \sim 3370$Å, with NH contributing only a portion of this absorption. Higher dispersion observations of this region would alleviate the situation, but background fogging on the photographic plate by ion noise in the image tube would prohibit the use of the coudé échelle. Therefore, the present data is the best currently obtainable at Mount Stromlo.

The other area where differences could arise is in the model atmospheric structure, particularly in the very outer surface layers, where the feature at $\lambda \sim 3360$ is forming. This would affect the weak-G-band star more than the Hyades giant, because of the higher N abundance and hence stronger NH lines in the former.

We also briefly investigated the lack of surface cooling by CO in HD 91805, which would result from its carbon deficiency (*cf.* Gustafsson *et al.* 1975). We increased the surface temperatures according to Figure 8 of Gustafsson *et al.*, making no attempt to adjust the other

FIG. 7. - Observations for HD 91805 and HD 100407 at the near-ultra-violet NH feature.

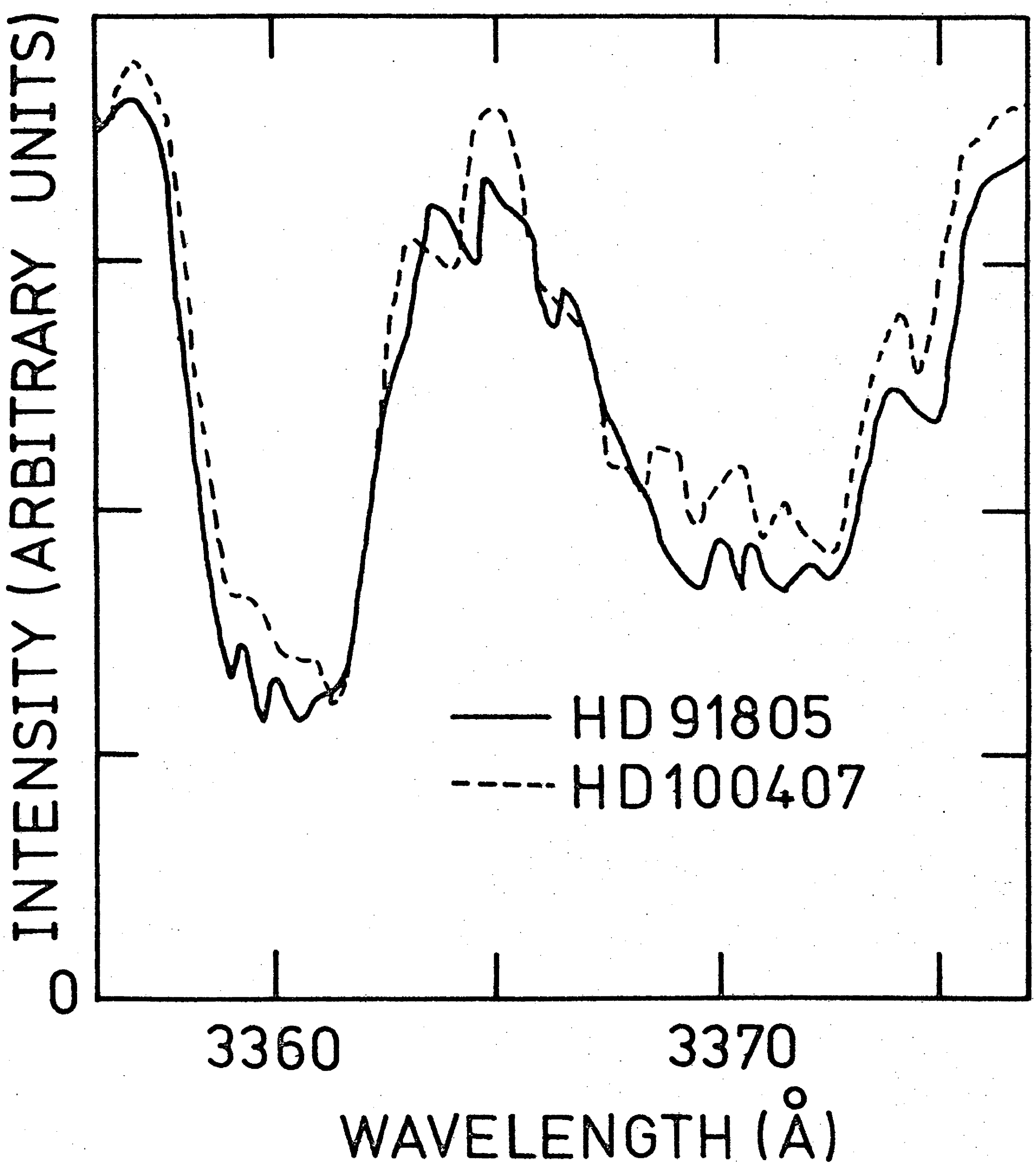
INTENSITY (ARBITRARY UNITS)
0
3360
3370
WAVELENGTH (Å)
HD 91805
HD100407

FIG. 8. - NH feature showing observed and synthetic spectra, (a) HD 91805, and (b) HD 100407. Convolving profile had FWHM = 1.5Å.

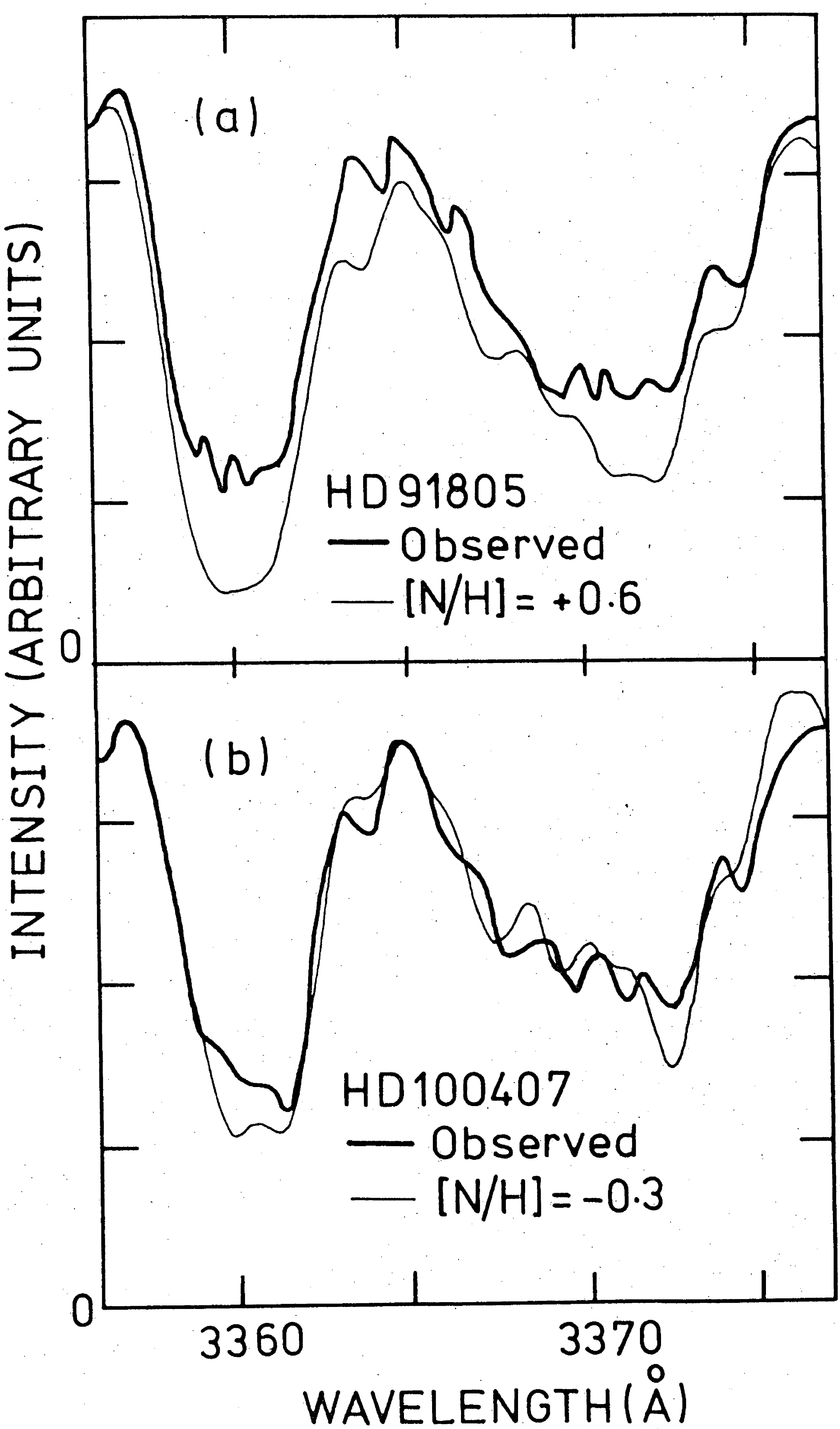
(a)
HD 91805
Observed
[N/H] = +0·6
(b)
HD 100407
Observed
[N/H] = −0·3
INTENSITY (ARBITRARY UNITS)
0
0
3360
3370
WAVELENGTH (Å)

parameters, i.e. P_e,P_g, etc. We found only a slight difference in the NH feature, ~1 percent. In view of the ad hoc nature of our method, however, it would be premature to place emphasis on this result. More work on the atmospheric structure of stars with peculiar CNO abundances is necessary before this problem can be clarified.

The CNO abundances for HD 91805 in Table 4 are most readily explained in terms of the mixing to the surface of material processed in the CN cycle. The normal oxygen abundance implies that the NO cycle has not operated. In view of the fact that a similar result has been obtained for HR 6766 by Sneden and Peterson (1977), it seems reasonable to assume that this is a general property of the Bidelman-MacConnell weak-G-band stars. We shall now consider the possible evolutionary phases at which this peculiarity might be produced.

IV. THE EVOLUTIONARY STATUS OF THE BIDELMAN-MACCONNELL WEAK-G-BAND STARS

Figure 9 shows the DDO observations from Table 1 in the [C(45-48), C(42-45)] - plane, where only stars with multiple observations have been plotted, together with the Population I sequences of Osborn (1971). The most striking feature is the concentration of points at [C(45-48), C(42-45)] ~ (1.18, 0.72).[1] We have also plotted in the figure the Hyades group members (Eggen 1972) for which Boyle and McClure (1975) find Hyades like CN band strengths (δCN $\gtrsim$ 0.05). These are stars which one may consider

---

[1] Two stars in Table 1 deserve further investigation. BD + 5°593 could be metal weak, according to its position in both Figure 9 and in the [C(45-48), C(38-42)] - plane. If true, it would be the brightest Population II weak-G-band star. BD-19°967 appears to be a dwarf in all DDO planes, and has the colors of a G4V star (*cf.* Osborn 1971). It is difficult to understand G-band weakness in such an object.

FIG. 9. - The weak-G-band stars and the Hyades group members in the [C(45-48), C(42-45)] - plane. The Population I sequences of Osborn (1971) are also shown.

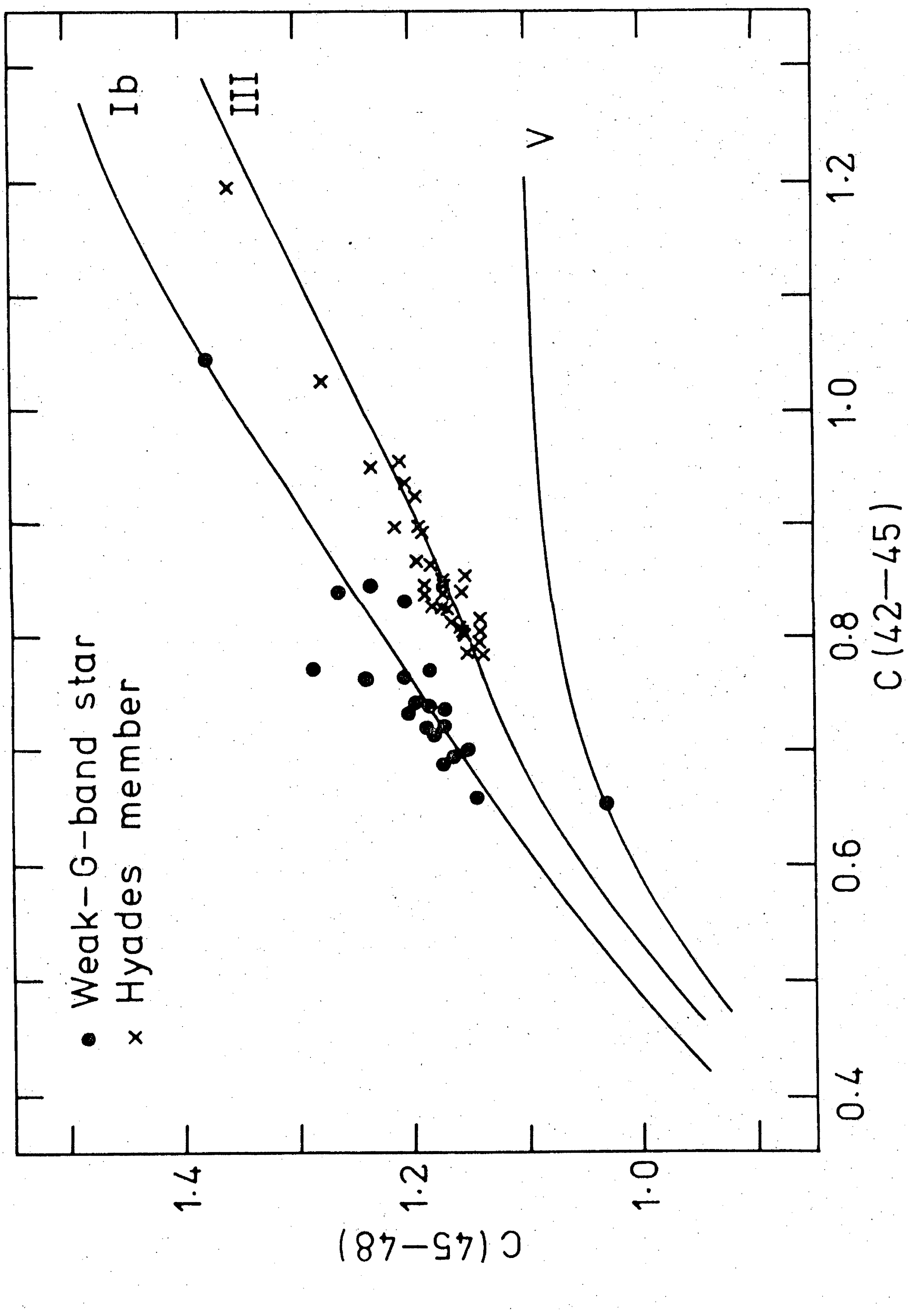
Weak-G-band star
Hyades member
Ib
III
V
C (42—45)
C (45—48)
0.4
0.6
0.8
1.0
1.2
1.4
1.2
1.0

to be Hyades group members on both kinematic and abundance grounds. Here too we see a strong grouping (the well known clump), at [C(45-48), C(42-45)] ~ (1.17, 0.82). We suggest that the two groups seen in Figure 9 represent the same evolutionary phase, with the difference in position being caused by differences in CH blocking. We reason as follows: There are many CH lines in the 42 bandpass, but virtually none in either the 45 or 48 bandpasses. The color C(45-48) will thus be unaffected by CH-blocking differences, while in the weak-G-band stars (which have less blocking in the 42 bandpass) C(42-45) will be somewhat bluer. We may estimate the size of the effect by comparing our spectra of the weak-G-band star HD 91805 and the Hyades cluster member HD 28307, each of which is typical of the two groupings seen in Figure 9. In particular we have blue spectra of the two stars (*cf.* §IIa) taken consecutively with the same equipment. We have used tracings of these spectra, together with the response functions of our 42 and 45 filters, to estimate the change induced in C(42-45) by the CH blocking around λ4250Å. We find that HD 91805 is 0.18 and 0.04 mag bluer in the 42 and 45 bands respectively, leading to a C(42-45) color bluer by 0.14 mag. The observed difference between the two stars is 0.12 mag (Table 1; Boyle and McClure 1975).

The most likely evolutionary phase of the stars in the two clumps in Figure 9 is the core helium burning phase which follows the helium flash[2] (*cf.* Cannon 1970; Faulkner and Cannon 1973). We are unable to say whether the cooler and more luminous weak-G-band stars in Figure 9 are the progenitors or progeny of the clump, and will not discuss these stars further.

---

[2] It should be noted that we have applied no reddening corrections to our observations. If the majority of our stars are clump objects having M_V ~ 0.7 (*cf.* Eggen 1972), it obtains that they have reddenings E(B-V) ≲ 0.1 (*cf.* FitzGerald 1968, esp. Figure 1) which will have little effect on our conclusions.

Given, however, that most of the weak-G-band stars are burning helium in their core, it goes without saying that helium shell flashes can have little to do with G-band weakness. The same conclusion has previously been reached for Population II stars by Norris and Zinn (1977). We may also place important constraints on the masses and structure of the weak-G-band stars. To have experienced a core helium flash their total mass must have been less than $2.2M_\odot$ (Iben 1967), while their helium core mass must be ~0.4 to $0.5M_\odot$ (*cf.* Sweigart and Gross 1977). A lower limit to the total mass may be inferred from the horizontal branch models of Gross (1973). For a metal abundance $Z \sim 0.02$ his results suggest that in order for such stars to fall in a clump near the giant branch, rather than at higher temperatures on a horizontal branch, the ratio of core mass to total mass must be smaller than ~0.85. Adopting the above core mass limits, this leads to a lower limit to total mass of ~0.5 to $0.6M_\odot$. We thus have an allowed mass range $0.5 \lesssim M/M_\odot \lesssim 2.2$. The most important point that may be culled from this discussion, however, is that the weak-G-band stars have considerable envelope masses, lying in the range 0.1 to $1.8M_\odot$. Assuming that the weak-G-band phenomenon is not confined to the atmosphere, but extends throughout the envelope, any production mechanism must have been able to process virtually all of the envelope carbon into nitrogen. This result must be achieved without processing oxygen, which - according to both Sneden and Peterson (1977) and the present work - is normal in these stars. That is, only the CN cycle may be invoked.

There seems little reason to suspect that G-band weakness is induced during the clump phase. In the next section we confine our attention to three other possible sites - the helium core flash, the red giant branch, and the main sequence.

V. THE ORIGIN OF THE WEAK-G-BAND PHENOMENON

(a) The helium core flash

It seems difficult to reconcile the observed CNO abundances and the inferred lower limit to the envelope masses with any once-only, short-duration, phenomenon such as the helium core flash. Unless the envelope is largely processed through the CN cycle at the time of the flash, which seems to us unlikely, the original carbon will still be seen in the outer layers. If the envelopes contain at least 15 percent of the total mass, and if before mixing the carbon abundance was normal (i.e. ~ solar), then the final carbon abundance cannot be less than ~ 15 percent solar. This is considerably larger than the observed carbon abundance.

It is perhaps important to note that this result somewhat contrasts the opinion expressed by Norris and Zinn (1977) in their discussion of the weak-G-band effect in Population II stars. Since, however, we have no estimates of abundances in the Population II objects, we cannot yet rule out the helium core flash as the relevant phase in globular cluster evolution.

(b) The giant branch

There is a growing opinion that existing stellar evolution computations underestimate the amount of nuclearly-processed material which is convectively mixed to the surface during the red giant phase. Observed $^{12}C/^{13}C$ ratios are consistently lower than predicted (Dearborn, Eggleton, and Schramm 1976, and references therein). The observed range in G-band strength on the lower giant branch of several globular clusters (Norris and Zinn 1977) is also suggestive of such a shortcoming. According to Dearborn, Eggleton, and Schramm (1976), and Norris and Zinn (1977) the most likely explanation of these phenomena lies in some combination of mass loss and possible hydrogen shell instability. We consider each in turn.

(i) Mass loss

Dearborn, Kozlowski, and Schramm (1976) have made the case that extensive mass loss is required in the immediate post main sequence phase to explain a range of astronomical observations. According to Iben (1967) a $2.25M_{\odot}$ star possesses a large nitrogen-rich, carbon-depleted region exterior to the hydrogen burning regions as it leaves the main sequence. Since at this mass most energy generation on the main sequence occurs in the CN cycle, the oxygen abundance in this region is normal. *Extensive* mass loss at this stage could thus lead to the abundances seen in the weak-G-band stars. The Bidelman-MacConnell sample would be the stars in which the mass loss is most extreme. To explain the observations, mass must be lost right down to the enriched regions. The mass fraction involved is ~0.5, and although such a possibility is not dismissed by Dearborn, Kozlowski, and Schramm (1976) in the context of the $^{12}C/^{13}C$ problem, it seems to us a rather radical solution.

(ii) Instability of the hydrogen burning shell

Repeated thermal instability in the hydrogen burning shell, and subsequent convective mixing of CN processed material to the surface could also enhance the N/C ratio above that found in the standard computations (*cf.* Bolton and Eggleton 1973; Dearborn, Bolton, and Eggleton 1975). If, however, thermal instability exists as a universal phenomenon in all stars, one would not expect to find a large range in G-band strengths. A coupling of variable mass loss and thermal instability, on the other hand, might overcome this problem.

The present observations place important constraints on this mechanism. At the center of the hydrogen burning shell conditions are favourable for the ON cycle to be in equilibrium; only in the outer layers of the shell could one expect a normal oxygen abundance (Sweigart and

Gross 1977). If we insist on maintaining a normal surface oxygen abundance, any mixing must therefore occur only from the outer layers of the shell. Let us suppose that the upper one fifth of the shell is mixed to the surface during each instability, and that the envelope mass that must be processed by repeating the instability is $0.1M_{\odot}$ - the lower limit inferred in §IV. From Iben (1967) we estimate that a typical red giant of intermediate luminosity would have a shell of mass $\sim 0.003M_{\odot}$. Then assuming that all carbon has been transformed to nitrogen in the material to be mixed up, we estimate that some 500 instabilities are required to reduce the surface abundance to one twentieth its original value.

Dearborn, Bolton, and Eggleton (1975), on the other hand, expect ~100 shell instabilities during the giant branch evolution of a $0.75M_{\odot}$ Population II star. They note further that fewer instabilities are expected in more massive stars because of their more rapid evolution on the giant branch. We conclude that the present estimates, while rough, offer little support for thermal instability as the cause of G-band weakness.

(c) The main sequence and meridional mixing

Paczyński (1973) has predicted that meridional circulation in rapidly rotating $3\text{-}10M_{\odot}$ stars can bring CN processed material from just outside the convective core to the surface layers. In his $3M_{\odot}$ model, in particular, the N/C ratio increases to 200 during the main sequence lifetime. For masses less than or equal to $1.5M_{\odot}$ the mechanism fails to work because of molecular weight gradients set up by the p-p cycle. No models were computed in the intermediate mass range, $1.5 \lesssim M/M_{\odot} \lesssim 3.0$.

The weak-G-band stars, on the other hand, have N/C ~ 25, masses less than $\sim 2.25M_{\odot}$, and the low rotational velocities generally associated with late type giants (for HD 91805 our spectra show no line broadening relative to the Hyades giants HD 28307 and HD 100407). Little imagination is required to see how such stars could be produced by the Paczyński mechanism. First, the abundance anomaly is produced during the main sequence phase of rapidly rotating stars having masses greater than some critical value, lying in the range 1.5 to $3M_{\odot}$. The Bidelman-MacConnell weak-G-band stars probably represent the extreme N/C enhancement and most likely correspond to the most rapidly-rotating main sequence stars. The oxygen abundance, of course, would be normal. Second, the red giant phase is accompanied by considerable loss of mass and angular momentum, reducing the mass (if necessary) below that necessary for the helium core flash, and the angular momentum to the low value presently observed. The association of rotation and loss of mass and angular momentum in the red giant phase is not new, and has been previously invoked to explain the low rotational velocities universally observed in late type giants, some of which must have been rapidly rotating while on the main sequence (Kraft 1970; Strittmatter and Norris 1971).

Of the several mechanisms we have considered, meridional mixing alone invokes no radical postulates and violates none of the observational constraints. It should be noted, however, that such a process cannot be invoked to explain the G-band weakness observed in globular cluster giants, which have masses considerably smaller than those considered here.

Acknowledgements

P. L. Cottrell wishes to acknowledge the support of an Australian National University Postgraduate Award, which enabled access to the UNIVAC 1100/42 Computer, operated by the Australian National University Computer Center.

REFERENCES

Bell, R. A., Ericksson, K., Gustafsson, B., and Nördlund, Å. 1976, *Astr. Ap. Suppl.*, 23, 37.

Bidelman, W. P. 1951, *Ap. J.*, 113, 304.

Bidelman, W. P., and MacConnell, D. J. 1973, *A. J.*, 78, 687.

Blackwell, D. E., Ibbertson, P. A., and Petford, A. D. 1975, *M.N.R.A.S.*, 171, 195.

Bolton, A. J. C., and Eggleton, P. P. 1973, *Astr. Ap.*, 24, 429.

Boyle, R. J., and McClure, R. D. 1975, *Pub.A.S.P.*, 87, 17.

Bridges, J. M., and Kornblith, R. L. 1974, *Ap. J.*, 192, 793.

Butler, D., Carbon, D., and Kraft, R. P. 1975, *Bull. AAS*, 7, 239.

Cannon, A. J. 1912, *Harvard Ann.*, 56, 104.

Cannon, R. D. 1970, *M.N.R.A.S.*, 144, 449.

Carbon, D., Butler, D., Kraft, R. P., and Nocar, J. L. 1977, in *CNO Isotopes in Astrophysics*, ed. J. Audouze, vol. 67 of Astrophysics and Sp. Sc. Library (Dordrecht: Reidel), p. 33.

Childs, D. R. 1974, *J. Quant. Spectrosc. and Rad. Transf.*, 4, 283.

Dean, C. A., Lee, P., and O'Brien, A. 1977, *Pub.A.S.P.*, 89, 222.

Dearborn, D. S., Bolton, A. J. C., and Eggleton, P. P. 1975, *M.N.R.A.S.*, 170, 7P.

Dearborn, D. S., Eggleton, P. P., and Schramm, D. N. 1976, *Ap. J.*, 203, 455.

Dearborn, D. S., Kozlowski, M., and Schramm, D. 1976, *Nature*, 261, 210.

Eggen, O. J. 1971, *Pub.A.S.P.*, 83, 271.

———. 1972, *Pub.A.S.P.*, 84, 406.

———. 1977, *Ap. J.*, 215, 812.

Faulkner, D. J., and Cannon, R. D. 1973, *Ap. J.*, 180, 435.

FitzGerald, M. P. 1968, *A. J.*, 73, 983.

Greenstein, J. L., and Keenan, P. C. 1958, *Ap. J.*, 127, 172.

Griffin, R. F. 1968, *Photometric atlas of the spectrum of Arcturus:* $\lambda\lambda$*3600-8825Å* (Cambridge: Cambridge Phil. Soc.).

———. 1969, *M.N.R.A.S.*, 143, 381.

Gross, P. G. 1973, *M.N.R.A.S.*, 164, 65.

Gustafsson, B., Bell, R. A., Eriksson, K., and Nördlund, Å. 1975, *Astr. Ap.*, 42, 407.

Herzberg, G. 1959, *Molecular Spectra and Molecular Structure I. Spectra of Diatomic Molecules* (New York: Van Nostrand).

Iben, I. Jr. 1967, *Ap. J.*, 147, 650.

Johnson, H. L. 1966, *Ann. Rev. Astr. Ap.*, 4, 193.

Kraft, R. P. 1970, in *Spectroscopic Astrophysics: An Assessment of the Contributions of Otto Struve*, ed. G. H. Herbig (Berkeley: Univ. of Calif. Press), p. 385.

Krupp, B. M. 1974, *Ap. J.*, 189, 389.

Kurucz, R. L. 1970, *SAO Spec. Rept.*, No. 309.

Kurucz, R. L. and Peytremann, E. 1975, *SAO Spec. Rept.*, No. 362.

Lambert, D. L. 1968, *M.N.R.A.S.*, 138, 143.

Liszt, H. S., and Hesser, J. E. 1970, *Ap. J.*, 159, 1101.

Mallia, E. A. 1975, *M.N.R.A.S.*, 170, 57P.

May, M., Ritcher, J., and Wichelmann, J. 1974, *Astr. Ap. Suppl.*, 18, 405.

McClure, R. D. 1976, A. J., 81, 182.

Minnaert, M., Mulders, G. F. W., Houtgast, J. 1940, *Photometric Atlas of the Solar Spectrum* (Amsterdam: Schnabel).

Moore, C. E., Minnaert, M. G. J., and Houtgast, J. 1966, *NBS Monog.*, No. 61.

Norris, J. and Bessell, M. S. 1977, *Ap.J. (Letters)*, 211, L91.

Norris, J., and Zinn, R. 1977, *Ap. J.*, 215, 74.

Osborn, W. 1971, Ph.D Thesis, Yale Univ.

Paczyński, B. 1973, *Acta Astr.*, 23, 191.

Pagel, B. E. J. 1964, *Roy. Obs. Bull.*, No. 87.

Schadee, A. 1964, *Bull. Astr. Neth.*, 17, 311.

————. 1968, *Ap. J.*, 151, 239.

Sneden, C. 1974, Ph.D Thesis, University of Texas at Austin.

Sneden, C., and Peterson, R. 1977, *Bull. AAS*, 9, 365.

Spindler, J. R. 1965, *J. Quant. Spectrosc. and Rad. Transf.*, 5, 165.

Strittmatter, P. A., and Norris, J. 1971, *Astr. Ap.*, 11, 477.

Sweigart, A. V., and Gross, P. G. 1978, *Ap. J. Suppl.*, 36, 405.

Tatum, J. B. 1966, *Pub.D.A.O.*, 13, No. 1.

Weast, R. C. 1965, in *Handbook of Chemistry and Physics* (Cleveland: Chemical Rubber Co.), p. E-143.

Zinn, R. 1973, *Ap. J.*, 182, 183.

————. 1977, *Ap. J.*, 218, 96.

APPENDIX

	λ	Mult	$-\log {}^{W}/_{\lambda}$ HD 28307	$-\log {}^{W}/_{\lambda}$ HD 91805	$-\log {}^{W}/_{\lambda}$ HD 100407
FeI	5213.35	1165		5.19	5.01
	5213.81	962		5.39	5.16
	5217.40	553		4.49	4.51
	5217.92	880		4.75	4.66
	5223.18	880		4.90	4.87
	5225.54	1		4.55	4.53
	5226.04	716		5.01	4.94
	5232.95	383		4.26	4.15
	5242.50	843		4.58	4.58
	5243.78	1089		4.65	4.68
	5247.06	1		4.46	4.52
	5250.22	1			4.48
	5285.13	1166		4.84	4.93
	5288.53	929		4.70	4.65
	5293.97	1031		4.85	4.92
	5294.55	875		5.11	5.04
	5298.79	875		4.87	4.74
	5315.08	1147	4.84	4.83	4.71
	5315.77	877	5.49	5.45	5.51
	5317.55	1032	5.16	5.31	5.31
	5321.12	1165	4.90	4.87	4.85
	5322.05	112	4.70	4.61	4.55
	5324.19	553	4.21	4.29	4.25
	5326.82	1147	5.10	5.25	5.27
	5339.94	553		4.50	4.41
	5358.12	628		5.16	5.15
	5364.88	1146		4.54	4.52
	5365.41	786		4.62	4.65
	5367.48	1146		4.50	4.48
	5369.97	1146		4.48	4.46
	5460.88	464		5.28	
	5461.56	1145		5.03	
	5464.28	1030		4.80	
	5466.41	1144		4.64	
	5467.76	741		5.28	
	5470.09	1144		5.00	5.01
	5473.17	1064		5.07	5.03
	5478.46	1062		4.77	4.74
	5487.16	1143		4.80	4.78
	5491.84	1031		5.19	5.07
	5494.48	1024		4.95	5.13
	5496.53	1281		5.22	5.25
	5497.53	15		4.39	4.43
	5501.49	15		4.40	
FeI (cont.)	6003.02	959	4.72		
	6007.97	1178	4.77		
	6012.76	1198	5.61		
	6015.25	63	5.17		
	6019.37	780	5.39		
	6024.07	1178	4.66		
	6027.06	1018	4.73		
FeII	5234.62	49		4.86	4.90
	5325.56	49	4.90	4.82	4.90
CrI	5214.13	193		5.20	4.97
	5214.61	189		4.95	4.78
	5238.96	59		5.10	5.01
	5241.46	59		5.45	5.42
	5243.35	201		4.84	4.81
	5247.57	18		4.57	4.54
	5287.17	225		5.20	5.14
	5296.70	18		4.52	4.54
	5300.75	18		4.63	4.68
	5312.86	225	4.93	5.11	5.13
	5318.77	225	5.14	5.15	5.07
	5329.15	94	4.67	4.67	4.66
	5340.45	225		5.09	4.93
	5344.76	225			5.19
	5345.81	18		4.39	4.41
	5348.33	18		4.47	4.48
	5480.52	204		5.37	5.13
CrII	5305.86	24		4.93	5.00
	5308.43	43		4.90	4.93
	5313.57	43	5.01	4.85	4.89
	5502.09	50		5.01	5.10
TiII	5211.53	103		4.81	4.85
	5336.80	69		4.57	4.62
	5492.89	68		4.97	5.10
[OI]	6300.30	1F		4.99	5.29

C H A P T E R 3

CARBON AND NITROGEN ABUNDANCES IN THE CARBON-RICH CEPHEID V553 CENTAURI

P. L. Cottrell

SUMMARY

A spectroscopic and photometric analysis of the carbon-rich Cepheid V553 Centauri has been undertaken, and the following results were obtained: using spectrum synthesis techniques, [C/Fe] = +0.8 and [N/Fe] = +0.5, while from a differential curve-of-growth analysis [Fe/H] = -0.1; all values relative to the Sun. Finally, this research considers the nuclear processes and evolutionary status of a variable star having the above abundances. The near-solar composition means that V553 Cen must have an extremely small envelope to be evolving in the instability strip with its derived luminosity, log $L/L_\odot$ of ~2. The most plausible interpretation of V553 Cen is as the progeny of the strong-lined RR Lyrae stars. This object has evolved to a position above the horizontal branch and is currently either a suprahorizontal branch star or a loop Cepheid. The latter explanation provides a more turbulent site for the carbon and nitrogen enhancements to be attained.

I. INTRODUCTION

Strong bands of C_2, CH, and CN were first noted in the spectra of V553 Centauri (HD 129981 ≡ CoD $-31^{\circ}11449$) by Herbig (1952). In recent work Lloyd-Evans, Wisse, and Wisse (1972) have shown low dispersion spectra which illustrated the strong carbon bands in V553 Cen relative to a Cepheid of similar temperature, V381 Cen. From V553 Cen's strong-lined spectrum and its low radial velocity, the latter authors suggested that this star appeared to belong to Population I. However, light curves by the above authors and Landolt (1975) indicated that V553 Cen more closely resembled Cepheids in the globular clusters. This similarity is twofold: (a) the presence of a shoulder on the fall from maximum light, and (b) the hump on the rise to maximum light.

In the present work both a photometric and a detailed spectroscopic analysis were undertaken on this peculiar Cepheid. The photometric results are discussed in §III*a*, where data are included on the light and (R-I) colour curves. A discussion and estimate of the reddening was also incorporated in this section. This enabled a temperature table to be derived, which was used in §III*b* to deduce the overall abundance and then in §III*c* to construct synthetic spectra of some of the carbon molecular bands, viz., CH and CN. Finally in §IV the implication of the abundances derived in §III was considered with respect to current evolutionary theories.

II. OBSERVATIONS

(a) Photometry

Broad-band VRI photometry was obtained in 1976 July and August and 1977 March using a GaAs photomultiplier tube attached to the single-channel photon counting system on the 76cm telescope at Mount Stromlo. The filter set used was the same as that described by Bessell (1976) and has been specifically designed for use with a GaAs tube. In addition to V553 Cen, a number of late-type B stars within a few degrees of this star were also observed in order to derive the amount of reddening. In columns (1) to (4) of Table 1 the identification, right ascension, declination and spectral type of all these stars are given. To transform these photometric observations on to a standard system, the E-region standards of Cousins (1973, 1974) were included in the observing program. An estimate of the reddening was extracted from intermediate band uvbyβ photometry of the B stars in Table 1, acquired by Dr. M. S. Bessell using the 40cm telescope at Siding Spring in 1978 February.

(b) Spectra

Extensive high dispersion observations were obtained for V553 Cen, as well as several spectra of a comparison star, the short period δ Scuti variable, ρ Puppis, which is a subgiant of similar temperature to V553 Cen (see Bessell 1969). All spectroscopic measurements were acquired at the coudé focus of the 1.9m telescope at Mount Stromlo.

For the differential curve-of-growth analysis between V553 Cen and ρ Puppis spectra were recorded using the échelle grating, the 40cm camera, and a Carnegie image tube. This gave good wavelength coverage between λλ~4750 and ~5100Å, with a reciprocal plate dispersion of ~3.6Åmm^{-1}. Within each spectral order the total wavelength coverage was approximately 80Å. However, only about 50Å of this was of high enough quality for accurate equivalent width measurements to be made. The remainder was either under- or over-exposed because of the curved response function of the échelle grating system.

In addition to the above spectroscopic plates used in the curve-of-growth treatment, spectra were taken in blue spectral regions which covered the major molecular features of CH and CN, viz., the G-band for CH, and the

TABLE 1

BASIC DATA

Star Name (1)	Spectral Type (2)	V (3)	α (1950) (4)	δ (5)	b-y (6)	m_1 (7)	c_1 (8)	β (9)	distance (pc) (10)	U,V,W,[##] (11)
-31° 11449 (≡ V553 Centauri)	F5 - GO[†]	8.23-8.75	$14^h43^m32^s$	$-31^{\circ}58'$	-	-	-	-	800[**]	-8,-32,-65
-31° 11560	B9[‡]	8.61	$14^h33^m40^s$	$-30^{\circ}49'$	0.020	0.136	0.885	2.841	300[#]	-
-30° 11624	B9[‡]	6.37	$14^h38^m52^s$	$-30^{\circ}43'$	-0.017	0.125	0.608	2.738	200[#]	-
-32° 10301	B9[‡*]	8.23	$14^h38^m58^s$	$-32^{\circ}36'$	0.028	0.148	1.142	2.854	-	-

† From Lloyd-Evans *et al.* (1972).

‡ From SAO Star Catalog (Whipple 1966).

** Assuming $<M_V> \sim -1.0$.

* ~A2 from uvbyβ photometry.

\# Using $M_V - \beta$ relation (Crawford 1978).

\## Using proper motions from SAO Star Catalog (Whipple 1966).

TABLE 2

EQUIVALENT WIDTHS

			$-\log W/\lambda$					$-\log W/\lambda$	
λ	Mult	χ	ρ Puppis	V553 Cen	λ	Mult	χ	ρ Puppis	V553 Cen
4745.13	67	2.21	5.26		4982.51	1067	4.09	4.24	
71.70	67	2.19	5.02		83.26	1067	4.14	4.38	4.51
76.08	635	3.30	5.01		.86	1066	4.09	4.16	
79.44	720	3.40	5.16		85.26	984	3.91	4.56	4.77
85.96	1044	4.12	5.22		.55	318	2.85	4.31	4.48
86.81	467	3.00	4.21		86.24	1070	4.20	4.83	5.26
87.84	384	2.99	5.25		.90	1092	4.24	5.23	
89.65	753	3.53	4.44		88.96	1066	4.14	4.66	4.66
4848.90	114	2.27	4.45	4.59	91.85	1094	4.20	5.33	5.01
68.38	38	1.55	5.24		94.13	16	0.91	4.68	4.72
4871.32	318	2.85	4.30	4.32	5049.83	114	2.27	4.66	4.65
72.14	318	2.87	4.32	4.41	67.16	1092	4.20	4.82	4.91
75.89	687	3.32	4.87	5.01	68.77	383	2.93	4.40	4.47
85.44	966	3.86	4.74	4.76	74.76	1094	4.20	4.31	4.53
86.34	1066	4.14	5.02	4.83	76.29	1089	4.28	4.55	4.71
88.65	1066	4.09	4.77	4.76	83.34	16	0.95	4.64	4.54
90.76	318	2.86	4.38	4.52	90.79	1090	4.24	4.61	4.71
91.50	318	2.86	4.36	4.42	5109.66	1089	4.28	4.77	4.82
4946.39	687	3.35	4.71	4.62	10.41	1	0.00	4.49	4.68

$\Delta v = 0$ and -1 bands for CN. These spectra were acquired using the same combination as above. The reciprocal dispersion in this instance was ~3.3Åmm^{-1}.

For V553 Cen a large number of spectra were procured, covering all phases between maximum and minimum light. This enabled the largest temperature variation to be observed, and consequently the greatest changes in band strengths.

As well as the spectra using the échelle grating, several blue spectra were taken using the B grating, the 81cm camera, and the two-stage Carnegie image tube. This combination gave a reciprocal dispersion of ~10Åmm^{-1} on the plate.

Hydrogen sensitized IIaO emulsions were used to record all the spectroscopic data, and they were traced on the Göttingen microphotometer which was programmed with an intensity calibration. The latter was acquired using the same systems as have been described above. The line strengths measured from the tracings of the redder échelle plates are shown in Table 2, and will be used in the construction of the curves of growth.

III. RESULTS

(a) Photometry

Light and colour curves were constructed from the VRI photometry of V553 Cen. The uvbyβ photometry of the B stars has been used in obtaining an estimate of the reddening, E(B-V). This latter parameter will be discussed later in this section. The infrared (R-I) colours of V553 Cen have been dereddened, which gave intrinsic colours and thus a temperature scale for this star. Let us now consider the photometry in more detail.

(i) Light and colour curves

The V magnitudes and observed (R-I) colours are tabulated in columns (3) and (4) of Table 3 and are also shown in Figures 1a and 1b, respectively. The Julian Day and phase are respectively shown in columns (1) and (2) of this Table. The phase was determined using the ephemeris adopted by Lloyd-Evans *et al.* (1972), viz.,

$$\text{Max} = 2441124\overset{d}{.}28 + 2\overset{d}{.}06051 \times E,$$

where $2\overset{d}{.}06051$ is the period of V553 Cen, and E is an integer. The above relation then gives the J.D. of maximum light. In Figure 1a the data of Dean *et al.* (1977) were also included, and the good agreement attests to the reliability of the present observations.

(ii) Reddening

In the present work two reddening estimates were made: one was dependent on observational data, while the other was determined using a relation derived by Kron (1978). We shall consider each estimate in the following paragraphs.

FIG. 1. - (a) Light curve for V553 Centauri, with observations from Dean *et al.* (1977) (▲), and the author (●).

(b) The variation in the observed R-I colour with phase.

(c) Effective temperature T_e against phase. This temperature is determined from the dereddened R-I observations.

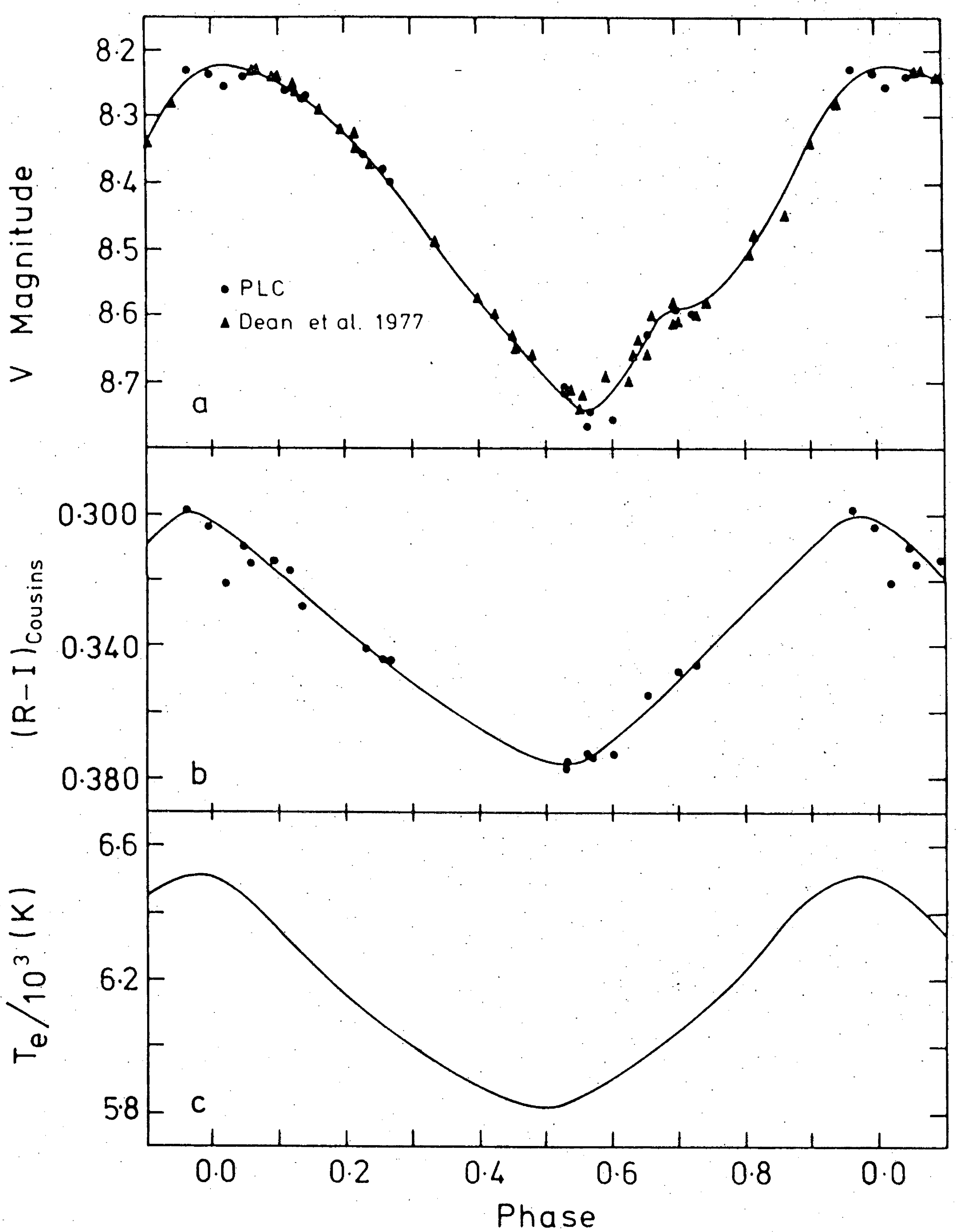

V Magnitude
8·2
8·3
8·4
8·5
8·6
8·7
● PLC
▲ Dean et al. 1977
a
(R−I)Cousins
0·300
0·340
0·380
b
Te/10³ (K)
6·6
6·2
5·8
c
0·0
0·2
0·4
0·6
0·8
0·0
Phase

TABLE 3

VRI OBSERVATIONS FOR V553 CENTAURI

Julian Date 2440000 + (1)	Phase (2)	V (3)	(R-I) (4)
2980.918	0.0569	8.234	0.315
2986.905	0.9630	8.230	0.299
2986.971	0.9950	8.237	0.304
3001.955	0.2670	8.397	0.344
3003.937	0.2293	8.356	0.341
3003.967	0.2556	8.378	0.344
3004.899	0.6957	8.590	0.348
3004.954	0.7227	8.597	0.346
3008.928	0.6511	8.627	0.355
3009.883	0.1145	8.260	0.317
3009.924	0.1344	8.271	0.328
3258.000	0.5300	8.708	0.375
3258.077	0.5674	8.744	0.374
3258.145	0.6004	8.755	0.373
3259.002	0.0164	8.254	0.321
3259.069	0.0488	8.240	0.310
3259.161	0.0936	8.271	0.314
3260.059	0.5290	8.718	0.377
3260.125	0.5610	8.767	0.373

First, Kron concluded that reddening material is present in two forms: (1) concentrated in clouds and (2) a relatively uniform layer about 500pc thick, with the Sun approximately at the centre. However, the Sun is south of the centre with respect to the clouds. The uniform layer reddens material according to

$$E(B-V) = 0\overset{m}{.}082\ D\ ,$$

where D is the distance (in kpc) which the starlight travels within this layer. For V553 Cen, assuming $\langle M_V \rangle \sim -1.0$, the above formula gives $E(B-V) = 0\overset{m}{.}05$, shown in column (1) of Table 4.

Second, in column (2) of Table 4, $E(B-V) = 0\overset{m}{.}06$ was determined using the uvbyβ filter system of Strömgren (1966). The individual colours for the B stars are shown in columns (6) to (9) of Table 1. Although the distances

TABLE 4

E(B-V) ESTIMATES

Uniform Layer* (1)	Intermediate Band Photometry (2)	Cosec Formula† (3)	Intrinsic Colours‡ (4)
$0^{m}.05$	$0^{m}.06$	$0^{m}.08$	$0^{m}.14$

* From Kron (1978).
† From Arp (1962).
‡ From Johnson (1966).

to these stars, column (10) of this table, are smaller than that derived for V553 Cen, this method for determining the reddening gave a reliable lower limit, similar to the value obtained using the formula of Kron (1978). In their discussion Lloyd-Evans *et al.* (1972) adopted a value of E(B-V) = $0^{m}.10$. This was based on two estimates, (1) the cosec formula of Arp (1962) and (2) the intrinsic colours of Johnson (1966). Both of these are shown respectively in columns (3) and (4) of Table 4. However, the relationship of Kron (1978) appears superior to (1) above, while the intermediate band photometry provides a better estimate of the reddening than trying to match an intrinsic colour to V553 Cen.

Thus, for the reddening in the direction of V553 Cen, E(B-V) = $0^{m}.06$ was adopted, which is a weighted mean of the Strömgren photometry and Kron's formula, a larger weight being assigned to the observational data.

Before we consider the abundances in the atmospheres of both V553 Cen and ρ Puppis, effective temperatures and gravities are required to be used in the model atmosphere calculations.

(b) Atmospheric parameters

(i) Effective temperature

An effective temperature, T_e = 6600 K, was derived for ρ Puppis from

TABLE 5

ATMOSPHERIC PARAMETERS

Star (1)		T_e (2)	T_{exc} (3)	log g (4)	[Fe/H] (5)	[C/Fe] (6)	[N/Fe] (7)
ρ Puppis		6600	6300	3.4†	+0.36†	-0.3 ± 0.2	- ‡
V553 Centauri							
Phase =							
(1)	0.00	6500	6200	2.0	-0.1 ± 0.3	+0.9 ± 0.3	+0.5 ± 0.4
(2)	0.61	5925		2.0	-0.1*	+1.0 ± 0.3	
(3)	0.45	5850		2.0	-0.1*	+0.6 ± 0.3	+0.5 ± 0.4

† From Bessell (1969).

‡ No value determined (see text).

* Value adopted from Phase = 0.00 observations.

the (I-K) measurement of Neugebauer and Leighton (1969), and the (R-I) colour of Iriarte *et al.* (1965).

For V553 Cen the effective temperature can be derived using Johnson's (1966) (R-I) $-T_e$ scales for supergiants. The observed (R-I)'s are in Cousins' (1974) system, but they can easily be transformed to Johnson colours using relationships given by Bessell (1977) and Eggen (1974). Consequently, if one adopts the reddening determined in §IIIa*(ii)*, namely E(B-V) ~ $0^m.06$, the variation in effective temperature with phase can be extracted from these observations. This is shown in Figure 1c.

(ii) Gravity

The values chosen for this parameter are shown in column (4) of Table 5. For ρ Puppis, a value of log g = 3.4 was adopted following Bessell's (1967) research, in which he used undisturbed atmospheric calculations.

The surface gravity for V553 Cen was determined using two basic relationships, namely that the luminosity, $L \propto R^2 T_e^{\,4}$ and the gravity,

$g \propto M/R^2$ where M, R, and T_e are respectively the mass, radius and effective temperature of the star. With respect to the Sun,

$$\log g = \log M/M_\odot + 4 \log T_e - \log L/L_\odot - 10.61,$$

where g is in cgs units. This required independent estimates of both the mass and luminosity.

Christy (1966) illustrated that the phase of the "hump" on the light curves of RR Lyrae stars was related to the mass, and was independent of helium abundance. For V553 Cen this "hump" occurs at a phase of 0.70 (see Figure 1a) corresponding to a mass of ~0.5 $M_\odot$. Assuming an absolute magnitude of -1, the low systemic radial velocity for V553 Cen gives a large velocity component in the direction perpendicular to the galactic plane, which in turn suggests that this object is a member of the old disk population. This conclusion is supported by V553 Cen's height of ~300pc above the galactic plane.

Although Lloyd-Evans *et al.* (1972) considered V553 Cen to be a member of the disk population, they also noted this star's similarity to Type II Cepheids, in particular BL Her, viz., minimum radial velocity occurring very close to maximum light, and the ultra-violet excess between phases 0.5 and 0.8. In addition they point out that only short period stars of this type have been discovered. This latter condition also prevails in the dwarf spheroidal galaxies (see Norris and Zinn 1975) and in NGC 121, a red globular cluster in the Small Magellanic Cloud. Thus in order to derive a luminosity for this object let us assume that it obeys the P-L law of the dwarf spheroidal galaxies. Thus from Figure 2 of Norris and Zinn (1975), a luminosity (log $L/L_\odot$) ~ 2.4 is assumed, from which using (1) above, a gravity (log g) of ~ 2 is derived.

The temperatures and gravities discussed above will be used in §III*c* to derive a metal abundance, and in §III*d* to match the observed spectra with synthetic spectra of regions sensitive to changes in the carbon and nitrogen abundances.

(c) Iron Abundance Determination

In this analysis a differential curve-of-growth treatment between ρ Puppis and V553 Cen was employed. This has been described previously by Cottrell and Norris (1978), and follows the method of Pagel (1964). In particular the assumption $\Delta\theta_e \equiv \Delta\theta_{exc}$ was made. In Table 5 the parameters for both stars are tabulated.

Since spectroscopic observations of ρ Puppis covered a large wavelength interval, it was possible to make a comparison between the equivalent width measurements of this work and those of Bessell (1969), who also carried out a curve-of-growth analysis on this star. This comparison is shown in Figure 2 for about 35 lines which we had in common, and illustrates that the present measurements are on the same system as those of Bessell. Thus his value of the iron abundance, namely [Fe/H] = +0.36 relative to the Sun, was adopted for this analysis. In addition, Bessell's (1969) value of the atmospheric microturbulence of ~6 km s^{-1} was adopted for ρ Puppis.

For V553 Cen there were several échelle plates whose mean phase of exposure was centred around maximum light. These were used in the differential analysis of this star relative to ρ Puppis. The FeI curves-of-growth for both stars are shown in Figures 3a and 3b. From the horizontal shift required to move the V553 Cen curve on to that of ρ Puppis, and the marginally different temperature structure of these two stars, an iron abundance, [Fe/H] $\{$V553 Cen − ρ Puppis$\}$ ~ −0.45 was determined. Thus V553 Cen has a [Fe/H] ~ −0.10 relative to the Sun. The error associated with this parameter is a factor of 2, principally due to the errors associated with fitting the curve-of-growth from Bessell (1969) to the data shown in Figures 3a and 3b. No vertical shift and consequently no microturbulent

FIG. 2. - Comparison of equivalent width measurements for ρ Puppis from Bessell (1969) and the author (PLC). The line has a slope of 1 and passes through the origin.

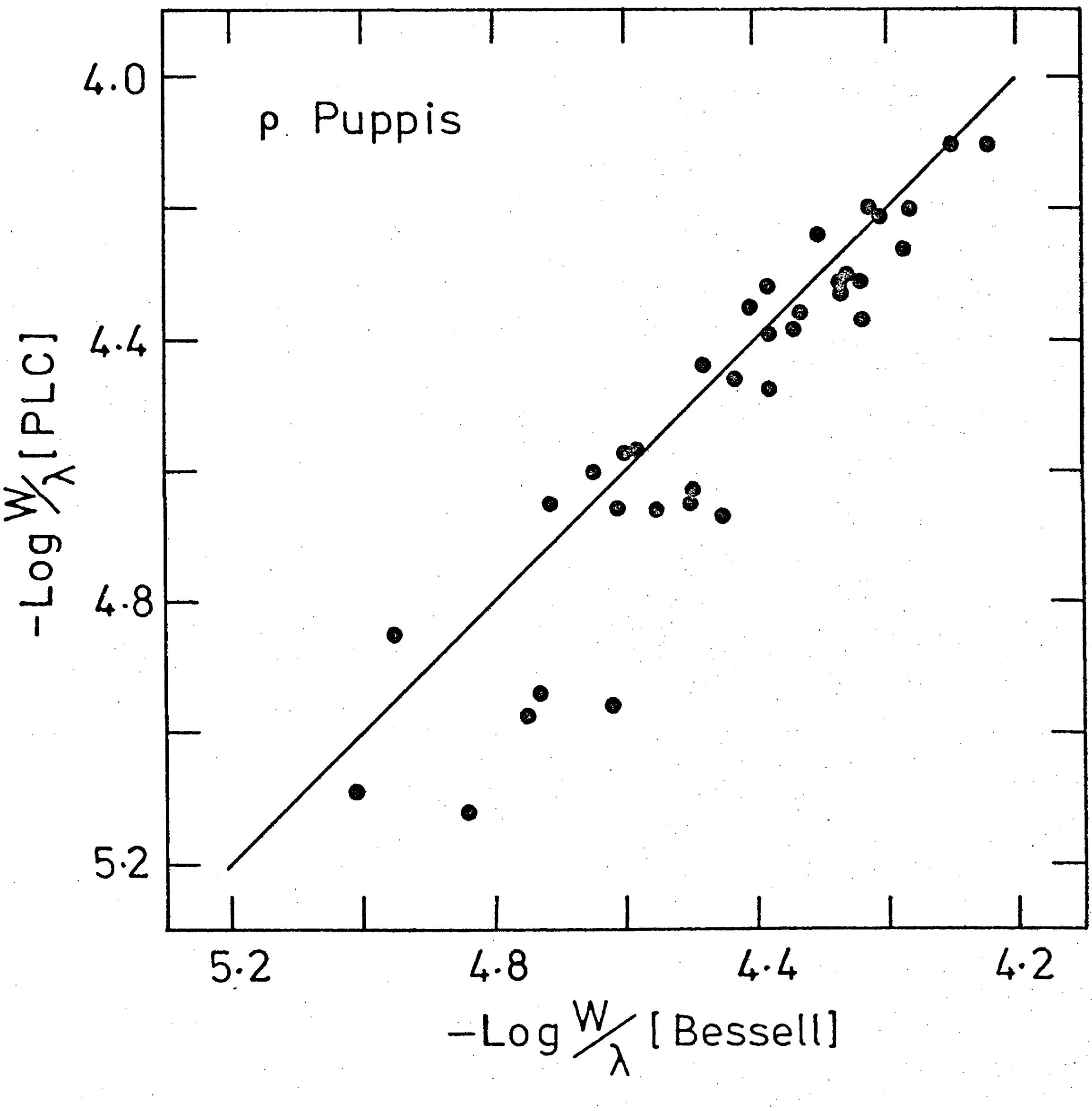

ρ Puppis
4.0
4.4
4.8
5.2
–Log W/λ [PLC]
5.2
4.8
4.4
4.2
–Log W/λ [Bessell]

FIG. 3. - FeI curves of growth for (a) V553 Centauri and (b) ρ Puppis.

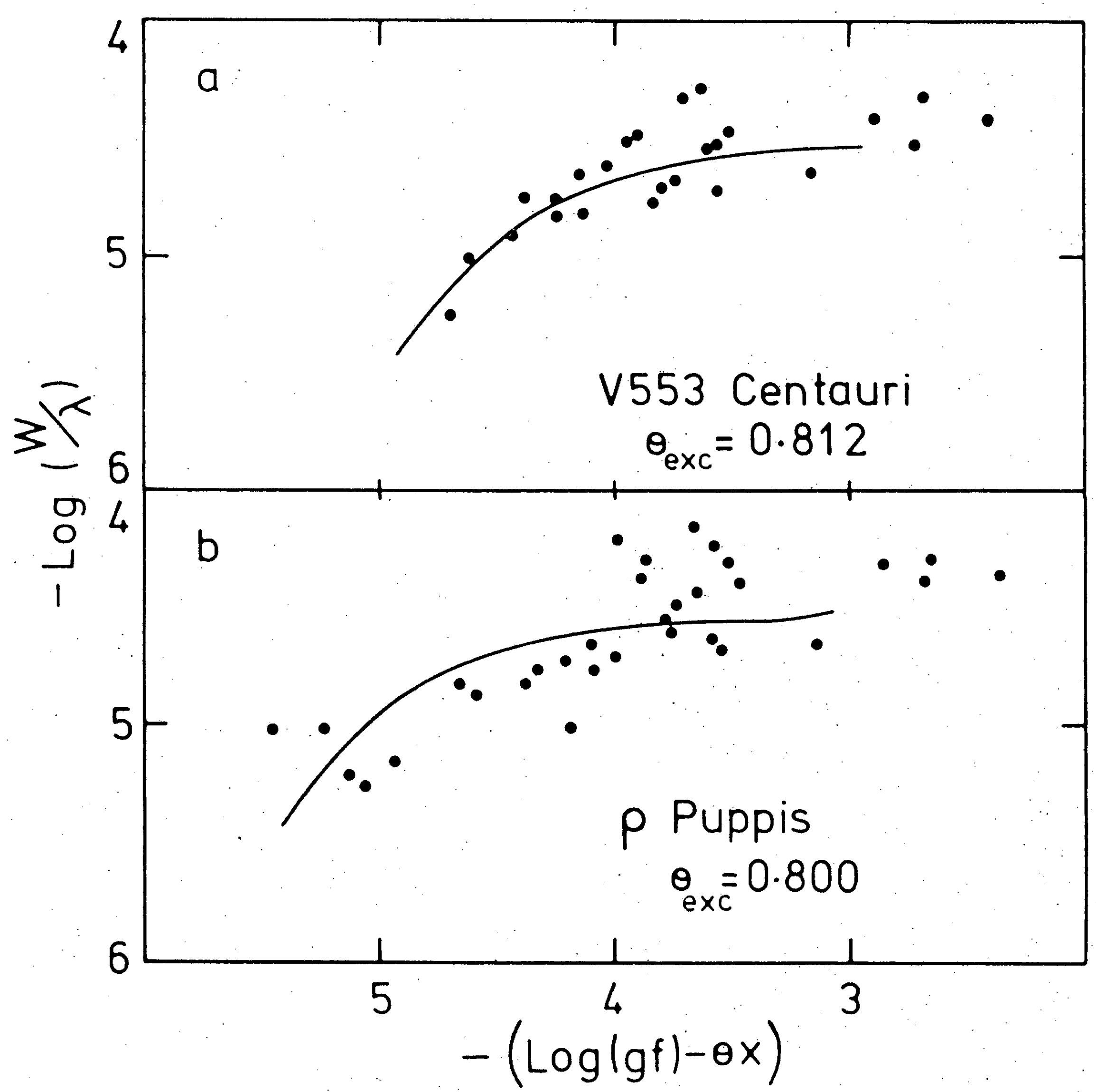
a
b
4
5
6
4
5
6
5
4
3
V553 Centauri
$\theta_{exc} = 0{\cdot}812$
ρ Puppis
$\theta_{exc} = 0{\cdot}800$
$-\mathrm{Log}\,(W/\lambda)$
$-(\mathrm{Log}(gf) - \theta x)$

velocity, v_t could be obtained from the V553 Cen and ρ Puppis curves-of-growth, because of the large scatter in Figures 3a and 3b. The value of v_t will be discussed in relation to the models used in the construction of the synthetic spectra.

(d) C and N abundances using spectrum synthesis

A number of assumptions had to be made before we could progress to the determination of the carbon and nitrogen abundances. These were: (1) that the iron abundance obtained in the last section could be applied to all elements except carbon and nitrogen, and (2) that the models of Bell, Eriksson, Gustafsson, Nördlund (1976) for which a microturbulent velocity, $v_t = 2$ km s^{-1} was generally adopted, could be used for stars in which the parameter had values up to 6 km s^{-1}. This is justified from Figure 10 of Gustafsson, Bell, Eriksson, and Nördlund (1975) where a change in v_t from 2 to 5 km s^{-1} resulted in ΔT's of less than 50 K. In addition, for V553 Cen it was assumed (1) that the atmospheric structure of the Bell *et al.* (1976) models was suitable for use in stars with peculiar C and N abundances and (2) that at any given phase the star could be represented by a static atmosphere.

An oxygen abundance could not be determined in either V553 Cen or ρ Puppis, because of the extreme weakness of the [OI] line at λ~6300.3 Å. For example in the Sun (T_e ~ 5780 K) the equivalent width of this line is only 5mA. Thus [O/Fe] = 0.0 was adopted. Next the carbon abundance for both the stars under investigation was derived using the G-band. The synthesis technique employed here has been developed by the author, and has been described by Cottrell and Norris (1978) and Cottrell (1978).

In Figure 4, the synthetic and observed G-band spectra for both ρ Puppis and V553 Cen are shown in the wavelength interval λλ4305 to 4325Å, in which the regions most sensitive to changes in the carbon abundance are

FIG. 4. - Synthetic and observed spectra of the G-band region between $\lambda\lambda$4305 and 4325Å. (a) ρ Puppis with v_t = 6 km s^{-1} (b) Synthetic spectra with same parameters except v_t. Two values of v_t, 2 and 4 km s^{-1}; the latter has the deeper lines. (c), (d), and (e) V553 Cen at phases of 0.0, 0.6, and 0.45 respectively. All three synthetic spectra have v_t = 4 km s^{-1}. Synthetic spectra in (a) to (d) have been convolved with a Gaussian whose FWHM = 0.5 Å. In (e) the FWHM = 0.9 Å. The curves in each Figure are indicated. The wavelength intervals most sensitive to carbon abundance changes are indicated by arrows.

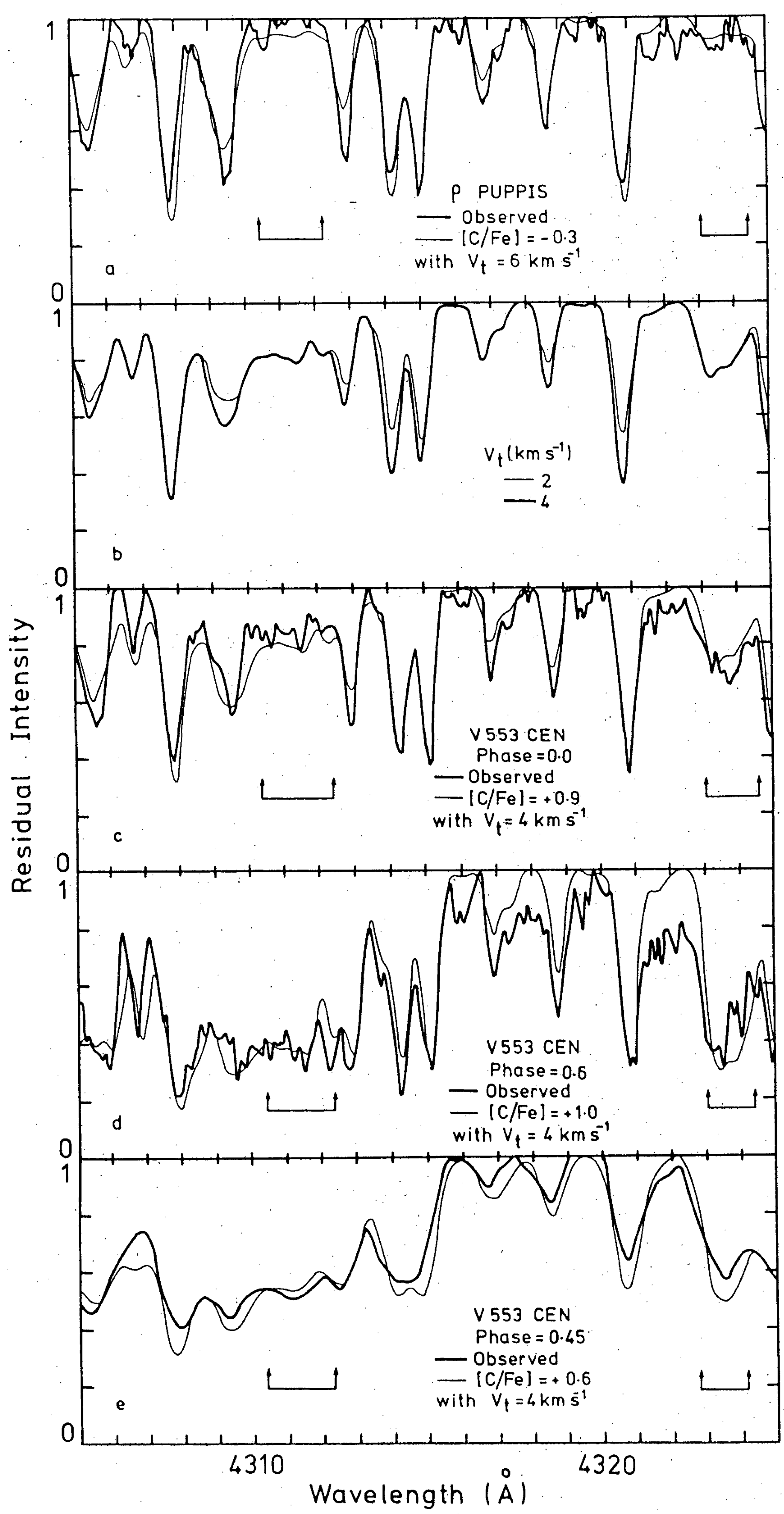
1
0
ρ PUPPIS
Observed
[C/Fe] = -0.3
with V_t = 6 km s^{-1}
a
V_t (km s^{-1})
2
4
b
V 553 CEN
Phase = 0.0
Observed
[C/Fe] = +0.9
with V_t = 4 km s^{-1}
c
V 553 CEN
Phase = 0.6
Observed
[C/Fe] = +1.0
with V_t = 4 km s^{-1}
d
V 553 CEN
Phase = 0.45
Observed
[C/Fe] = + 0.6
with V_t = 4 km s^{-1}
e
Residual Intensity
4310
4320
Wavelength (Å)

indicated. The C abundances derived from these figures are shown in column (6) of Table 5. From Figure 4a, ρ Puppis has a slight carbon deficiency relative to iron. The weakness of the CH features at this effective temperature made it difficult for a precise C abundance to be evaluated, but this value gives a good fit to the observational data. A microturbulent velocity of 6 km s^{-1} (Bessell 1969) was used to construct this synthetic spectrum.

Before continuing with the comparison of synthetic and observed G-bands of V553 Cen, we must determine a value of v_t to be used for *this* object. Figure 4b shows synthetic spectra with v_t's of 2 and 4 km s^{-1}. The latter gives a better fit to the observations as shown in Figure 4c and 4d. These figures illustrate V553 Cen at phases of ~0.0 and ~0.6 respectively, which approximately correspond to the maximum and minimum atmospheric temperatures. Osmer (1970) in his study of F supergiants of luminosity classes Ia and Ib, derived microturbulent velocities of ~5 km s^{-1}. Thus the adoption of 4 km s^{-1} for V553 Cen, classified as belonging to class II, appears justified.

Figures 4c, 4d and 4e yield C abundances of +0.9 dex, +1.0 dex, and +0.6 dex respectively, relative to the iron abundance. Thus carbon is over-abundant in the atmosphere of V553 Cen by a factor of ~7 relative to iron.

All the synthetic spectra illustrated so far, except Figure 4e, have been convolved with a Gaussian of full width at half maximum (FWHM) equal to 0.50Å, which compares favourably with the width of individual spectral lines obtained using the échelle system. For Figure 4e a FWHM = 0.90Å was used to match the synthetic spectrum with observations of V553 Cen obtained with a normal grating system, which had a significantly lower resolution.

Next the nitrogen abundance was derived using the strongest features of the blue CN system, namely the $\Delta v = 0$ band running blueward from λ3883Å and the $\Delta v = -1$ band, with bandheads at λλ~4216 and ~4197Å. Figures 5 and 6 illustrate the results for the $\Delta v = -1$ and $\Delta v = 0$ bands, respectively. The N abundances extracted from these curves are tabulated in column (7) of Table 5. For ρ Puppis no nitrogen abundance could be estimated, as a result of (1) the photographic plates at λ~3880Å being underexposed and (2) the high effective temperature (T_e = 6600 K) and intrinsic weakness of the $\Delta v = -1$ bands (a factor of ~10 weaker than the $\Delta v = 0$ bands). Similarly, at maximum light V553 Cen has no observable CN features in the wavelength range λλ4205 to 4220Å.

However, Figure 5 displays the result for V553 Cen at a phase of ~0.45, with the synthetic spectrum parameters shown in Table 5. As with Figure 4e, this figure has been convolved with a Gaussian whose FWHM = 0.90Å.

Finally in Figure 6a, a synthetic spectrum of the $\Delta v = 0$ blue CN system is compared with coudé échelle data of V553 Cen at a phase of ~0.0. At a phase of ~0.45, theoretical and observed data are superimposed in Figure 6b, where the FWHM = 0.90Å. This latter figure illustrates an effect previously noted by Cottrell and Norris (1978). For very strong features, that is those which are formed in the top two or three depth points of the model atmosphere, large anomalies will result in the central depth. Thus, in order to derive a nitrogen abundance from a band of this type, one should consider features which are formed at larger optical depths, and features 2 - 3 Å away from the bandhead.

From the CN spectra in Figures 5 and 6a, a nitrogen enhancement of a factor of ~4 relative to iron was determined. Therefore the synthesis technique applied here gave an enrichment of both carbon *and* nitrogen relative to iron, by factors of approximately 7 and 4 respectively. These anomalous abundances were determined at both maximum and minimum light, and

FIG. 5. - Synthetic and observed spectrum of the $\Delta v = -1$ region of the blue CN system. V553 Cen at a phase of 0.45. The synthetic spectrum was convolved with a Gaussian which had a FWHM = 0.90 Å. The positions of the bandheads of the $\Delta v = -1$ system are indicated.

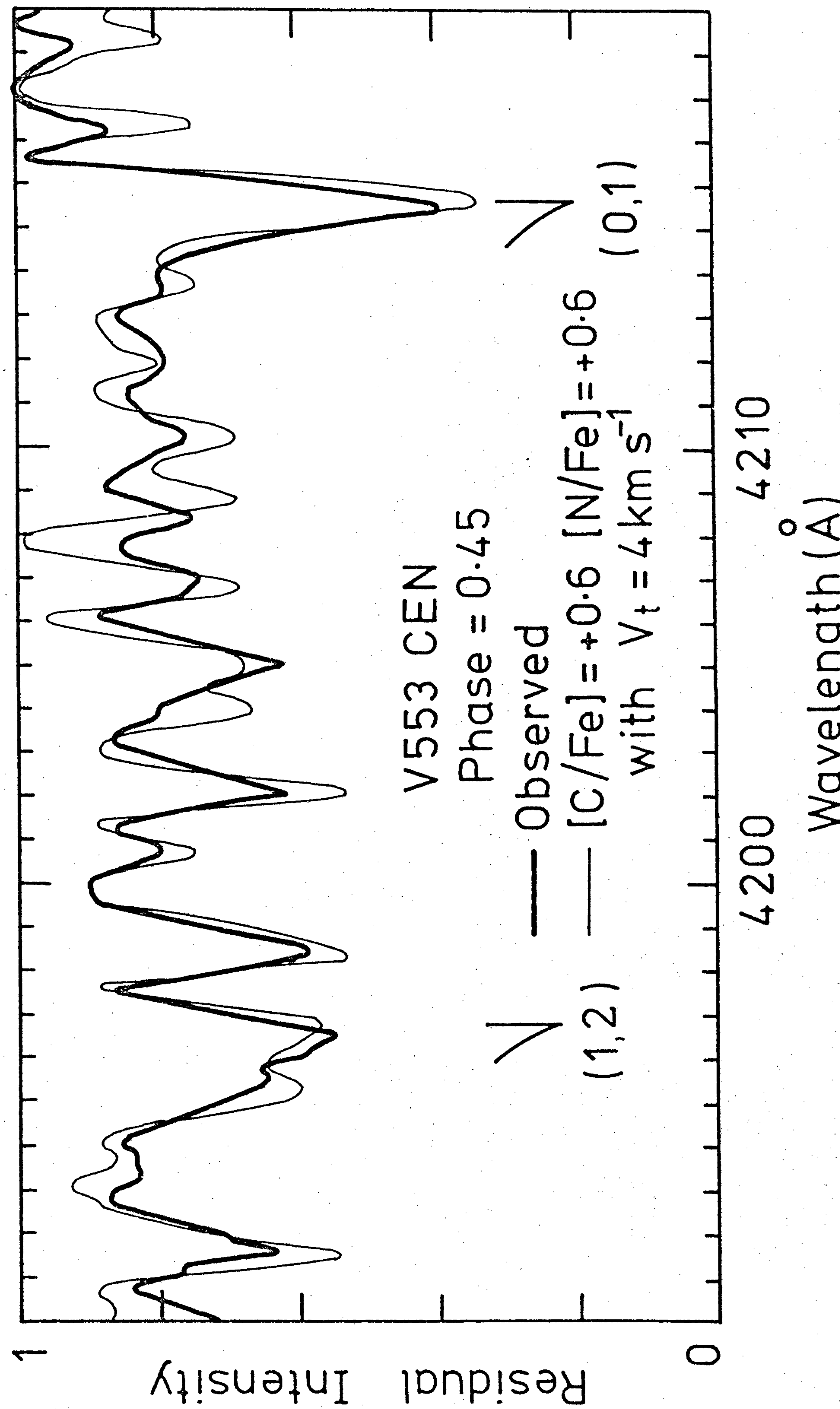

V553 CEN
Phase = 0·45
— Observed
— [C/Fe] = +0·6 [N/Fe] = +0·6
with V_t = 4 km s^{-1}
(1,2)
(0,1)
Residual Intensity
1
0
4200
4210
Wavelength (Å)

FIG. 6. - Synthetic and observed spectra for the $\Delta v = 0$ bands of the blue CN system. (a) V553 Cen at a phase of 0.0, convolved with a Gaussian with FWHM = 0.50Å (b) V553 Cen at a phase of 0.45; convolving profile has FWHM = 0.90Å. The positions of the bandheads are also indicated.

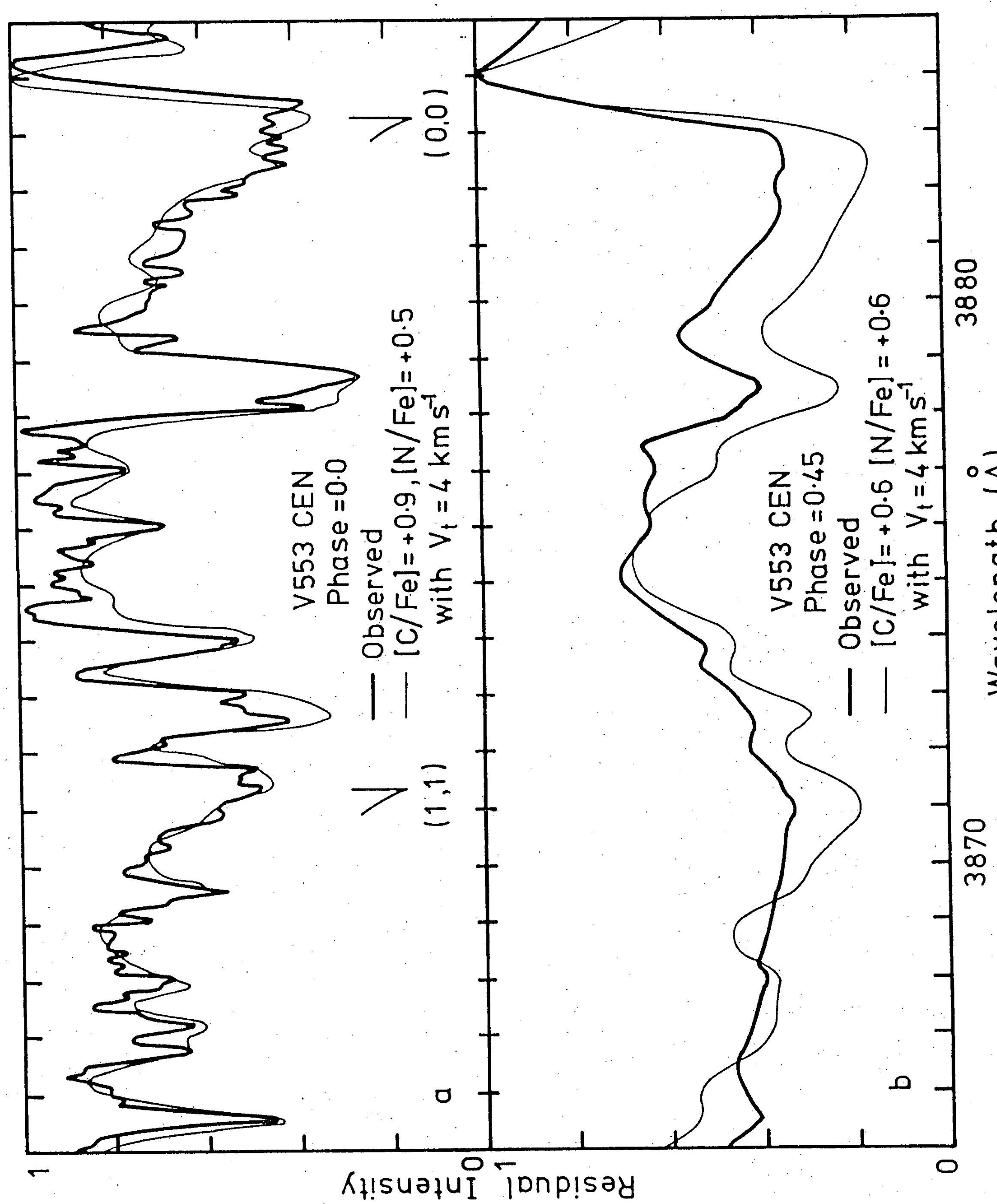
a
V553 CEN
Phase =0.0
— Observed
— [C/Fe]= +0.9, [N/Fe]= +0.5
with Vt = 4 kms-1
(1,1)
(0,0)
b
V553 CEN
Phase =0.45
— Observed
— [C/Fe]= +0.6 [N/Fe] = +0.6
with Vt = 4 kms-1
3870
3880
Wavelength (Å)
Residual Intensity
0
1

consequently reflect the good choice of atmospheric parameters at each of these phases.

Two error analyses were undertaken to determine the affect on the C and N abundances as well as the microturbulent velocity with changes in the gravity and overall metal abundance. A $\Delta\log g = +0.5$ required the C abundance to be lowered by 0.2 dex, and the nitrogen to be enhanced by an additional 0.1 dex relative to iron. A $\Delta[A/H] = -0.3$ leads to an increase in v_t from 4 to 6 km s^{-1}, as well as an increase in the carbon and nitrogen abundances by 0.4 and 0.3 dex, respectively. Neither of these error estimates alter the major result of this research, namely that both carbon and nitrogen are enhanced in the atmosphere of V553 Cen.

Before concluding this section some comment must be made concerning the s-process elements barium and strontium. The échelle plates obtained for this analysis did not enable examination of the BaII lines at either $\lambda\lambda\sim4554$ or 4934Å. The only s-process line accessible on these plates was the SrII line at $\lambda4215.5$Å, which coincides with a $\Delta v = -1$ bandhead of CN. The observed spectra of ρ Puppis and V553 Cen, the latter at maximum light, correspond to almost identical effective temperatures, and at $\lambda\sim4215$ there appeared to be no significant enhancement of this line in the Cepheid. However, additional spectra should be obtained to investigate these species, before a conclusion can be reached concerning the abundance of barium and strontium.

From the above discussion, carbon and nitrogen are enhanced in the atmosphere of V553 Cen by +0.7 and +0.4 dex respectively, relative to the Sun, while the s-process element strontium (on the basis of a single line) appears to be normal. The implications of these abundances on the evolutionary status of this star will be considered in §IV.

IV. EVOLUTIONARY CONSIDERATIONS

In an attempt to interpret the results derived for V553 Cen, let us begin with a summary of the properties of this Cepheid. From §III, the overall metal abundance, except for carbon and nitrogen, is slightly deficient in V553 Cen relative to the Sun. Carbon and nitrogen are enhanced relative to solar abundances by factors of 5 and 3 respectively. On the basis of current evolutionary theory of single stars this would require material, processed by *both* the triple - α and CN processes, to be mixed into the surface layers. This scheme of enrichment was discussed recently by Bessell and Norris (1976) as one scenario for the abundance peculiarities in ω Cen. For triple - α processing the star must have evolved beyond the red giant branch phase.

From §III*b* the present mass of V553 Cen was estimated to be ~$0.5M_\odot$ (following Christy 1966). However, following the He-flash a star with solar composition must have an extremely small envelope mass to evolve as far blueward as the instability strip. According to Gross (1973), a $0.50M_\odot$ solar composition star with a core mass of $0.45M_\odot$ would have its helium-core burning (horizontal branch, HB) evolution to the blue of the instability strip. Subsequent evolution off the HB into the region of the suprahorizontal branch (above horizontal branch, AHB) could produce stars with solar abundance, and even variables with periods longer than those of the RR Lyraes. Thus V553 Cen could be the progeny of the strong-lined RR Lyrae stars of Preston (1959). The evolution of these stars has been considered by Kraft (1972). Kraft's interpretation was that they started with masses much larger than their globular cluster counterparts, but lost more mass during their evolution to the HB. However, to attain a carbon-nitrogen-rich atmosphere at this stage, enriched material would have to be mixed either at the He-flash or during the quiescent He-burning stage on the HB. The latter has not been demonstrated in any evolution calculations to date. The former, which could produce the required carbon enrichments, would not have sufficient time to process the carbon to nitrogen. Thus we have to consider a later stage of evolution, namely the asymptotic giant branch (AGB), to explain the abundances derived for V553 Cen.

A $0.5M_{\odot}$ HB star with an envelope mass of $\sim 0.05M_{\odot}$ could pass through the instability strip at a log $L/L_{\odot}$ of ~2 if it continues to lose mass as it evolves up the AGB. Theoretical calculations (Mengel 1973; Gingold 1974) have shown that stars with envelope masses of $\sim 0.01 - 0.02M_{\odot}$ evolve away from the AGB, towards the white dwarf region. Thus, V553 Cen could be a loop Cepheid (as defined by Kraft 1972) evolving through the instability strip with a luminosity only slightly above the AHB. The anomalous carbon and nitrogen abundances could have been obtained during He-shell flashes on the AGB, following CN-processing on the products of the triple - α reaction. Only relatively small amounts of this enriched material are required to be mixed into the envelope as these layers contain so little mass ($\lesssim 0.05M_{\odot}$). If these types of Cepheids loop off at comparatively low luminosity, this could explain why no carbon-rich Cepheids have been discovered at longer periods, i.e. > 2^{d} (see Lloyd-Evans *et al.* 1972).

Although the above scenario provides an interpretation of the abundances obtained in §III, it is necessary to consider how large amounts of mass can be lost from the envelope of a star. V553 Cen could either be a member of a binary system in which it lost mass to a secondary star, or some property of this star has induced it to lose mass at a greater rate than other objects. While the binary star proposition could be investigated further by a detailed photometric and radial velocity search for secular variations in the light and radial velocity curves of V553 Cen, a more fruitful exercise would be to follow the evolution of a solar composition star through the He flash, He-core and He-shell burning, with large amounts of mass loss to investigate the phases at which CN-rich material can be mixed into the outer layers.

Finally, let us consider that a star is completely mixed at the helium core flash. The subsequent evolution of these objects has been considered by two groups of researchers. Petersen (1972) evolved helium dominated models in the log L - log T_e plane, and these show that a $0.7M_{\odot}$ star with an hydrogen mass fraction of 0.2 will evolve off the He-rich main sequence and through the instability strip with a luminosity similar to that of V553 Cen. The enhanced C and N abundances are respectively accounted for by the triple - α reaction at the core flash and subsequent CNO processing. A slightly different approach was investigated by Paczyński and Tremaine (1977), who artificially produced off-centre helium core flashes. These led to mixing of the helium core with the envelope, and although no details of these objects' movements in the HR diagram are given these authors suggested that this process could produce the subgiant CH stars discussed by Sneden and Bond (1976). These objects could in turn by the progenitors of stars like V553 Cen. Further model calculations using He-dominated atmospheres could provide additional constraints on the amount of helium enrichment required before helium opacities, namely He^{-}, become the principal source of continuum opacity. However, both the production of fully mixed models and off-centre core flashes have not been constructed without altering currently accepted, basic input physics.

Consequently although extensive mass loss is required in the interpretation of V553 Cen as a loop Cepheid, this explanation alleviates the problem of the apparent non-existence of longer period carbon-rich Cepheids.

V. SUMMARY

In this research the carbon-rich Cepheid V553 Centauri was analysed and the following results were determined: (1) the iron abundance in this star is close to solar; (2) the carbon and nitrogen abundances are enhanced by factors of 5 and 3 respectively relative to the Sun, and (3) the solar abundance for iron applies equally well to the other elements, as shown in the synthetic spectra constructed in the neighbourhood of the molecular features. From the above investigation, V553 Cen is thus a carbon-nitrogen-rich Cepheid with a near-solar metal abundance.

Finally it is suggested that V553 Cen is most appropriately interpreted as a loop Cepheid with a luminosity only slightly higher than the suprahorizontal branch. The carbon and nitrogen enrichments are a result of He-shell flashes, prior to the stars final evolution away from the giant branch on its way to becoming a white dwarf.

Acknowledgements

I would like to thank Dr. M. S. Bessell for obtaining the Strömgren photometry of the B stars near V553 Centauri, and also for his and Dr. John Norris' comments on the manuscript. In addition I wish to acknowledge the support of an Australian National University Post-graduate award which enabled access to the UNIVAC 1100/42 Computer, operated by the Australian National University Computer Services Centre.

REFERENCES

Arp, H. 1962, *Ap. J.*, 135, 971.

Bell, R. A., Eriksson, K., Gustafsson, B., and Nördlund, Å. 1976, *Astr. Ap. Suppl.*, 23, 37.

Bessell, M. S. 1967, *Ap. J.*, 149, 167.

———. 1969, *Ap. J. Suppl.*, 18, 167.

———. 1976, *Pub.A.S.P.*, 88, 557.

———. 1977, private communication.

Bessell, M. S., and Norris, J. 1976, *Ap. J.*, 208, 369.

Christy, R. F. 1966, *Ap. J.*, 144, 108.

Cottrell, P. L. 1978, *Ap. J.*, July 15 issue (Chapter 5).

Cottrell, P. L., and Norris, J. 1978, *Ap. J.*, May 1 issue (Chapter 2).

Cousins, A. W. J. 1964, *M.N.A.S.S.A.*, 23, 175.

———. 1973, *Mem. R.A.S.*, 77, 223.

———. 1974, *M.N.A.S.S.A.*, 33, 149.

Crawford, D. L. 1978, *A. J.*, 83, 48.

Dean, J. F., Cousins, A. W. J., Bywater, R. A., and Warren, R. R. 1977, *Mem. R.A.S.*, 83, 69.

Eggen, O. J. 1974, *Pub.A.S.P.*, 86, 697.

Gingold, R. A. 1974, *Ap. J.*, 193, 177.

Gross, P. G. 1973, *M.N.R.A.S.*, 164, 65.

Gustafsson, B., Bell, R. A., Eriksson, K., and Nördlund, Å. 1975, *Astr. Ap.*, 42, 407.

Herbig, G. H. 1952, *Trans. I.A.U.*, 8, 807.

Iriarte, B., Johnson, H. L., Mitchell, R. I., and Wisniewski, W. K. 1965, *Sky and Telescope*, 30, 21.

Johnson, H. L. 1966, *Ann. Rev. Astr. Ap.*, 4, 193.

Kraft, R. F. 1972, in *The Evolution of Population II Stars*, ed. A. G. D. Philip, Dudley Obs. Report No. 4, p. 69.

Kron, G. E. 1978, preprint.

Landolt, A. U. 1975, *Pub.A.S.P.*, 87, 373.

Lloyd-Evans, T., Wisse, P. N. J., and Wisse, M. 1972, *M.N.R.A.S.*, 159, 67.

Mengel, J. G. 1973, in *Variable Stars in Globular Clusters and in Related Systems*, ed. J. D. Fernie (Dordrecht: Holland), p. 214.

Neugebauer, G., and Leighton, R. B. 1969, *Two-Micron Sky Survey - A Preliminary Catalog*, (Scientific and Technical Information Division, NASA: Washington).

Norris, J., and Zinn, R. 1975, *Ap. J.*, 202, 335.

Osmer, P. S. 1970, Ph.D Thesis, California Institute of Technology.

Paczyński, B., and Tremaine, S. D. 1977, *Ap. J.*, 216, 57.

Pagel, B. E. J. 1964, *Roy. Obs. Bull.*, No. 87.

Petersen, J. O. 1972, *Astr. Ap.*, 19, 197.

Preston, G. 1959, *Ap. J.*, 130, 507.

Sneden, C., and Bond, H. E. 1976, *Ap. J.*, 204, 810.

Strömgren, B. 1966, *Ann. Rev. Astr. Ap.*, 4, 433.

Whipple, F. L. 1966, *Smithsonian Astrophysical Observatory - Star Catalog*.

CHAPTER 4

EXTREMELY METAL-WEAK STARS: CARBON AND NITROGEN ABUNDANCES IN GIANTS

P. L. Cottrell

ABSTRACT

Seven extremely metal-weak giant stars have been analysed. Five of these were selected from the objective prism survey of Bidelman and MacConnell. Carbon and nitrogen abundances were determined for all seven stars by constructing synthetic spectra of regions which contain many lines of the CH, CN, and NH molecules. The following correlation between the carbon to nitrogen ratio and gravity was obtained:

$$[C/N] = 0.5(\log g) - 1.3.$$

In addition, a slight enhancement of nitrogen (relative to the metals) was determined as the gravity was reduced (i.e., with increasing luminosity). The above relationship can be interpreted in a similar manner to the $^{12}C/^{13}C$ ratios discussed by Dearborn, Eggleton, and Schramm, namely that as stars evolve to higher luminosities, there is mixing of CNO-processed material into the outer layers. The evolutionary phase at which mixing can occur, as well as the nature of the mixing processes, are briefly discussed.

I. INTRODUCTION

The detailed analysis of metal-poor stars provides an opportunity to investigate the properties of objects which were probably formed during the early evolution of the Galaxy. Dwarf stars, in which no products of nuclear processing are expected in the outer layers, will therefore still be exhibiting their primordial abundances. However, giants have evolved sufficiently that their outer layers could have become contaminated with the products of interior burning. Many schemes have been discussed which have endeavoured to interpret various extreme surface abundance anomalies, viz., CH stars (both giant and subgiant), and BaII stars (see Sackman, Smith and Despain 1973; Ulrich and Scalo 1972, 1973). In addition, there are a number of giant stars having more subtle peculiarities in their atmospheric layers. Such peculiarities include the variation in the $^{12}C/^{13}C$ ratio as a function of the star's position on the giant branch (Dearborn, Lambert, and Tomkin 1975), the CN strong stars in the globular cluster M5 (Osborn, 1971; Zinn 1977), and the weak-G-band stars in both globular clusters (Zinn 1973, 1977), and the field (Cottrell and Norris 1978; Sneden *et al.* 1978).

The extremely metal-deficient population II field star HD 122563 has been the subject of many abundance analyses (Wallerstein *et al.* 1963; Wallerstein and Helfer 1966; Pagel 1965; Ball and Pagel 1967; Wolfram 1972; Sneden 1973). Wallerstein *et al.* (1963) determined that this star was deficient in iron by a factor of 800 relative to the Sun. A reanalysis of the data, using an improved temperature estimate, reduced this deficiency to 500 (Wallerstein and Helfer 1966). The most recent fine analysis (Wolfram 1972) confirmed this latter result, that is [Fe/H] = -2.7 ± 0.3. Wolfram also derived a C abundance from his observations, [C/Fe] = -0.4 ± 0.4. Sneden (1973), using these parameters, obtained a nitrogen abundance, [N/Fe] = +1.2 ± 0.5. Sneden assumed [O/Fe] = 0. However, Lambert, Sneden, and Ries (1974) have since determined an oxygen abundance, using a coudé échelle scanner in the region of the [OI] line at λ~6300.3Å. From this feature an overabundance of oxygen relative to iron was derived, quantitatively, [O/Fe] = +0.6. No redetermination of the carbon and nitrogen abundances was made. Lambert *et al.* (1974) briefly discussed the evolutionary implication of their result, and concluded that the enhancement of oxygen must have been primordial, since CNO nuclear-burning processes lead only to the *destruction*, not the formation of oxygen.

Sneden (1974) determined carbon and nitrogen abundances in 10 additional metal-poor stars, having gravities, log g, between 1.3 and 3.8. Using spectrum synthesis techniques he found that the giants, with log g's $\lesssim$ 2.4 had [C/N] $\lesssim$ -1.0, whereas for gravities larger than this value, [C/N] $\gtrsim$ +0.0. He interpreted the low C/N values as indicating that the products of CNO burning had been mixed into the surface layers, with the mixing becoming significant at a log g = 2.4. If one makes some assumption about the mass, namely log $M/M_\odot$ = 0 for these population II giants, a luminosity, log $L/L_\odot$ ~ 2 is determined. Examination of Figure 3 of Dearborn *et al.* (1975) shows that this is the same luminosity at which the $^{12}C/^{13}C$ ratio in red giant stars, is consistently being observed with values (~15) significantly lower than the solar value (~90). Theoretical calculations, involving burning via the CNO cycle, indicate that both the lowering of the $^{12}C/^{13}C$ ratio and a decrease in the value of C/N are produced (see Dearborn, Eggleton, and Schramm 1976), although their calculations cannot interpret the extremely low $^{12}C/^{13}C$ values (~5-10), observed in a few stars.

In the present work a larger sample of stars with log g < 2 has been analysed. In particular, carbon and nitrogen abundances have been determined (§IV). The observational data, both spectroscopic and photometric (RI and

DDO), are described in §II, with the DDO photometry being the basis for the gravity and metal abundance determinations (§III). Finally, the abundance results are discussed (§V) with particular reference to the work of Sneden (1974) and Dearborn *et al.* (1976).

II. OBSERVATIONS

In this analysis, the program stars have come principally from the extensive tabulations of Bidelman and MacConnell (1973). Generally, stars in their Table V, which had an extreme degree of metal-line weakening, were selected. All the stars studied here are shown in column (1) of Table 1. Two previously studied weak-lined stars were also included, viz., HD 122563 and HD 165195. A carbon and nitrogen abundance analysis of HD 122563 enabled a comparison with other determinations (see Sneden 1973). Alexander (1971), in his search for metal-deficient stars in the Cape Photographic Catalogue, had 2 stars in common with Bidelman and MacConnell (1973). One of these, HD 184711, was analysed in this research. According to Bidelman and MacConnell, this star had only a moderate degree of metal-line weakening.

(a) Spectra

Using the coudé focus of the 1.9m telescope at Mount Stromlo, and various combinations of gratings and cameras, spectroscopic data were acquired which were centred on two wavelength regions. These regions contained molecular bands which are sensitive to changes in the carbon and nitrogen abundances. In particular, spectra around λ~4300Å (the G-band) and the CN features at λ~3880Å were obtained. The dispersion of the observational data was dependent on the brightness of each object at the chosen wavelength. For example, for HD 122563 the coudé échelle and the 40cm camera combination gave a reciprocal dispersion of ~3-4Å mm^{-1}. However for all other objects, reciprocal dispersions between ~7 and ~14Å

TABLE 1

BASIC DATA FOR PROGRAM STARS

Star (1)	C(45–48)* (2)	C(42–45)* (3)	C(38–42)* (4)	$(R-I)_J$** (5)	E(B–V)† (6)	M_V* (7)	B.C.## (8)	V_r* (9)
HD 21022	1.195	0.675	-0.682	0.575	0.024	-1.58	-0.51	+107
$+6^{\circ}648$	1.299	0.862	-0.500	0.769	0.25‡	-1.04	-0.60	-150
HD 36702	1.307	0.772	-0.396	0.688	0.040	-2.14	-0.73	+111
HD 84903	1.256	0.688	-0.614	0.750	0.082	-2.19	-0.79	+80
HD 122563	1.178	0.622	-0.750	-	-	-	-	-26#
HD 165195	1.338	0.790	-0.410	0.783	0.25#	-1.10	-0.63	-27
HD 184711	1.352	0.798	-0.435	0.811	0.049	-2.55	-0.91	+94§

* From Bessell and Norris (1978).

** From Eggen (1974), except for HD 165195 and HD 184711.

† Using formula from Kron (1978), except where indicated otherwise.

‡ Using Stromgren photometry.

\# From Wallerstein *et al.* (1963).

\## From Böhm-Vitense (1973, 1975).

§ For HD 184711, Alexander (1971) gives $V_r = 119 \pm 2$ km s^{-1}.

mm^{-1} were obtained using either the B or C gratings, in combination with either the 40cm or 81cm cameras. For two stars, HD 122563 and HD 21022, spectroscopic data of the NH features near λ~3360Å were acquired using the cassegrain spectrograph on the 1.9m telescope at Mount Stromlo. For this data the reciprocal dispersion was ~33Å mm^{-1}, and the resolution was slightly lower than that obtained using the coudé focus with a reciprocal dispersion of ~14Å mm^{-1}. Image intensifier tubes were attached to all cameras. The spectra were recorded on either nitrogen or hydrogen sensitised IIaO emulsions. Where possible, two spectra of each region were obtained for each star. Having traced the spectrograms, using the Göttingen microphotometer (which was programmed with an intensity calibration), the measured residual intensities were punched into a computer. For a given star and wavelength interval, the intensities were added numerically, and then spline interpolated to give a smooth spectrum. The spectral observations were then in a form which could be compared directly with the instrumentally convolved spectrum synthesis data of the same wavelength region.

For one of the objects, HD 84903, an IPCS spectrum near the CN features at λ~3883Å was acquired by Dr. M. S. Bessell, using the 3.9m Anglo-Australian Telescope. This observation had a reciprocal dispersion of ~5Å mm^{-1}, and to match the resolution, the synthetic spectrum was convolved with a Gaussian having a full width at half maximum (FWHM) of 0.3Å.

(b) Photometry

DDO photometry was acquired for all the program stars, except HD 122563, by Bessell and Norris (1978). The observed C(45-48), C(42-45), and C(38-42) colours are given in columns (2) to (4) of Table 1. Some of the stars in this table have $(R-I)_K$ colours from Eggen (1974). The remainder were observed using the 76cm telescope at Mt. Stromlo, employing a single-channel photon-counting system, with a GaAs photomultiplier tube and the RI filters of Bessell (1976). All the observations were transformed to $(R-I)_J$ (Eggen 1974), and are shown in column (5) of Table 1. This enabled an effective temperature to be derived, using an estimate of the reddening E(B-V), and the T_{eff} - $(R-I)_J$ calibration of Johnson (1966).

Norris, Bessell, and Pickles (1978) have embarked upon a detailed DDO analysis of a large number of stars from Bidelman and MacConnell's (1973) lists of weak-lined objects. From the DDO photometry, an absolute magnitude, M_V, and a metal abundance, [M/H] have been extracted, using the theory developed by Osborn (1971). ([M/H] is the logarithmic difference in the abundance of all metals between the star under investigation and the Sun.)

Bessell and Norris (1978) have also determined a reddening in the direction of one star, $+6^{o}648$, and E(B-V) for another, HD 165195 has been taken from Wallerstein *et al.* (1963). For all other stars, for which no reddening was available, the statistical method of Kron (1978) was used. This gives a lower limit of the reddening, dependent on the distance which starlight has to travel through a uniformly absorbing layer, 500pc thick. The Sun is considered to be at the centre of this layer. E(B-V) adopted for each star are shown in column (6) of Table 1.

III. ATMOSPHERIC PARAMETERS AND THE REDUCTION TECHNIQUE

From the photometry described in the previous section, the basic atmospheric parameters for each star can be derived. The effective temperature, gravity, and metal abundance for all the program stars are shown in columns (2), (3), and (4) of Table 2. The effective temperatures have been determined by applying the reddening corrections to the observed $(R-I)_J$ colours, while the metal abundance has been extracted from Figure 3.8 of Osborn (1971). To derive a value of the gravity from M_V (column (7) of Table 1), the following relationships were applied,

TABLE 2

ATMOSPHERIC PARAMETERS

Star (1)	T_{eff} (^{o}K) (2)	log g (3)	[M/H] (4)
HD 21022	4550	1.30	-2.5
+6^{o}648	4400	1.35	-2.7
HD 36702	4200	0.80	-2.0
HD 84903	4100	0.80	-2.7
HD 122563*	4600	1.20	-2.7
HD 165195	4350	1.35	-2.5#
HD 184711	3950	0.50	-3.0

* Parameters from Wolfram (1972).

\# From Wallerstein and Helfer (1966).

$$L = 4\pi R^2 \sigma\, T_{eff}^{4},\; g = GM/R^2,\text{ and } L = 10^{0.4(4.75 - M_{bol})},$$

which gives

$$\log g = 4 \log T_{eff} + 0.4M_{bol} + \log M/M_{\odot} - 12.52.$$

Bolometric corrections for Population II giants have been taken from Böhm-Vitense (1973, 1975), and are given in column (8) of Table 1. To evaluate this expression some assumption has to be made about the mass of these stars. From the low metal abundance (column (4) of Table 2) and the large radial velocities (column (9) of Table 1), these objects can be considered to belong to the halo population (Population II). Thus masses in the range 0.6 to 1.0 $M_{\odot}$ can be considered (see Gingold 1974; Schwarschild and Härm 1967). Applying the upper limit, log $M/M_{\odot}$ = 0, the gravities, shown in column (3) of Table 2, are obtained. The error in this parameter is of the order of 0.3 dex. The metal abundance is uncertain by a slightly larger factor.

Using the parameters given in Table 2, model atmospheres were interpolated or extrapolated from within the extensive grid constructed by Bell, Eriksson, Gustafsson, and Nördlund (1976). These were subsequently used to compute synthetic spectra in the following wavelength intervals: (1) $\lambda\lambda 4300 - 4330\text{Å}$ to determine the carbon abundance, (2) $\lambda\lambda 3860 - 3885\text{Å}$ to derive a nitrogen abundance, and finally for stars where the observational data were acquired, (3) $\lambda\lambda 3355 - 3380\text{Å}$ for an additional estimate of the nitrogen abundance. The synthesis technique has been described in more detail by Cottrell and Norris (1978) and Cottrell (1978).

In this abundance analysis two assumptions have been made in the construction of the synthetic spectra: (1) that [O/M] = 0, and (2) that a microturbulent velocity, v_t of 2 km s^{-1} can be applied to all stars. The observational data is not of high enough resolution for these parameters to be derived. Variations in v_t will be considered in the discussion of errors (§IV*c*). Sneden (1974) considered variations in the oxygen abundance, and consequently they will not be considered further in this research.

IV. MOLECULAR BAND ANALYSIS

(a) Carbon and nitrogen abundances

In the determination of these abundances, the following sequence was employed. The fluxes for the G-band were computed for the parameters shown in Table 2, and initially,

$$[C/M] = [N/M] = 0.$$

(We recall from the previous section that [O/M] = 0 has been adopted.) These fluxes were then convolved with the appropriate instrumental profile and superimposed on the observational data. The carbon abundance was then adjusted until a good fit to the observations was procured. If NH observations had been acquired, synthesis of this feature now proceeded, first adopting [N/M] = 0, and subsequently altering this value (if required), to obtain an acceptable fit to the observations. The NH region is contaminated by atomic lines, and the spectroscopic data are of low resolution, so the blue $\Delta v = 0$ CN features were used to derive an additional nitrogen abundance. In fact, these latter features were the sole source of the nitrogen abundance in all except HD 122563 and HD 21022.

Using the above sequence, carbon and nitrogen abundances were determined for all the stars shown in Table 1, and are displayed in Table 3. To investigate any systematic errors between this work and that of Sneden (1973, 1974), the observed and synthetic spectra for HD 122563 are shown (Figure 1). A short description of the abundance results for this star is given in the following paragraphs. Comments on all the other objects will be given in §IV*b*, and in §IV*c*, the errors will be discussed in detail.

TABLE 3

CARBON AND NITROGEN ABUNDANCES

Star (1)	[C/M] (2)	[N/M] (3)	[C/N] (4)
HD 21022	-0.1	+0.4	-0.5
$+6^{\circ}648$ §	-0.1	+0.2	-0.3
HD 36702	-0.6	-0.2	-0.4
HD 84903	-1.1	+0.4	-1.5
HD 122563	-0.1	+0.6*	-0.7
	-0.4	+0.9†	-1.3
HD 165195	-0.6	+0.4	-1.0
HD 184711#	-0.6	+0.4	-1.0

§ Using M/H = -2.4, instead of -2.7 (see text, §IV*b*).

* From G-band, CN features (see text, §IV*a*).

† Using (1,1) band of NH, CN features (see text, §IV*a*).

Using M/H = -2.7, instead of -3.0 (see text, §IV*b*).

Figures 1a-d show respectively the observed and synthetic spectra of the G-band, NH feature, and two $\Delta v = 0$ CN bands for HD 122563. As seen in Table 3, carbon is only slightly deficient, while nitrogen is not enhanced by as large a factor as determined by Sneden (1973). The errors associated with these values are illustrated well in Figures 1c and 1d. In Figure 1c the nitrogen abundance has been determined using the CN features, having adopted the carbon abundance from the G-band. However, in Figure 1d, having established a nitrogen abundance from the NH features (principally the (1,1) band near λ~3370Å), the carbon abundance was derived using the CN bandheads. All the abundance determinations are within the error bars given by Sneden (1973). The (0,0) band of the NH feature, at a wavelength of ~3360Å, shows a similar effect to that described by Cottrell and Norris (1978), that is for features formed in the top two or three depth points of the model atmosphere, large errors resulted in the central depth.

There was one difference between this analysis and that undertaken by Sneden (1973, 1974). It concerned the dissociation potential (D_o) of CN, for which a value of 7.89 eV was used in the present work, compared with 7.55 eV adopted by Sneden. The higher value is now believed to be closer to the correct value (see Arnold and Nicholls 1973). This effect was shown in Figure 4a of Sneden (1973), in which the higher D_o produced the stronger features. Thus if Sneden had adopted the higher value of D_o he would have had to lower his N abundance to fit the CN features around λλ~3871 and ~3883Å. This would mean that both his and the present observations would be more closely aligned.

(b) Comments on the C and N abundances in individual stars

In this section, some observed and synthetic spectra will be included to illustrate the fit obtained in deriving the C and N abundances.

HD 21022 — The G-band, $\Delta v = 0$ CN around λ~3880Å, and the NH features

FIG. 1. - Observed and synthetic spectra for HD 122563. (a) The G-band region, (b) the near ultra-violet NH features, (c) and (d) the $\Delta v = 0$ CN features. Each of the curves is identified. The abundances for the computed spectra are given in the legend. The synthetic spectra in (a), (c), and (d) were convolved with an instrumental profile with a full width at half maximum (FWHM) of 0.3Å. The convolved profile in (b) had a FWHM = 1.0Å.

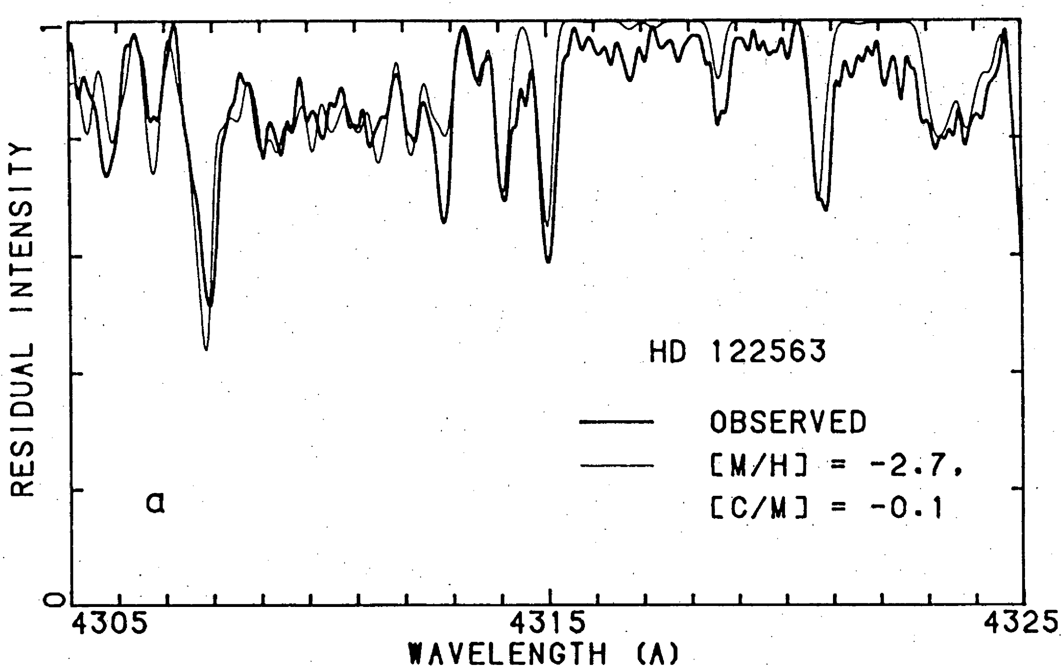
RESIDUAL INTENSITY
1
0
4305
4315
4325
WAVELENGTH (A)
HD 122563
OBSERVED
[M/H] = -2.7,
[C/M] = -0.1
a

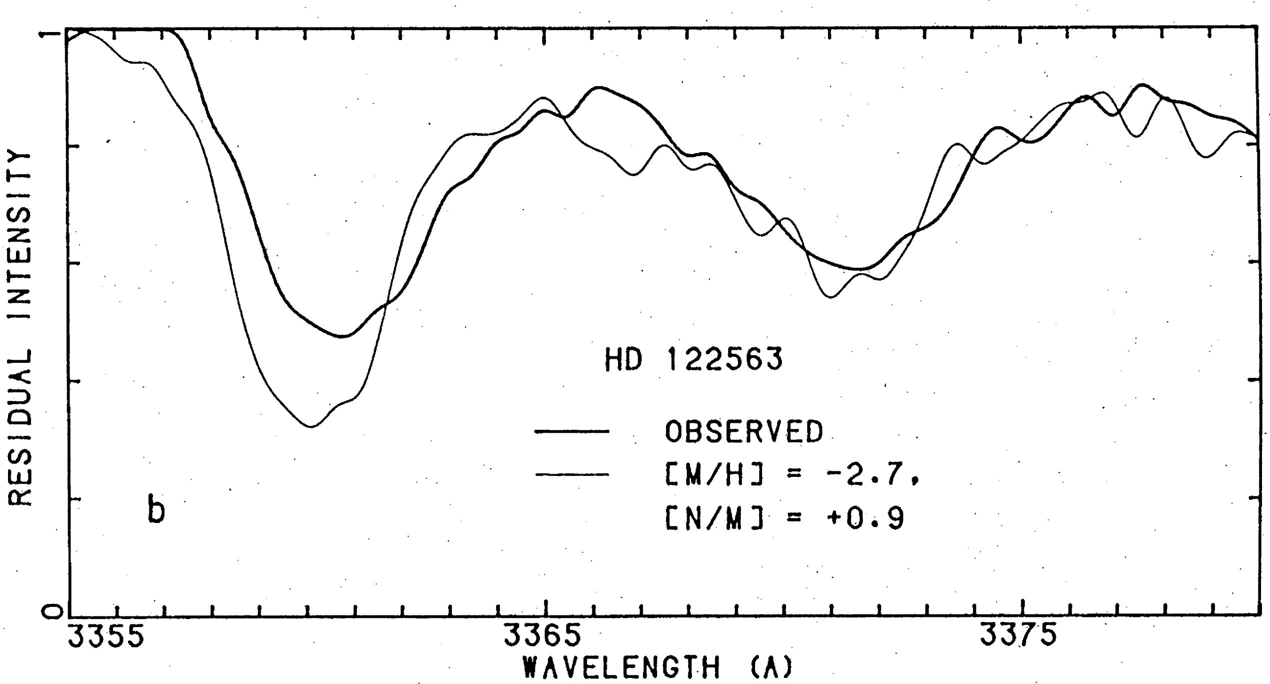
RESIDUAL INTENSITY
1
0
3355
3365
3375
WAVELENGTH (A)
HD 122563
OBSERVED
[M/H] = -2.7,
[N/M] = +0.9
b

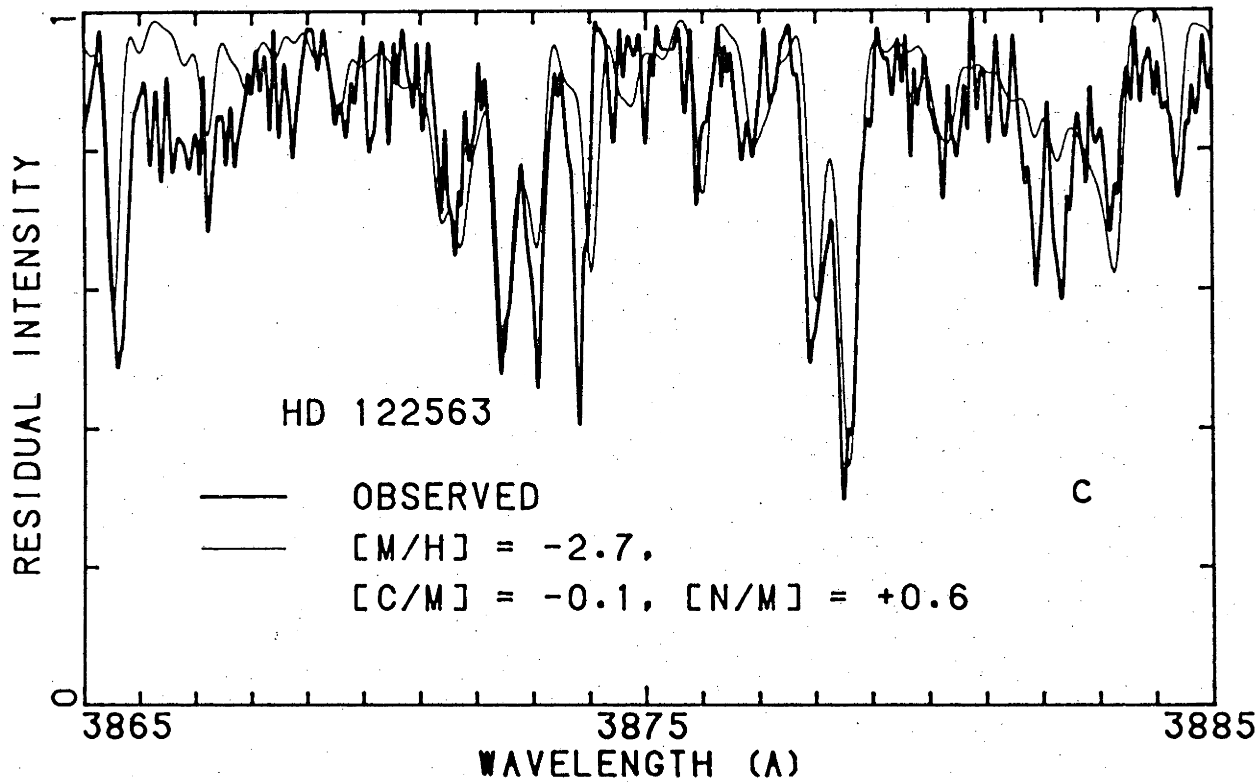
RESIDUAL INTENSITY
WAVELENGTH (A)
3865
3875
3885
HD 122563
OBSERVED
[M/H] = -2.7,
[C/M] = -0.1, [N/M] = +0.6
c

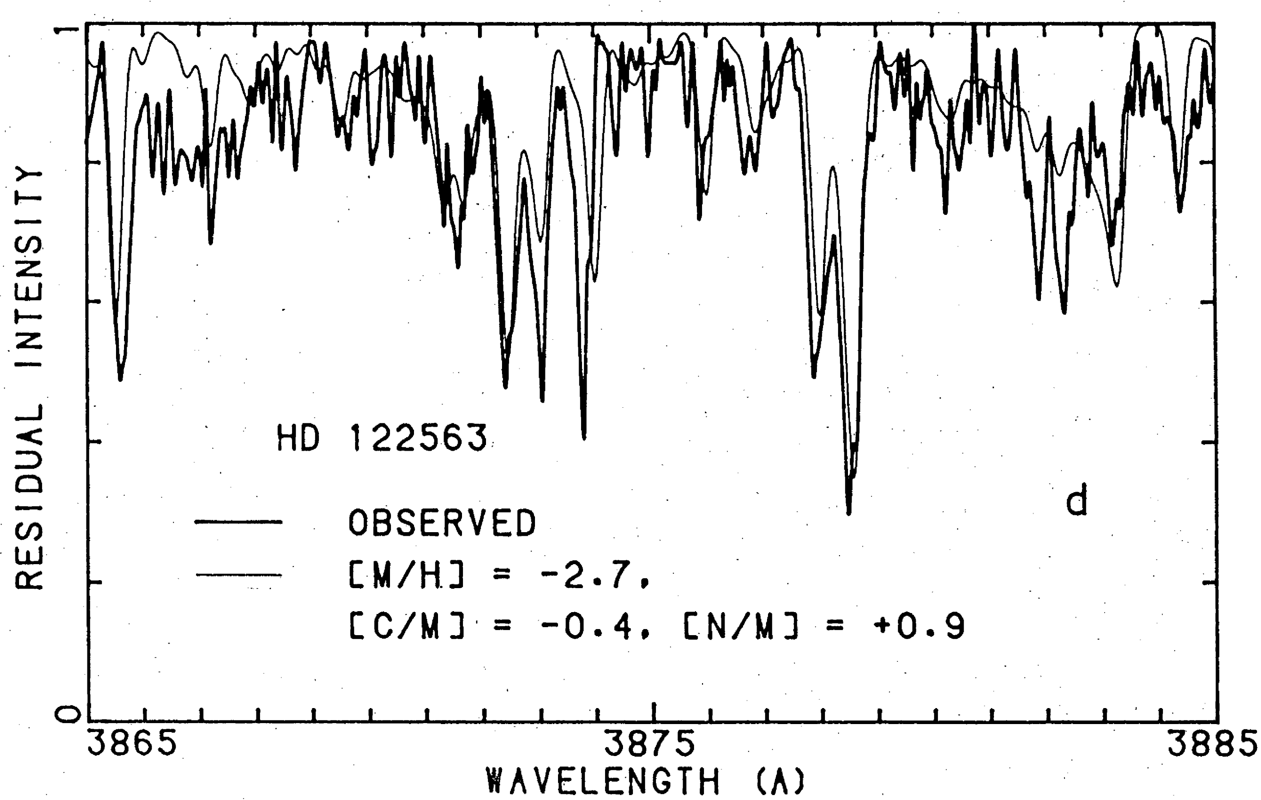
RESIDUAL INTENSITY
WAVELENGTH (A)
3865
3875
3885
HD 122563
OBSERVED
[M/H] = -2.7,
[C/M] = -0.4, [N/M] = +0.9
d

are shown in Figures 2a-c. This object has only a small carbon deficiency (relative to the metals), and a slight enrichment of nitrogen, the latter result obtained using both the CN and NH features. The metal abundance derived from the DDO photometry gave a reasonable fit to the atomic lines, although a complete match was not obtained for all features.

+6°648 — Using the metal abundance shown in Table 2, the synthesised atomic lines were much weaker than the observed metal line profiles. Therefore, the [M/H] was increased by a factor of 2, and this was used in the calculation of the carbon and nitrogen abundances. The fit was still not perfect, with the error probably due to an uncertainty in either the effective temperature, as a result of the large E(B-V), or the microturbulence. In fact, despite the high galactic latitude (30° below the plane), E(B-V) = 0.25, which transformed to a $\Delta T_{eff} \approx 500$ K. If this reddening had been overestimated, the cooler temperatures would give stronger neutral lines, and therefore a better fit to the observational data. Synthetic spectra of the G-band and CN feature were reconstructed using the following atmospheric parameters,

$$T_{eff} = 4100 \text{ K}, \log g = 1.30, [M/H] = -2.7,$$

which required a slight readjustment of the C and N abundances, namely Δ[C/M] = −0.2 and Δ[N/M] = +0.1. Further data should be obtained to determine the effective temperature of this star.

HD 36702 — In determining the carbon abundance, a balance had to be made between fitting the bandhead at λ~4323Å and the region λλ~4310 - ~4313Å, which are both sensitive carbon abundance determinators. The metal lines gave a good fit for [M/H] = −2.0, while nitrogen was slightly underabundant. This was the only object in the group of stars under investigation for which a deficiency of nitrogen, relative to the metals, was obtained.

HD 84903 — Figures 3a-c show the synthetic and observed spectra of

FIG. 2. - Observed and synthetic spectra for HD 21022. (a) G-band (FWHM = 0.5Å), (b) CN features around λ~3880Å (FWHM = 0.9Å), (c) NH features (FWHM = 1.0Å).

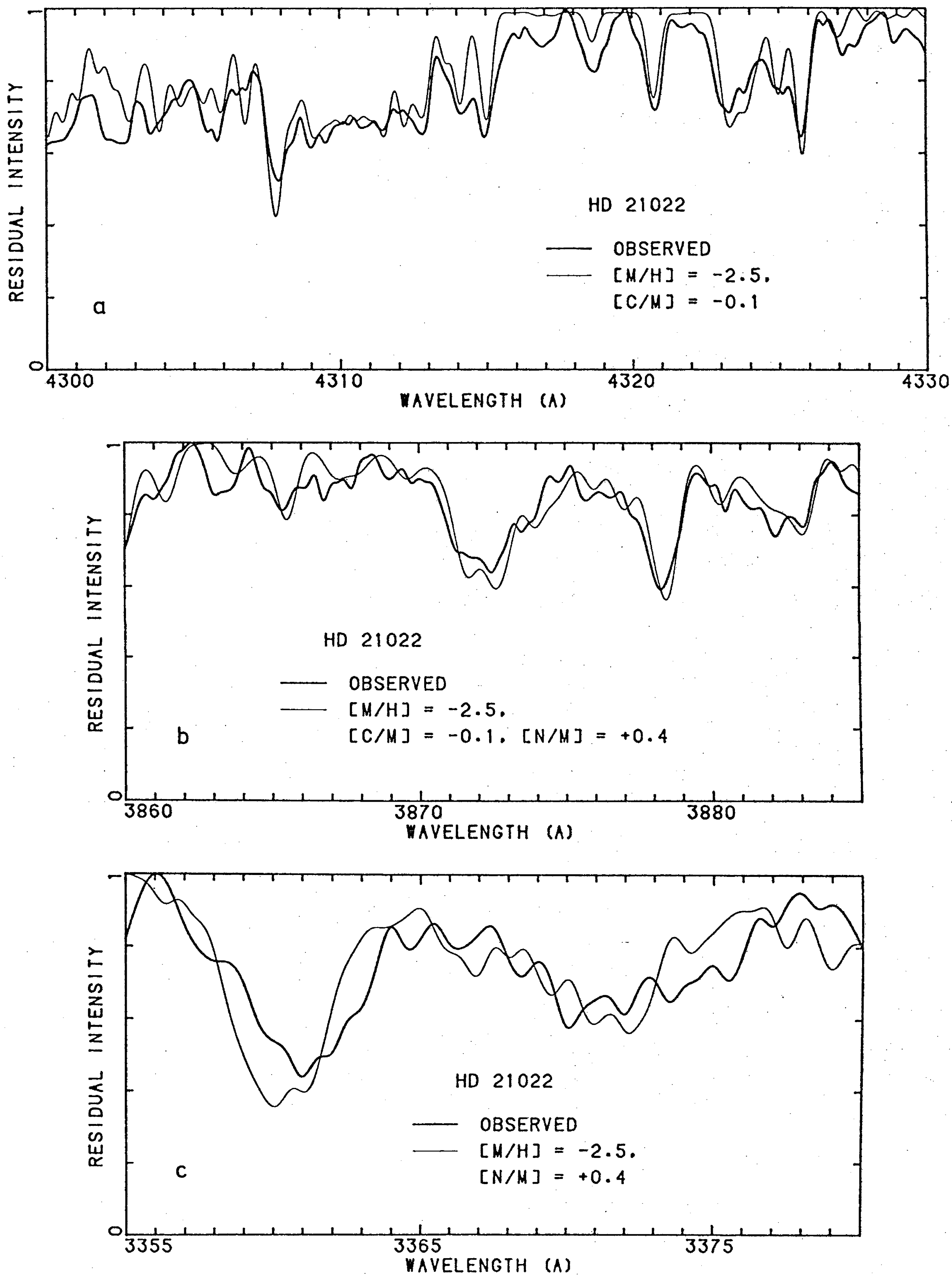
RESIDUAL INTENSITY
HD 21022
OBSERVED
[M/H] = -2.5,
[C/M] = -0.1
a
0
4300
4310
4320
4330
WAVELENGTH (A)
RESIDUAL INTENSITY
HD 21022
OBSERVED
[M/H] = -2.5,
[C/M] = -0.1, [N/M] = +0.4
b
0
3860
3870
3880
WAVELENGTH (A)
RESIDUAL INTENSITY
HD 21022
OBSERVED
[M/H] = -2.5,
[N/M] = +0.4
c
0
3355
3365
3375
WAVELENGTH (A)

FIG. 3. - Observed and synthetic spectra for HD 84903. (a) G-band (FWHM = 0.9Å), (b) and (c) $\Delta v = 0$ CN features. In (b), the synthetic spectrum is compared with data obtained using the coudé at Mount Stromlo (FWHM = 1.0Å), whereas higher resolution IPCS data (FWHM = 0.3Å), acquired using the 3.9m AAT, was the comparison in (c). The dotted curves in (a) and (b) are computed spectra from which all the CH and CN line contributions have been removed.

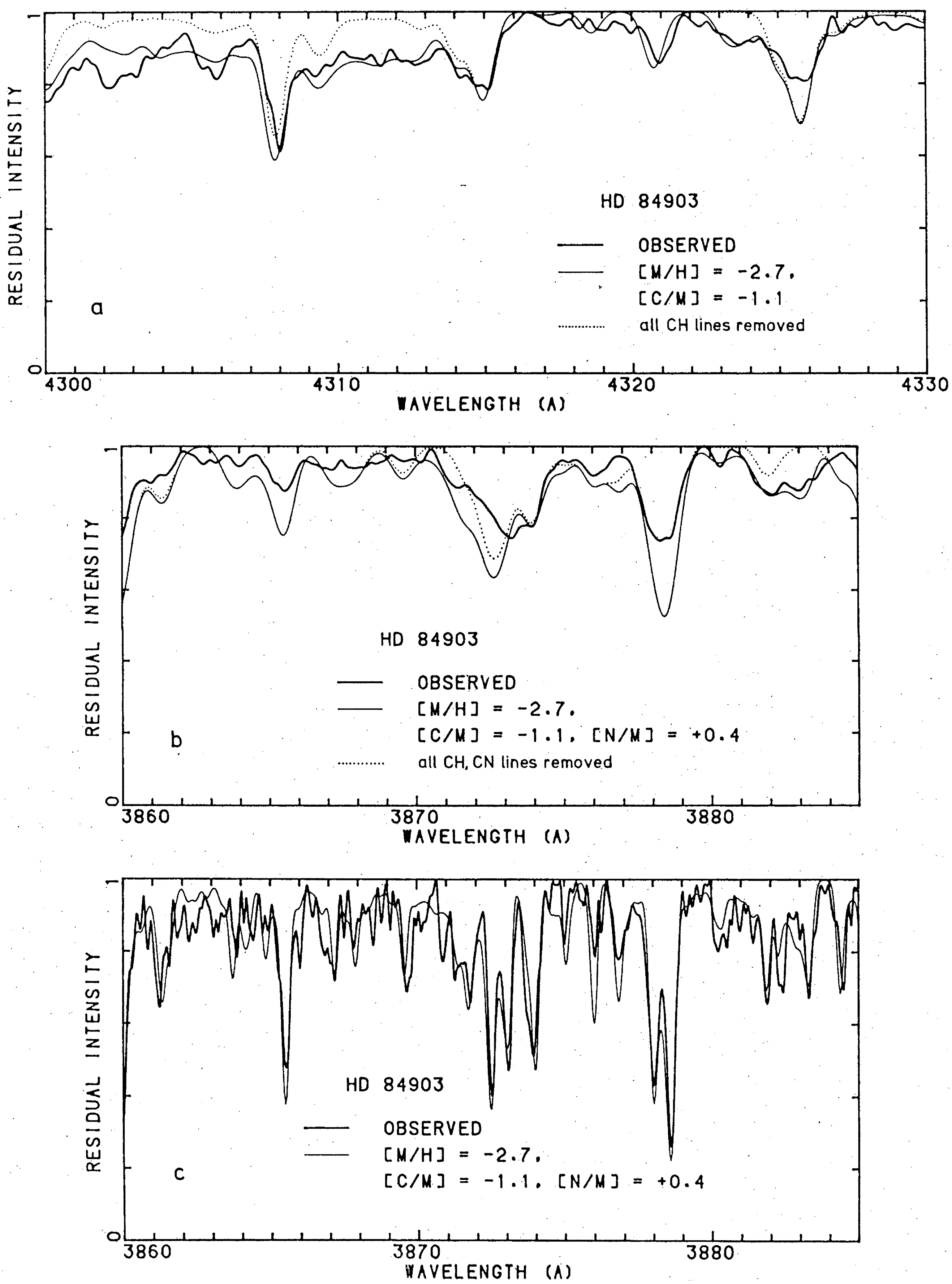

RESIDUAL INTENSITY
WAVELENGTH (A)
HD 84903
OBSERVED
[M/H] = -2.7,
[C/M] = -1.1
all CH lines removed
a
4300
4310
4320
4330
RESIDUAL INTENSITY
WAVELENGTH (A)
HD 84903
OBSERVED
[M/H] = -2.7,
[C/M] = -1.1, [N/M] = +0.4
all CH, CN lines removed
b
3860
3870
3880
RESIDUAL INTENSITY
WAVELENGTH (A)
HD 84903
OBSERVED
[M/H] = -2.7,
[C/M] = -1.1, [N/M] = +0.4
c
3860
3870
3880

this star. Also shown on Figures 3a and 3b are the computed spectra from which all the CH and CN contributions have been removed. Thus, although the molecular features are weak, they are a major contributor to the opacity in these regions. Figure 3c illustrates the same wavelength interval as Figure 3b, but shows the IPCS data, which gives better resolution than the camera/grating combinations employed in obtaining most of the other observations. One point which should be noted is the good fit to all the strong metal lines (in particular λλ~3872, ~3878Å) in the IPCS data, compared to the poor fit to these same lines in the spectra obtained using the coudé focus of the 1.9m telescope at Mt. Stromlo. Additional observations should be obtained to investigate this anomaly. This star, which is a typical member of this group, will be considered further in the error analysis (§IV*c*).

HD 165195 — An extremely good fit was obtained using the atmospheric parameters shown in Table 2, and the C, N abundances of Table 3. Hence, the metal abundance from Wallerstein and Helfer (1966) is well justified. These authors also indicated that this star was peculiar in the δ(U-B) - [Fe/H]-plane. However, if the reddening, E(B-V) was reduced from 0.25 to 0.18 this anomaly vanished. In the present analysis, the larger reddening, which gives a hotter effective temperature produces synthetic spectra which closely resemble the observations. Recent work by Böhm-Vitense and Szkody (1974) has shown that HD 165195 does not have a peculiar ultra-violet excess for the metal abundance adopted, namely [M/H] = -2.5.

HD 184711 — This object is the most metal-deficient star in this program ([M/H] = -3.0). In fact, on the basis of the DDO photometry, it is the most metal-poor star which has ever been analysed. However it should be noted that the abundance for this star was obtained by extrapolating outside the δC(38-42) - [Fe/H] calibration of Osborn (1971). From the C and N analysis, carbon is overdeficient by a factor of ~2, while nitrogen is overabundant by a factor of ~10. However the computed metal-line strengths did not fit the observations, so the gravity, metal abundance, and microturbulence were varied in an effort to clarify the situation. For a gravity, log g = 0.85 and a [M/H] = -3.0, a fit to both the G-band and λ~3883Å CN band was obtained for [C/M] = -0.7 and [N/M] = +0.6. With a [M/H] = -2.7 and a log g = 0.50, [C/M] = -0.6 and [N/M] = +0.4. These latter determinations are the values given in Table 3. All of the above values were derived for a microturbulent velocity, ξ_t, of 2 km s^{-1}. However, ξ_t was increased to 3 km s^{-1}, with [M/H] = -3.0 and log g = 0.50, and a better fit was obtained to the observations, in particular the metal lines, since this increase does not affect the strength of the molecular lines (see §IV*c*). An increase in the microturbulent velocity could be justified since this object has the highest luminosity, and thus the most extended, and possibly the most turbulent atmosphere.

(c) Error analysis

The errors associated with the determination of the carbon and nitrogen abundances were investigated by altering the atmospheric parameters of one star, HD 84903, which can be considered to be typical of this group of objects. The gravity, metal abundance, and microturbulence were all changed by a factor of 2(.3 dex), while the effective temperature was varied by ±250 K. Only one parameter was changed at any one time. The results of this analysis are illustrated in Table 4. The change required in each abundance is considered independently of the other two.

From Table 4 it can be seen that the carbon abundance determination is almost independent of changes in the temperature, gravity, and [M/H]. The small temperature and gravity dependence of the G-band have been shown previously by Schadee (1968), but the insensitivity to changes in [M/H] is

TABLE 4

ERROR ANALYSIS FOR HD 84903

Atmospheric Parameter (1)	Δ[C/M] (2)	Δ[N/M] (3)	Δ[M/H] (4)
$\Delta T_{eff} = \pm 250K$	±0.05	±0.50	±0.10
$\Delta \log g = \pm 0.3$	∓0.05	±0.05	±0.05
$\Delta [M/H] = \pm 0.3$	∓0.05	∓0.30	-
$\Delta \log \xi_t = +0.3$	0.00	0.00	-0.50

Note: The order of the sign for each abundance corresponds to the order shown for each atmospheric parameter.

more interesting. As the metal abundance is lowered in these cool model atmospheres, the dominant continuous opacity source, H^- is also decreased, since it is dependent on the metals for its supply of electrons. In addition, the number density of CH molecules declines in unison with the metals. Thus the molecular line strength, which is determined by the ratio of line to continuous opacity, remains almost constant as the metal abundance is altered by a factor of 2. Consequently, the carbon abundances indicated in Table 3 are probably accurate to about ±0.2 in the logarithm. However, this does not take into account any errors which could be introduced due to variations in the oxygen abundance. This error estimate was not examined in this research, as it has been done previously by Sneden (1974; in particular see Table 5). For a star of about the same temperature, gravity and metal abundance as HD 84903, Sneden gave Δ[C/M] ~ ±0.30 for a Δ log O = ±0.50.

In contrast to the carbon abundance, nitrogen is much more sensitive to changes in some of the atmospheric parameters. The notable exception is the only slight Δ[N/M] for a Δ log g = 0.3, even though CN is normally a luminosity indicator. Over a factor of 2 in the gravity this effect is not apparent.

The strong temperature dependence of the nitrogen abundance determination, using bands of CN, has been discussed earlier by Sneden (1974). It is a result of the larger dissociation energy of CN (*cf.* CH, $D_o = 3.5$ eV) and thus its greater sensitivity to changes in the effective temperature, via the dissociation equation.

It was shown that the carbon abundance, determined from CH, is unaffected by changes in the overall metal abundance. If the abundance of nitrogen was derived from NH features, a similar conclusion could be applied to this element. However, the paucity, and lower resolution of the NH observations, compared with the CN bands, meant that one has to rely on the CN features. As the metal abundance is lowered, the CN number density declines as the square of the metal abundance, whereas the continuous opacity (H^-) is a linear function of [M/H]. Thus, in order to fit the CN bandheads, one has to increase the N abundance by approximately the same amount that the metals have been reduced. This effect can be seen in Figure 4, in which the nitrogen to overall metal abundance, [N/M], has been plotted as a function of [M/H], using values from Table 3 for all the program stars. The horizontal and vertical arrows summarize the above discussion. Figure 4 also illustrates a possible correlation between nitrogen enrichment and metal abundance. This will be discussed further in §V.

The overall metal abundance is the only parameter which is significantly affected by the microturbulence, since the molecular lines, from which [C/M] and [N/M] are derived, are on the linear portion of the curve-of-growth (see Sneden 1974). However, the original choice of $\xi_t = 2$ km s^{-1}, which gives a good fit to most of the observational data, also compares favourably with values given by Sneden (1974).

In summary, the carbon abundances are well determined in this analysis,

FIG. 4. - [N/M] vs. [M/H] for the giants observed in this study. The horizontal and vertical arrows show that if the metal abundance is reduced by 0.3 dex, the nitrogen abundance must be enhanced by a similar factor. Thus for reliable nitrogen abundances, a reasonable fit is required between the observed and computed atomic lines.

FIG. 5. - [M/H] vs. log g for the giants analysed in this work, ●, and those investigated by Sneden (1974), ○.

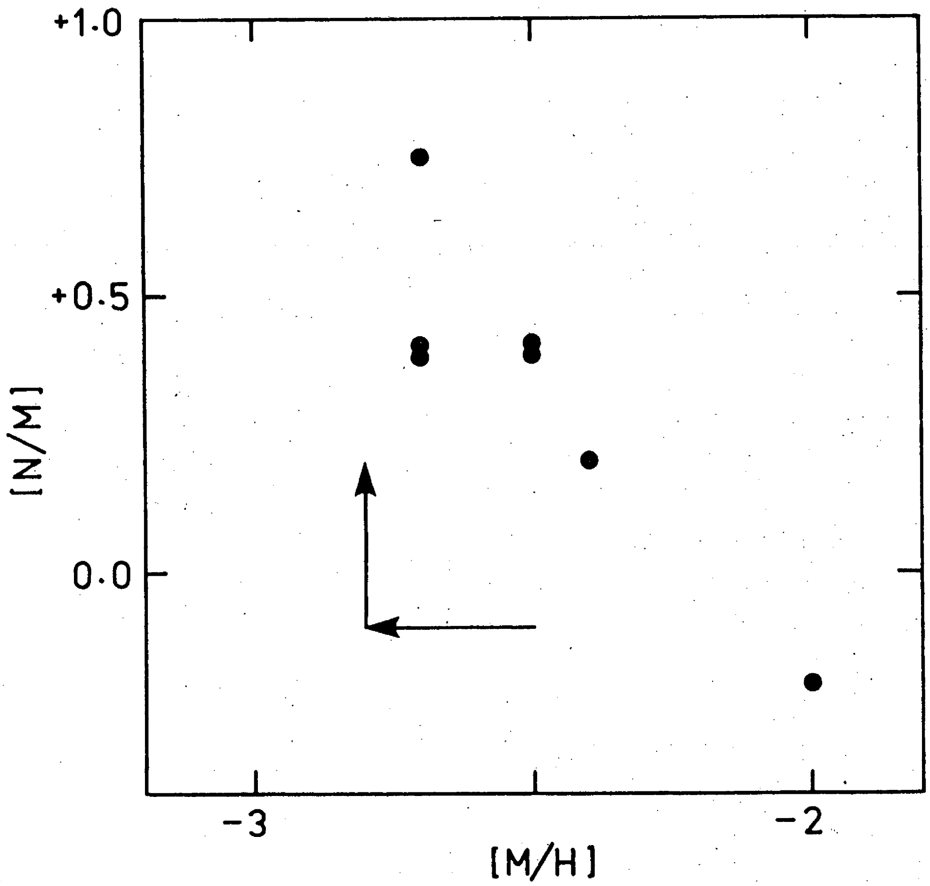
+1.0
+0.5
0.0
[N/M]
−3
−2
[M/H]

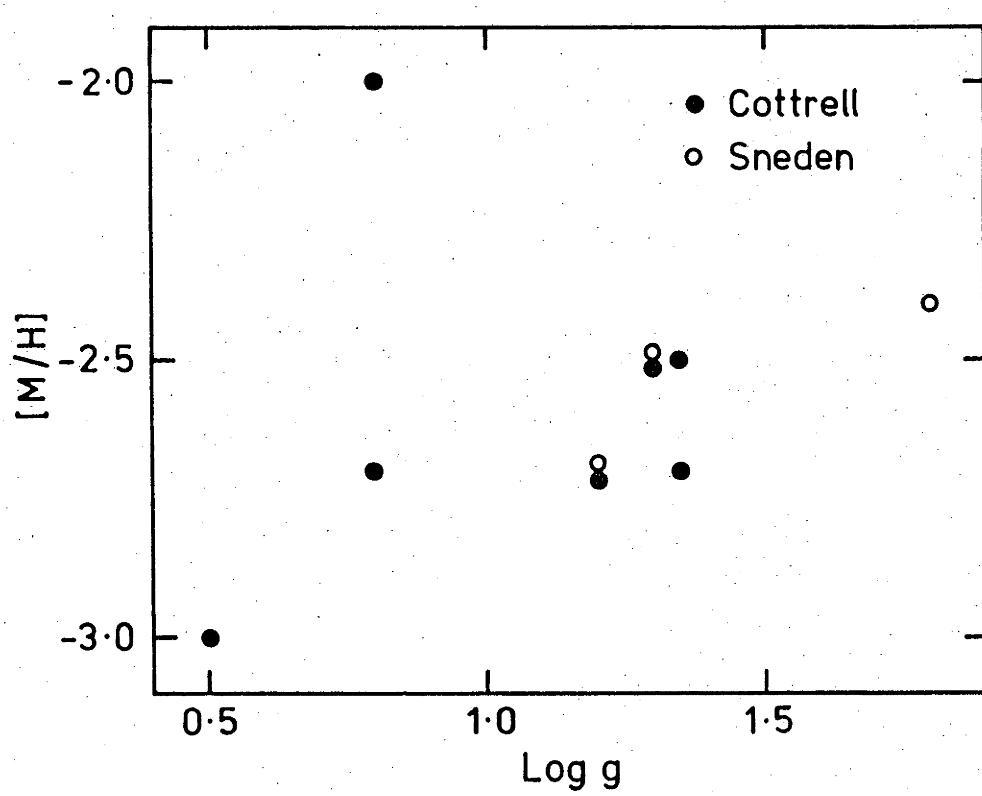
-2.0
-2.5
-3.0
[M/H]
0.5
1.0
1.5
Log g
Cottrell
Sneden

whereas the derived nitrogen abundances are sensitive to changes in the effective temperature and [M/H].

V. DISCUSSION OF THE CARBON AND NITROGEN ABUNDANCE RESULTS

This research has analysed a small sample of extremely metal-poor giants, in order to investigate the possible effects of mixing in highly evolved objects. Sneden (1974) undertook a similar investigation, but he considered objects which had a larger range in gravity, $1.2 \lesssim \log g \lesssim 3.8$. However, three of his objects had similar gravities to those considered in this work. One star, HD 122563 was common to both studies. All of these stars are shown in the [M/H]-log g plane (Figure 5), where the [M/H] and log g's for the program stars have been taken from Table 2. By identifying individual points in Figure 4, there is a general trend for the objects with the lowest gravities to be those with the largest nitrogen enhancement. This last relationship, [N/M] versus log g, is shown in Figure 6. Thus for conclusions to be drawn from the abundance results obtained in the previous section, the effect shown in Figure 5, that the lowest metal abundance objects have the smallest gravities, has to be considered. This is well-illustrated in Figure 4, where one could propose that there was a strong correlation between nitrogen enrichment and metal abundance. This correlation could be misleading due to the small sample of stars which have been analysed.

In addition to the nitrogen enhancement, [C/N] shows a strong correlation with gravity (Figure 7); the lower the gravity, the smaller is the value of [C/N]. A least squares fit to this data is

$$[C/N] = 0.5(\log g) - 1.3.$$

This general result appears similar to that obtained by Dearborn *et al.* (1976) in their investigation of the $^{12}C/^{13}C$ ratio in red giant stars.

FIG. 6. - [N/M] vs. log g for the program stars. The error bar is for HD 184711, and indicates the effect on the abundance for small changes in the atmospheric parameters (see text, §IV*b*).

FIG. 7. - [C/N] vs. log g for the program stars. The error bar is as for Fig. 6.

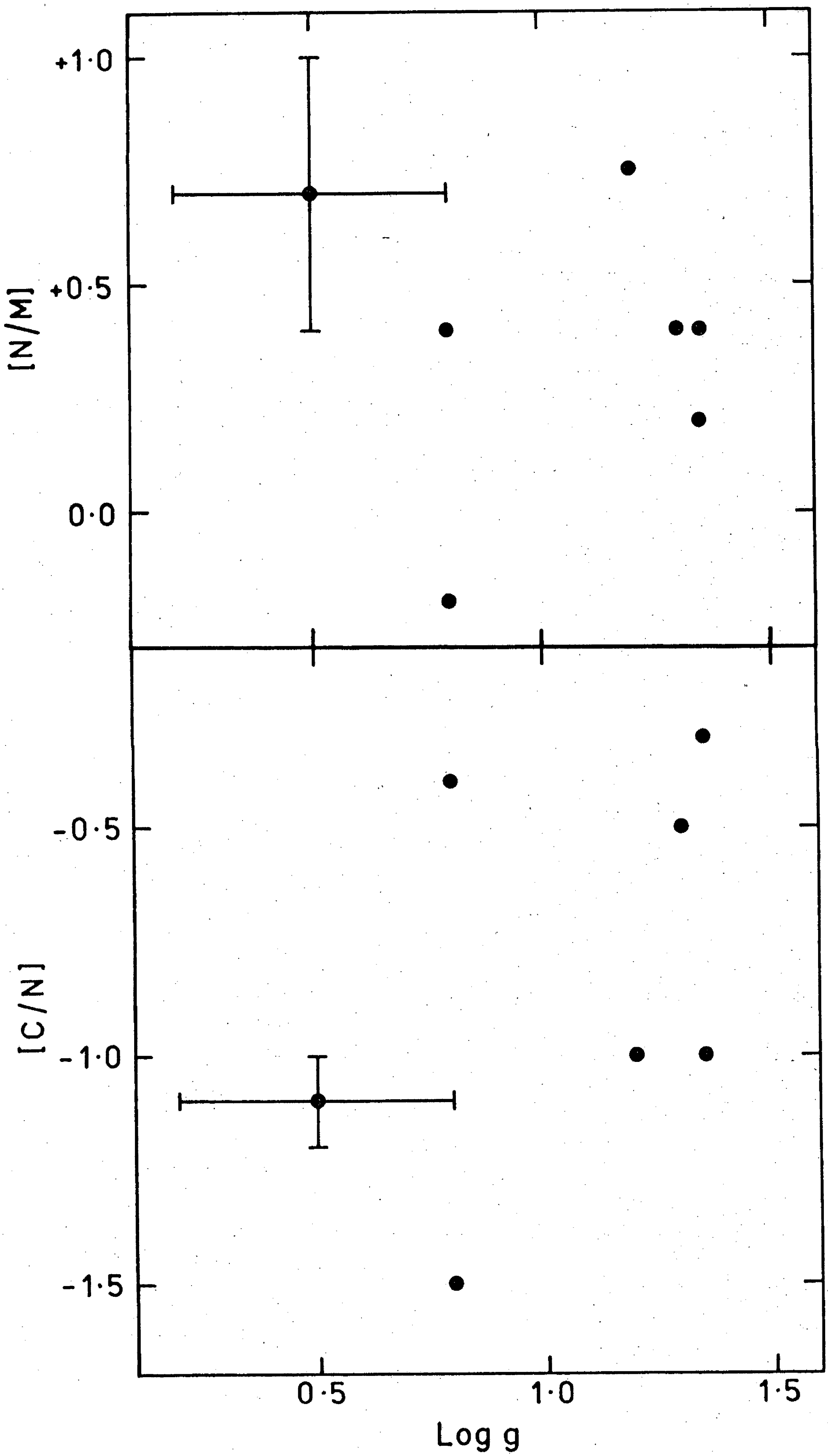
+1·0
+0·5
0·0
[N/M]
-0·5
-1·0
-1·5
[C/N]
0·5
1·0
1·5
Log g

They found that with increasing luminosity this ratio decreased from near solar values (~90) at $\log L/L_\odot \sim 0.5$ to values of ~10 at $\log L/L_\odot \sim 3.0$.

The connection between $^{12}C/^{13}C$ and C/N was also discussed by Dearborn *et al.* (1976). During main-sequence evolution, ^{12}C is burned via the CNO cycle. One of the products of this burning is ^{13}C. However, the ultimate product is N. As the star evolves off the main sequence, a deepening surface convection layer can mix both ^{13}C and N into the outer layers, producing both low $^{12}C/^{13}C$ and low C/N. For Dearborn *et al.*'s (1976) group of stars, this once only deep penetration of the surface convective zone is not sufficient to produce the extremely low $^{12}C/^{13}C$ ratios of ~5-10 observed in some of their objects. The above authors considered that mass loss and hydrogen-shell instabilities could reproduce their observations, without having to invoke abnormally low $^{12}C/^{13}C$ ratios in the interstellar medium. However, the artificial nature of these instabilities must always be remembered.

For the above arguments to be applied to the objects studied here, it is necessary to establish that the program stars have luminosities lower than that required for He-shell flashing. Using

$$\log L/L_\odot = 0.4(4.75 - M_{bol}),$$

and the M_V's from column (7) of Table 1, we obtain luminosities between ~2.5 and ~3.3. Theoretical calculations for 0.6 $M_\odot$ and 1 $M_\odot$ Population II stars by Gingold (1974) and Schwarzschild and Härm (1967), indicate that helium-shell flashes begin at luminosities, $\log L/L_\odot$ of ~3 and ~2.7, respectively. Thus at least some of the objects in our sample are not sufficiently luminous for shell flashing to be the cause of the mixing phenomenon. Therefore similar reasoning to that discussed by Dearborn *et al.* (1976) could be applied to some of the Population II stars analysed in the present research.

However mixing of CNO-processed material during helium-shell flashes could be the process by which some of these stars obtained their peculiar abundances. Gingold (1974) was only able to produce a small change in the surface C and N abundances in the evolution of his 0.6 $M_{\odot}$ Population II model through 14 relaxation oscillation cycles. Thus either an increase in the efficiency of the mixing or substantial mass loss (or both) would be required to produce conditions under which the abundances observed in this analysis could be obtained at this phase of evolution. However a combination of mixing on both the first and second giant branches could also produce low carbon and enhanced nitrogen abundances in the surface layers. A larger sample of stars is required before the solution can be finally resolved, but if a two-phase process is operating, there should be a larger scatter in the [C/N]-log g plane for log g $\lesssim$ 0.80, compared with > 0.80, since objects with log $L/L_{\odot} \gtrsim 3$ could be in either phase of evolution.

VI. CONCLUSIONS

Using spectrum synthesis techniques, the carbon and nitrogen abundances have been determined in seven extremely metal-poor giants, selected mainly from the lists of Bidelman and MacConnell (1973). Considering the stars as a group, the C/N ratio exhibits a correlation with gravity, given by the following least squares fit to the data points,

$$[C/N] = 0.5(\log g) - 1.3,$$

for $0.50 \lesssim \log g \lesssim 1.35$. The higher gravity limit of this relation can be extended to 2.4, since Sneden's (1974) observations fit the above expression, within the errors quoted. Some of these objects are probably not sufficiently luminous for helium-shell flashing to have commenced, so these abundances would appear to be a result of mixing during the first ascent of the red giant branch. Thus the discussions of Dearborn *et al.* (1976), who investigated the $^{12}C/^{13}C$ ratio for stars in this evolutionary phase, appear to be relevant in the interpretation of the above results, since both ^{13}C and N are formed from ^{12}C in the CNO-burning cycle. This produces low $^{12}C/^{13}C$, enhanced nitrogen and a low C/N ratio. The variation with decreasing gravity (increasing luminosity) may be produced, according to Dearborn *et al.* (1976), by a combination of mass loss and hydrogen-shell instabilities, where each instability mixes some of the CNO-processed material into the surface layers. However, for objects more luminous than $\log L/L_{\odot} \sim 3$, the observed abundances could be a result of helium-shell flashes and/or the processes discussed above. Thus in a larger sample of objects, a large scatter in the [C/N]-log g relationship for $\log g \lesssim 0.8$ could indicate that both processes are involved.

Acknowledgements

I wish to thank Drs. John Norris and Mike Bessell for allowing me access to their photometric data of these objects prior to publication. In addition, Dr. John Norris has made many useful comments on the manuscript. I acknowledge the support of an Australian National University Post-Graduate Award, which enabled access to the UNIVAC 1100/42 Computer, operated by the Australian National University Computer Services Centre.

REFERENCES

Alexander, J. B. 1971, *M.N.A.S.S.A.*, 30, 139.

Arnold, J. O., and Nicholls, R. W. 1973, *J.Quant.Spectrosc. and Rad.Transf.*, 13, 115.

Ball, C., and Pagel, B. E. J. 1967, *Observatory*, 87, 19.

Bell, R. A., Ericksson, K., Gustafsson, B., and Nördlund, Å., 1976, *Astr. Ap. Suppl.*, 23, 37.

Bessell, M. S. 1976, *Pub. A.S.P.*, 88, 557.

Bessell, M. S., and Norris, J. 1978, private communication.

Bidelman, W. P., and MacConnell, D. J. 1973, *A.J.*, 78, 687.

Böhm-Vitense, E. 1973, *Astr. Ap.*, 24, 447.

————. 1975, in *Problems in Stellar Atmospheres and Envelopes*, ed. B. Baschek, W. H. Kegel, G. Traving (Berlin: Springer-Verlag), p. 21.

Böhm-Vitense, E., and Szkody, P. 1974, *Ap. J.*, 193, 607.

Cottrell, P. L. 1978, *Ap. J.*, July 1st issue (Chapter 5).

Cottrell, P. L., and Norris, J. 1978, *Ap. J.*, 221, 893 (Chapter 2).

Dearborn, D. S. P., Lambert, D. L., and Tomkin, J. 1975, *Ap. J.*, 200, 675.

Dearborn, D. S. P., Eggleton, P. P., and Schramm, D. N. 1976, *Ap. J.*, 203, 455.

Eggen, O. J. 1974, *Pub. A.S.P.*, 86, 697.

Gingold, R. A. 1974, *Ap. J.*, 193, 177.

Johnson, H. L. 1966, *Ann. Rev. Astr. Ap.*, 4, 193.

Kron, G. E. 1978, preprint.

Lambert, D. L., Sneden, C., and Ries, L. M. 1974, *Ap. J.*, 188, 97.

Norris, J., Bessell, M. S., and Pickles, A. 1978, private communication.

Osborn, W. H. 1971, Ph.D Thesis, Yale Univ.

Pagel, B. E. J. 1965, *R.O.B.*, No. 87.

Sackmann, I.-J., Smith, R. L., Despain, K. H. 1974, *Ap. J.*, 187, 555.

Schadee, A. 1968, *Ap. J.*, 151, 239.

Schwarzschild, M., and Härm, R. 1967, *Ap. J.*, 150, 961.

Sneden, C. 1973, *Ap. J.*, 184, 839.

————. 1974, *Ap. J.*, 189, 493.

Sneden, C., Lambert, D. L., Tomkin, J., and Peterson, R. C. 1978, preprint.

Ulrich, R. H., and Scalo, J. M. 1972, *Ap. J.*, 176, L37.

————. 1973, *Ap. J.*, 183, 151.

Wallerstein, G., Greenstein, J. L., Parker, R., Helfer, H. L., and Aller, L. H. 1963, *Ap. J.*, 137, 280.

Wallerstein, G., and Helfer, H. L. 1966, *A.J.*, 71, 350.

Wolfram, W. 1972, *Astr. Ap.*, 17, 17.

Zinn, R. 1973, *Ap. J.*, 182, 183.

————. 1977, *Ap. J.*, 218, 96.

CHAPTER 5

EXTREME SUBDWARFS. I MOLECULAR BAND STRENGTHS: A THEORETICAL APPROACH

P. L. Cottrell

ABSTRACT

For subdwarf stars with effective temperatures $\lesssim$ 5500 K, the G-band region, which is a conglomerate of many atomic and molecular (CH) lines, is shown by spectrum synthesis to be an extremely sensitive metal abundance discriminator. In particular, some of the spectra computed for metal-deficient model atmospheres in the wavelength interval 4290 to 4330Å show that this feature is *stronger* than that for the normal abundance model at the same effective temperature and gravity. Thus the "CH strong" red subluminous stars classified by Greenstein, can be adequately interpreted as belonging to this group of stars, rather than unevolved stars having an overabundance of carbon. The behaviour of CO, OH, and H_2O molecules in determining the amount of free carbon available for CH formation in stellar atmospheres is discussed for a grid of flux-constant model atmospheres. Synthetic G-bands constructed with this grid of dwarf and subdwarf model atmospheres enable metal abundances to be derived for subdwarf stars with effective temperatures between 4000 K and 6000 K. In addition, molecular bands of magnesium hydride were constructed for some of the coolest model atmospheres and these show that this feature is a similar metal abundance discriminator for subdwarfs with $T_{eff} \lesssim$ 4000 K.

I. INTRODUCTION

Greenstein (1971) discussed spectra of a number of large ultraviolet excess, high proper motion stars which he investigated in his search for possible degenerate objects. Although his research did not reveal many new degenerates, he commented on any peculiarities which he noticed in the spectra which he had obtained for these red subluminous stars. The most frequent remark concerned the strength of the G-band, which is an absorption feature near 4300Å and consists of a large number of atomic and molecular (CH) lines. Greenstein had both "CH strong" and "CH weak" categories for these metal-deficient main-sequence or subdwarf stars. In some of the cooler sample of these stars, with B-V's ~ 1.4, he noticed that the MgH bands of the A $^2\Pi$ - X $^2\Sigma$ system or the Mg *b* line region, which is situated near the (0,0) and (1,1) bandheads of this MgH system, were stronger than expected for a star's spectral type and metal abundance. This latter parameter was interpreted from other metal-line features. In a recent abstract, Bidelman and Smethells (1976) proposed that CaH and MgH bands are metal abundance discriminants, since they found considerable variation in CaH band strengths with stars of the same (TiO-band) spectral type for K and M dwarf stars identified on objective-prism plates. Hence Greenstein's (1971) comments about the MgH bands possibly refer to this metal abundance effect.

In the present work G-band and MgH-band synthetic spectra (§III) were computed for a grid of dwarf and subdwarf model atmospheres (§II). These spectra were then used to interpret Greenstein's "CH" and "MgH" classifications. These could either correspond to carbon and magnesium abundance anomalies (e.g., GH7-21 [Wegner 1975] and G77-61 [Dahn *et al.* 1977] for the "CH" designations) or could be explained by molecular association effects in the atmospheres of these stars. This was investigated by a detailed analysis of the molecular equilibria (§IV) in our grid of model atmospheres.

II. MODEL ATMOSPHERES AND THE SPECTRUM SYNTHESIS TECHNIQUE

The flux-constant model atmospheres used in this analysis were constructed in a similar manner to those discussed in Wickramasinghe, Bessell and Cottrell (1977, hereafter WBC I), using the ATLAS model atmosphere program (Kurucz 1970), and will be described elsewhere (Bessell, Cottrell, and Wickramasinghe (1978, hereafter WBC II). The basic parameters are shown in columns (1), (2), and (3) of Table 1, where [A/H] is the lograithmic abundance of all elements, except H and He, relative to the solar abundances of Lambert (1968). In particular, C, N, and O abundances are varied in unison with the overall metal abundance. A number of model atmospheres have also been included from Mould's (1976) grid of M-dwarfs, in particular, the cooler metal-rich models. In his treatment Mould included line blanketing, TiO, and H_2O opacity sources, and consequently his models are more realistic. Mould's models are indicated in Table 1. To derive molecular number densities of species required by our synthesis program, the following molecules were included in the equilibrium equations: H_2, H_2O, CH, CH_2, NH, OH, CO, CO_2, CN, NO, N_2, MgH, MgO.

Subdwarf analyses (*cf.* Hearnshaw 1976) indicate that log g = 5 is a representative value for the gravity of stars at the cool end, $T_{eff} \lesssim$ 5000 K, of the subdwarf sequence. However, for hotter and possibly more evolved subdwarfs, e.g., HD 140283 and HD 19445, with $T_{eff} \sim 5800$ K, log g ~ 4 has been determined to be a better estimate of the gravity (Cohen and Strom 1968). Thus we have computed some G-band synthetic spectra for both log g = 4 and 5 at effective temperatures of 4000 K, 4500 K, and 5000 K, to determine the gravity dependence of this feature.

Synthetic spectra were computed by using a similar technique to that employed by Cottrell and Norris (1978). The particular regions of interest were, (1) the G-band between 4290 and 4330Å, which generally has a large

TABLE 1

MODEL ATMOSPHERIC PARAMETERS AND EQUIVALENT WIDTHS (Å)

			G-band Strengths			MgH-band Strengths	
T_{eff} (1)	log g (2)	[A/H] (3)	Total (Emergent Flux) (4)	Convolved (FWHM = 2Å) (5)	Molecular Component (6)	Total (7)	Molecular Component (8)
3500	5.0	† 0	13.9	11.6	0.1	48.8	37.6
		† -1	-	-	-	49.7	40.4
		† -2	12.8	11.5	0.5	50.2	41.7
		-4	18.2	18.1	9.3	27.9	22.4
4000	5.0	† 0	14.0	11.4	0.5	44.8	30.9
		† -1	-	-	-	35.6	25.8
		-2	10.1	9.6	3.9	27.7	20.3
		-3	12.5	12.3	8.2	20.0	15.9
		-4	14.1	14.1	12.4		
		-5	11.1	11.1	10.4		
	4.0	-3	9.7	9.6	7.1		
4500	5.0	0	16.8	14.5	3.4		
		-3	8.0	8.0	6.2		
	4.0	0	-	-	-	32.5	20.4
		-2	12.0	11.8	8.3	9.1	5.9
		-3	7.8	7.8	6.5		
5000	4.0	0	15.4	13.3	5.0		
		-2	9.7	9.6	8.2		
		-3	3.6	3.6	2.8		
	5.0	-3	3.6	3.6	2.8		
5500	4.0	0	13.3	11.5	7.5		
		-2	4.2	4.0	2.9		
		-3	0.8	0.8	0.5		
6000	4.0	0	9.8	8.2	5.5		
		-2	1.3	1.1	-		

† Using models from Mould (1976).

amount of molecular, CH, absorption, and (2) the region between 5115 and 5215Å, in which we included the Mg *b* lines, and the lines of the $\Delta v = 0$ vibrational transitions of the MgH A $^2\Pi$ - X $^2\Sigma$ system. At these wavelengths H^- is the dominant continuous opacity source in all the model atmospheres, including the coolest models at T_{eff} = 3500 K. However, for all except the normal abundance, [A/H] = 0 models, with $T_{eff} \lesssim 4000$ K, the H_2 dipole opacity determines the atmospheric structure, since in the metal-deficient models there are very few metals which can provide electrons for H^- to form. The atmospheric structure of all the models in this grid will be discussed further in WBC II. One significant modification to the synthesis program used by Cottrell and Norris (1978) was the division of the line list into three segments, (1) strong metal lines, e.g., 4307.9Å, 4325.8Å for the G-band, and the Mg *b* lines for the MgH feature, (2) weak metal lines, and (3) all the molecular lines, CH lines for the G-band and MgH lines for the synthetic spectra between 5115 and 5215Å. For the MgH region, no weak metal lines were included, since our main purpose in computing this feature was to illustrate the great difference between the molecular feature and any atomic feature, i.e., the Mg *b* lines. The above segmentation enabled each portion of the line list to be treated differently as in a 4000 K normal abundance dwarf the strong lines have contributions at least 10Å away from their line centers, while the molecular lines only have significant contributions (>0.5%) within ~ 0.5Å of the central wavelength.

III. SYNTHETIC SPECTRA

(a) G-band spectra

As a consequence of the observations of Greenstein (1971) (see §I), we computed G-band synthetic spectra for our grid of model atmospheres shown in Table 1. Four synthetic spectra are shown in Figure 1, two each

FIG. 1. - Synthetic G-bands convolved with a Gaussian whose FWHM = 2Å. (a), (b), T_{eff} = 4000 K, log g = 5.0, [A/H] = 0,-3, respectively. (c), (d), T_{eff} = 5000 K, log g = 4.0, [A/H] = 0,-2, respectively. The solid line represents the total G-band, whereas the dashed line is just the atomic-line component of the G-band.

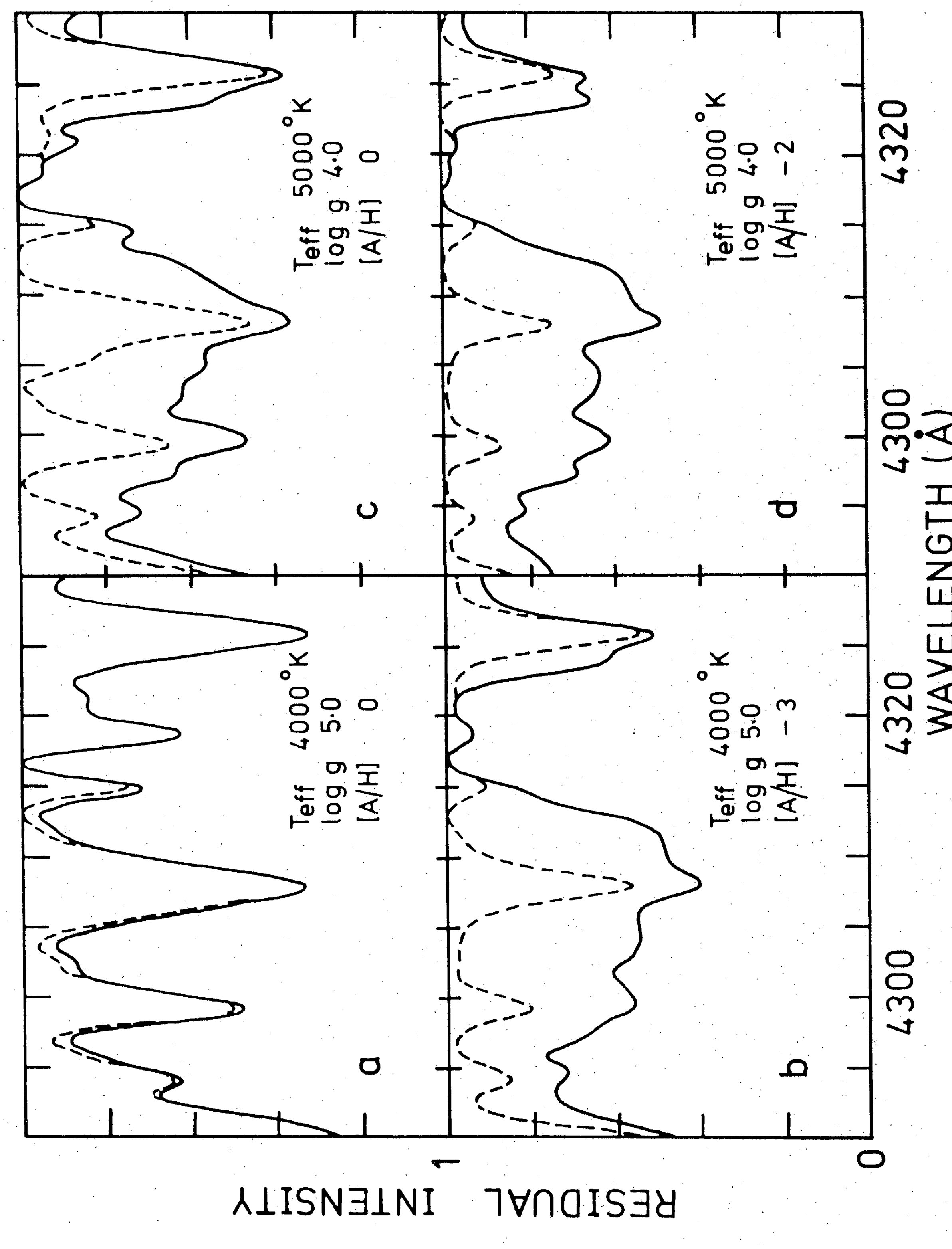

RESIDUAL INTENSITY
1
0
WAVELENGTH (Å)
4300
4320
4300
4320
a
Teff 4000°K
log g 5.0
[A/H] 0
b
Teff 4000°K
log g 5.0
[A/H] −3
c
Teff 5000°K
log g 4.0
[A/H] 0
d
Teff 5000°K
log g 4.0
[A/H] −2

at T_{eff} = 4000 K and 5000 K, and illustrate a major result of this research, namely, that the G-band strengthens or at least remains stronger than neighbouring purely atomic spectral regions as the metal abundance is lowered in cool, $T_{eff} \lesssim 5500$ K, dwarf atmospheres. In Figure 1 we have superimposed the metal-line component on the total G-band feature to emphasise the effect of metal abundance variations on the molecular component at these two temperatures. This gives an explanation for Greenstein's "CH strong" objects. A detailed analysis of individual stars from Greenstein's lists and other peculiar subdwarfs (e.g., GH7-21) will appear in a future paper of this series.

The equivalent width of the G-band between 4290 and 4330Å was computed for all the models in Table 1, and is shown in column (4) of this table. Also shown in column (6) of Table 1 is the molecular (i.e. CH) component of the G-band for most of these models. Although this parameter cannot be measured in any stellar spectrum, we tabulate it here to show the large temperature and metal abundance effect on this molecular feature. These two sets of data are also displayed in Figures 2a,b respectively. We have chosen two effective temperatures, 4000 K and 5000 K, to illustrate our results in detail.

Firstly, at T_{eff} = 4000 K, the total equivalent width of the G-band exhibits a complicated variation with decreasing metal abundance: the strength at first decreasing as the abundance goes from normal, [A/H] = 0, to [A/H] = -2, then increasing over the next two orders of magnitude, and finally decreasing again as the abundance is lowered to [A/H] = -5. This complexity can be understood by examining Figure 2b at T_{eff} = 4000 K, showing that the molecular component increases as the metal abundance is lowered from normal to [A/H] = -4. Thus the CH absorption is compensating, and in some instances overcompensating, for the decreasing atomic component of the G-band.

FIG. 2. - Synthetic G-band equivalent widths as a function of effective temperature (a) Total G-band strength. The equivalent width for the same region has been measured on the solar spectrum (Minnaert, Mulders, and Houtgast, 1940) and is shown in the Figure. This indicates the errors associated with these synthetic spectra. (b) The molecular, CH, component of the G-band. Metal abundances, [A/H] are shown on each of the curves. Open symbols correspond to log g = 4.0 models, and closed symbols to log g = 5.0 in both (a) and (b).

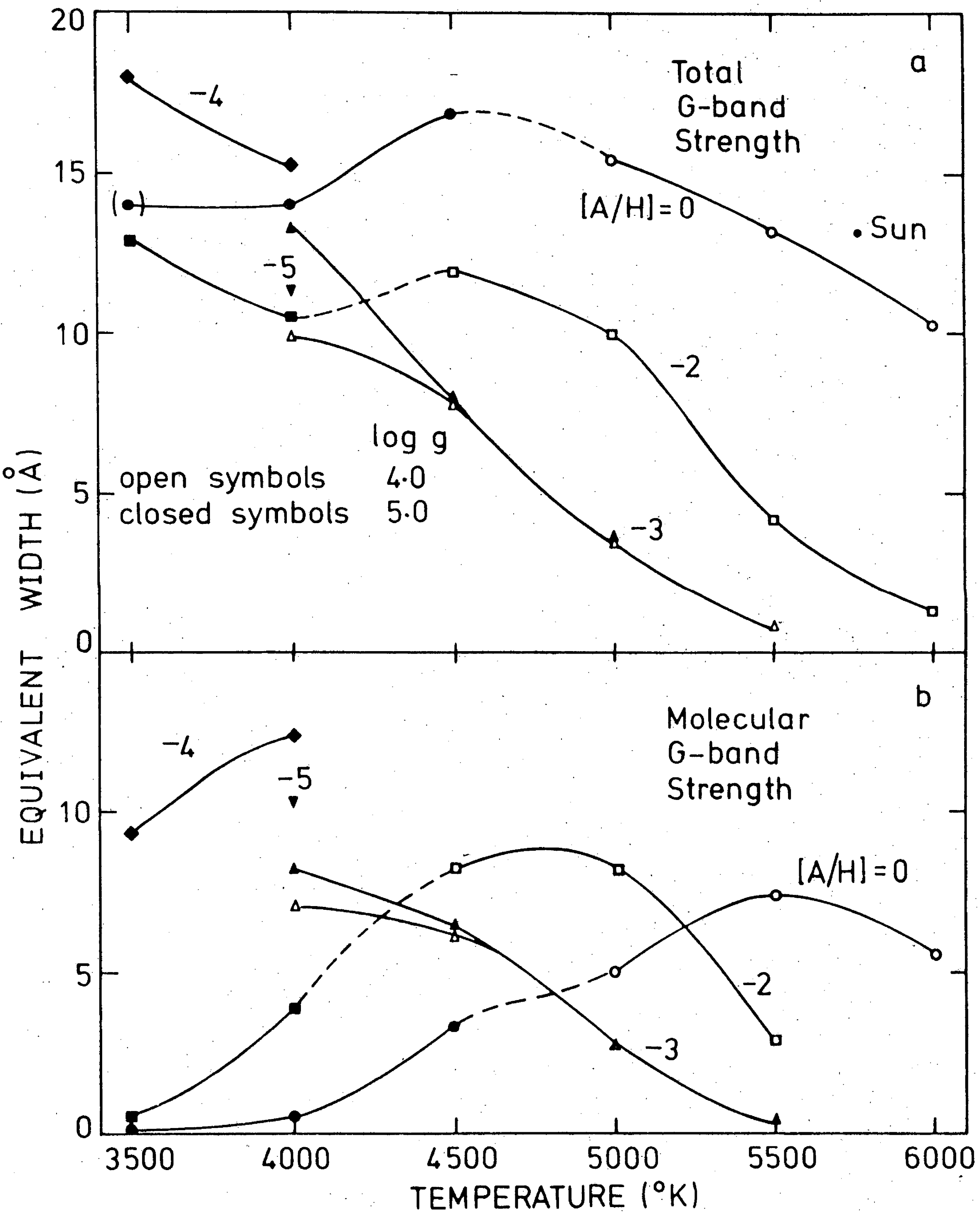
Total
G-band
Strength
a
-4
[A/H] = 0
• Sun
-5
-2
log g
open symbols 4·0
closed symbols 5·0
-3
EQUIVALENT WIDTH (Å)
20
15
10
5
0
b
Molecular
G-band
Strength
-4
-5
[A/H] = 0
-2
-3
10
5
0
3500
4000
4500
5000
5500
6000
TEMPERATURE (°K)

Secondly, at T_{eff} = 5000 K, although the same complex variation is not apparent as at 4000 K, molecular absorption over the first factor of 100 in metal abundance has a similar compensating function. Thus at this higher temperature, although the overall strength of the G-band decreases with a lowering of the abundance, the rate of decrease is not as steep as the weakening of the metal lines in adjacent regions of the spectrum (WBC II).

The equivalent widths plotted in Figures 2a and 2b are evaluated directly from the fluxes computed using our synthesis program. However, for comparison with data acquired at the telescope we have convolved these fluxes with a Gaussian profile which has a full width at half maximum (FWHM) of 2Å. The results are tabulated in column (5) of Table 1. The consequence of this convolution over such a small wavelength range is to depress the 'continuum' points, thus decreasing the theoretical strength of the G-band. This decrease is most extreme in the cool ($T_{eff} \leq$ 4500 K) metal-rich model atmospheres, as there are strong metal lines throughout the interval 4290 to 4330Å. However, in the metal-poor models, for example the T_{eff} = 4000 K, log g = 5.0, [A/H] = -4 model, the equivalent widths before and after convolution, columns (4) and (5) of Table 1 vary by less than one percent. In the above model ~70% of the absorption is produced by CH lines, and as there are none of these lines in the interval 4315 to 4323Å, as well as the lack of strong metal lines in this same interval, the emergent fluxes in this region remain unaffected by the convolution.

The gravity effect discussed in §II, that log g = 5 is the best estimate for cool subdwarfs, has only a minimal effect on our G-band strengths at both 4500 K and 5000 K. However, the lower gravity model at 4000 K has a total G-band strength which is only about 75% that of the log g = 5 model. Since, the atomic-line component is the largest factor in this decreasing strength one requires independent estimates of both the temperature and the gravity, in order to derive reliable abundances at this and cooler temperatures.

We conclude that for dwarf-type gravities, log g = 4 to 5, and effective temperatures ≲ 5500 K one can expect the G-band region to be stronger than neighbouring features in metal-deficient stars, provided most elemental abundances, in particular carbon and oxygen, behave in a similar manner. Thus the subluminous stars classified by Greenstein (1971) as having strong CH for their spectral type may not necessarily be overabundant in carbon (Greenstein 1969), but could belong to a group of stars for which we have computed synthetic spectra from our grid of model atmospheres. In the next section we show our results for the MgH bands.

(b) MgH spectra

Bands of magnesium hydride are observed in the region of the Mg *b* lines at λ~5200Å, and these bands were another distinguishing feature which Greenstein (1971) noted in some red subluminous stars.

In Figure 3 we show four representative MgH synthetic spectra at T_{eff} = 3500 K and 4000 K, with [A/H] = 0 and -2. These spectra, together with the band strengths shown in column (7) and (8) of Table 1 indicate that MgH bands in this temperature regime behave in a similar manner to the G-bands at temperatures of ~5000 K. That is, absorption by the MgH molecule for $T_{eff} \lesssim 4000$ K remains stronger than the absorption by neighbouring purely atomic-line regions of the spectrum as the metal abundance is lowered.

This is clearly evident at 3500 K, where lowering the abundance from normal to 10^{-2} actually results in a marginal strengthening of the MgH component. The Mg *b* lines, however, are reduced to 75% of their value at normal abundance. The effect at 4000 K is more subtle, but the decreasing strength of the molecular component is not as rapid as the decline in the Mg *b* line strengths.

FIG. 3. - Synthetic spectra between 5115 and 5215Å convolved with a Gaussian whose FWHM = 4Å. (a), (b), T_{eff} = 3500 K, log g = 5.0, [A/H] = 0,-2, respectively. (c), (d), T_{eff} = 4000 K, log g = 5.0, [A/H] = 0,-2, respectively. The solid line represents absorption by magnesium hydride plus that by the Mg*b* lines, whereas the dashed line is the Mg*b* line component.

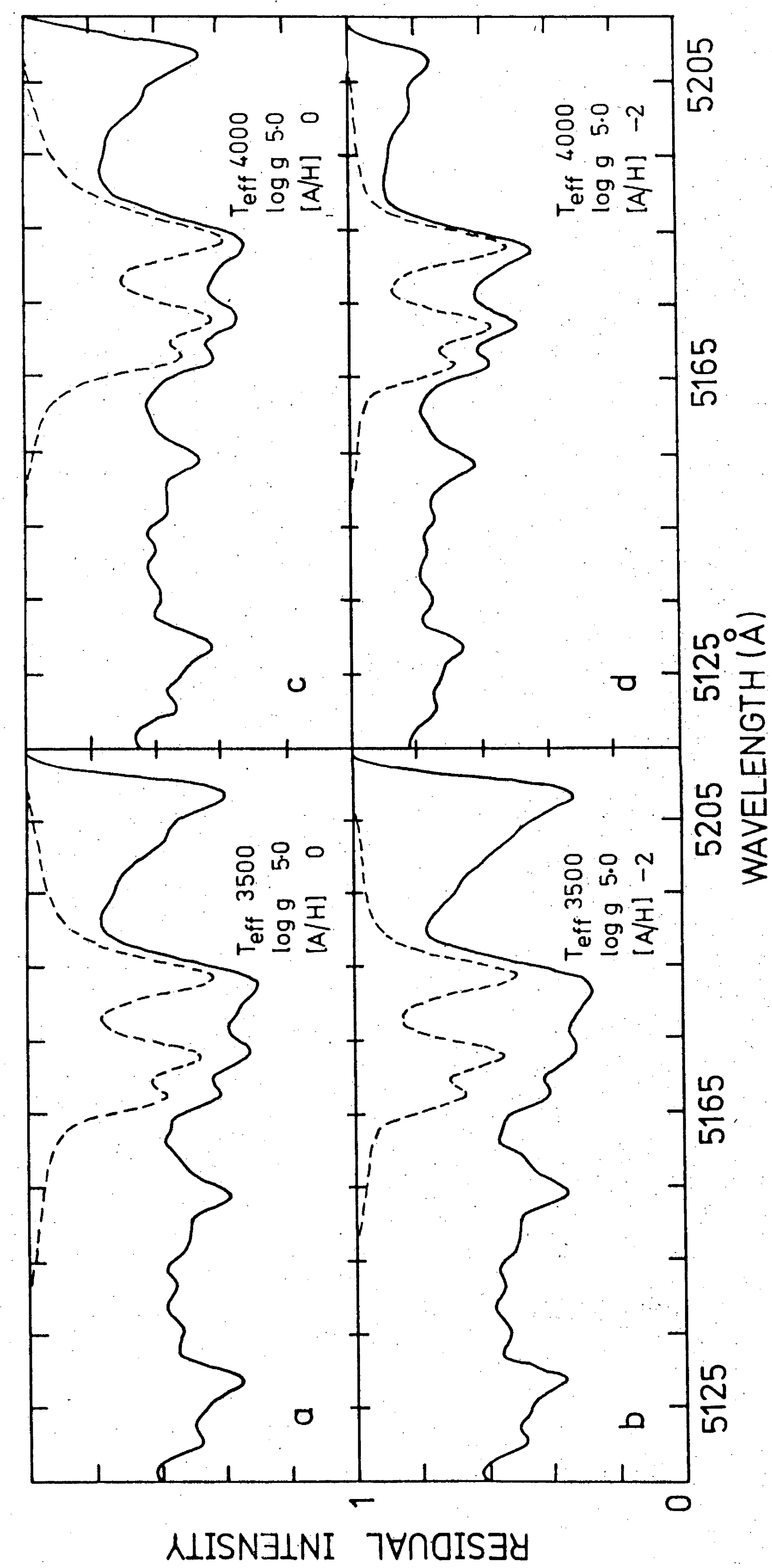
a
T_{eff} 3500
log g 5·0
[A/H] 0
b
T_{eff} 3500
log g 5·0
[A/H] −2
c
T_{eff} 4000
log g 5·0
[A/H] 0
d
T_{eff} 4000
log g 5·0
[A/H] −2
5125
5165
5205
WAVELENGTH (Å)
RESIDUAL INTENSITY
1
0

As the temperature is increased to 4500 K the effect disappears, and the MgH band and Mg *b* line strengths decline in unison. However, this is the regime where CH is becoming a good discriminant. Thus, for effective temperatures less than 5500 K we have two abundance discriminants, CH for the hotter stars, and MgH for the cooler ones. In §IV we will discuss the molecular equilibrium conditions so that we can understand the cause of the above effects.

IV. DISCUSSION OF MOLECULAR EQUILIBRIA

The variation in band strengths discussed in the previous section can be explained by scrutiny of the number densities of the relevant species in each of the model atmospheres. The molecular line strength can be expressed as

$$\mathcal{R} = \frac{\kappa_{line}}{\kappa_{cts}} \propto \frac{N_{line}}{N_{cts}} ,$$

where κ_{line}, κ_{cts} are respectively the line and continuous opacities, and N_{line}, N_{cts} are the number densities of species forming the line and continuous opacity. We consider CH and MgH separately.

(a) CH

For this molecule we again use the models at 4000 K and 5000 K to interpret the variation in strength of the G-band molecular component. Since H^- is the dominant continuous opacity source in all our models at $\lambda \sim 4300$Å, the relative strengths of the CH component of the G-band at a given effective temperature and for varying metal abundance can be compared directly by forming the ratio $N(CH)/N(H^-)$ over a range of optical depths (Rosseland mean optical depth, τ_{ROSS}, from 10^{-3} to 1). These are shown in Figures 4a,b for T_{eff} = 4000 K and 5000 K, respectively. The number densities for all relevant species in most of the 4000 K and 5000 K models are given in the Appendix.

FIG. 4. - Variation of the ratio of the number density of CH to the number density of H^-, the dominant continuous opacity source at $\lambda \sim 4300$ Å, with the Rosseland mean optical depth. (a) $T_{eff} = 4000$ K, log g = 5.0, (b) $T_{eff} = 5000$ K, log g = 4.0. A legend of metal abundances, [A/H], which applies to both sections of the figure is shown.

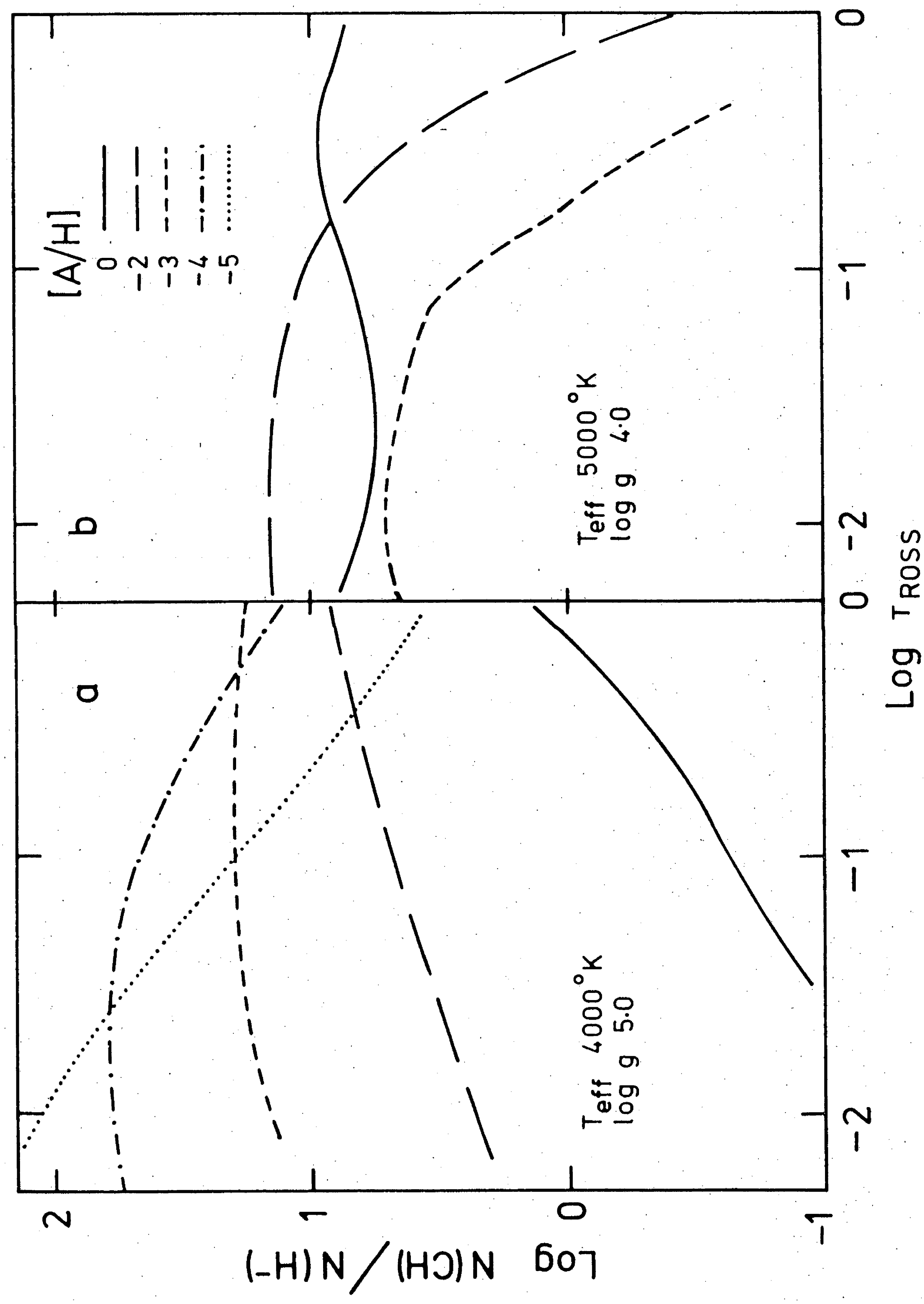

a
b
[A/H]
0
−2
−3
−4
−5
Teff 5000°K
log g 4.0
Teff 4000°K
log g 5.0
Log τROSS
Log N(CH)/N(H⁻)
2
1
0
−1
−2

The $N(H^-)$ as a function of τ_{ROSS} remains almost constant as the metal abundance varies, and so the great increase in line strength is a consequence of the large increase in the CH number density, a factor > 100 in the 4000 K models on lowering the metal abundance by 10^4 from [A/H] = 0, i.e. solar abundances. Hence the varying strength of the molecular component of the G-band, Figure 2b is explained by this rapidly changing ratio.

By using Figure 4 and the molecular band strengths tabulated in column (6) of Table 1, we can estimate where the CH lines make the largest contribution to the opacity, assuming that the dependence is independent of the metal abundance. Since the [A/H] = -5 model at T_{eff} = 4000 K has a computed strength which is midway between that of the [A/H] = -3 and -4 models, this restricts the depth at which the maximum of the CH contribution function occurs. From this we conclude that $\tau_{ROSS} \sim 0.05$ is the peak of this function for the 4000 K models. For T_{eff} = 5000 K the depth of formation is more difficult to determine but the peak of the distribution appears to be at approximately the same value of the mean Rosseland optical depth.

Further examination of the number densities reveals the cause of this rapid increase in the CH number density. The explanation of the above effect at our two chosen temperatures, which has so far followed a similar argument, diverges at this point in the discussion. Thus we will consider each independently, followed by a brief comment about other temperatures in our grid.

(i) T_{eff} = 4000 K

Figure 5 shows a plot of the major species influencing the CH formation at T_{eff} = 4000 K, log g = 5.0, and varying metal abundance. At normal abundance, CO has depleted the free carbon abundance to an enormous extent, particularly in the region of the peak CH line formation, $\tau_{ROSS} \sim 0.05$.

FIG. 5. - Plot of number densities against optical depth for the most important species which determine the amount of free carbon available for CH formation in models with T_{eff} = 4000 K, log g = 5.0 and the metal abundances indicated.

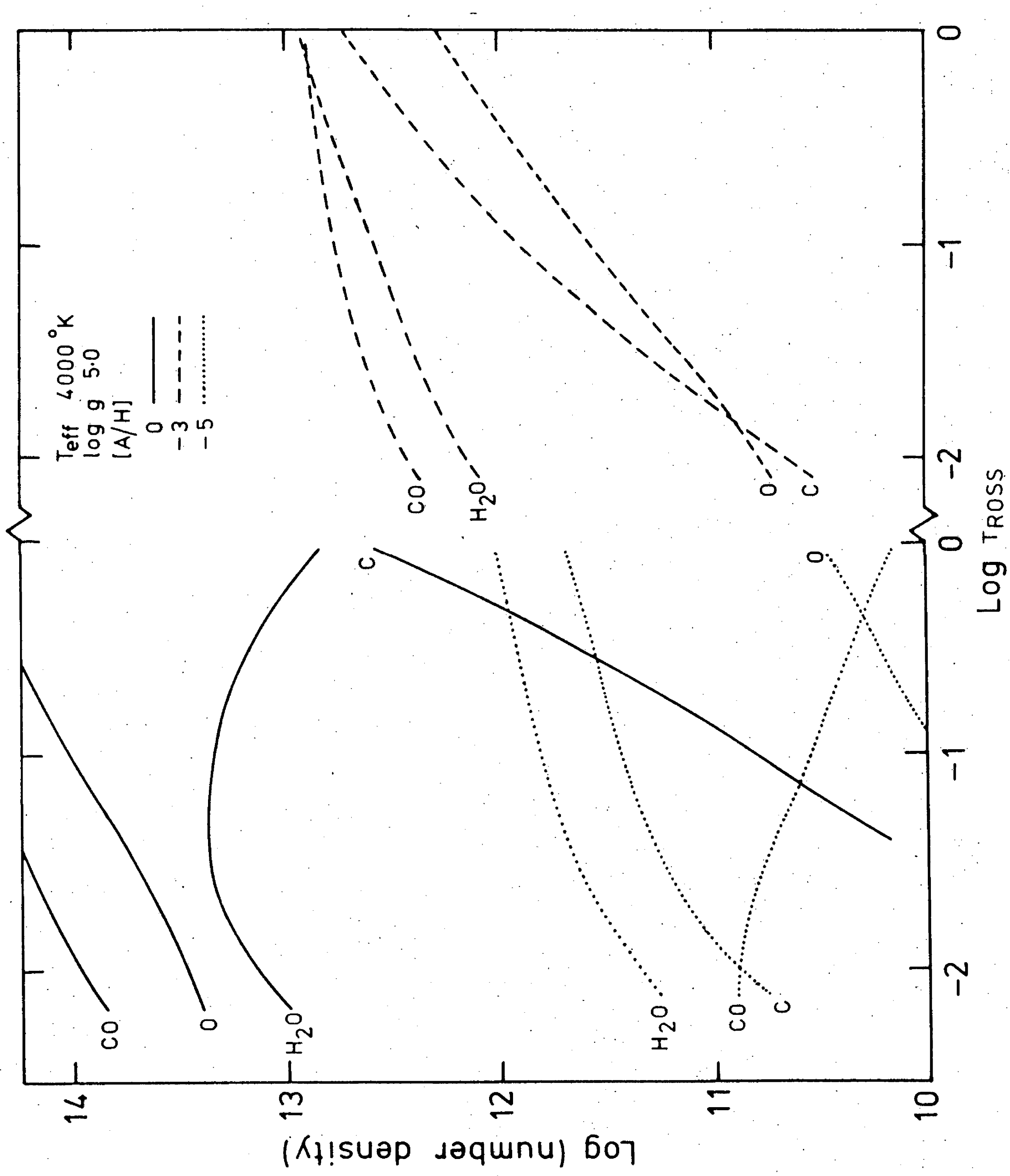
Log (number density)
Log τROSS
Teff 4000°K
log g 5.0
[A/H]
0
-3
-5
CO
O
H2O
C

However, in addition, H_2O and OH (the latter not shown in Figure 4) formation at these cool atmospheric temperatures have started to decrease the amount of free oxygen available. By [A/H] = -3, H_2O and CO number densities are of the same order of magnitude throughout the outer layers of the atmosphere. Also the N(OH) is only a factor of 3 more deficient than the $N(H_2O)$. Thus OH and H_2O have reduced the amount of free oxygen at $\tau_{ROSS} = 0.05$ by a factor of ~300 while the metal abundance was lowered by 10^3. Over the same range in abundance, the amount of free carbon has increased ~20 times. This is a consequence of the declining importance of CO relative to OH and H_2O with metal abundance, since the formation of CO depends on the product of the partial pressures of free carbon, p_C and oxygen, p_O, whereas H_2O and OH depend on $p_O \times (p_H)^2$ and $p_O \times p_H$, respectively. Since the partial pressure of hydrogen increases with decreasing metal abundance (see the Appendix), H_2O and OH become more favored species. Additionally, H_2O formation will be favored over OH association as the gas pressure increases in the metal-deficient models, since the dissociation potential of OH(D_o = 4.4ev) is significantly less than that of H_2O (D_o = 9.5ev).

Thus as the abundance is reduced from [A/H] = -3, more H_2O forms and there are fewer oxygen atoms free for CO formation. Therefore carbon is available to form bonds with other species, particularly hydrogen. This situation saturates when almost all the oxygen atoms in the outer atmospheric layers, τ_{ROSS} ~ 0.01 to ~1, become associated in H_2O molecules. The [A/H] = -5 curves in Figure 5 illustrate this effect. Further reduction in the metal abundance does not result in the release of any more carbon, in fact the abundance of all species decreases with metal abundance from [A/H] = -4. This latter result can also be inferred from the strength of the molecular component of the G-band (see Figure 2b), which peaks at [A/H] = -4 for an effective temperature of 4000 K.

(ii) T_{eff} *= 5000 K*

At this temperature the molecular equilibria have become considerably simpler. The temperatures are too hot to retain large amounts of OH and H_2O molecules in the atmosphere, so CO association is the only influencing species in determining the amount of free carbon available for the formation of CH. The situation is illustrated in Figure 6. At [A/H] = 0, carbon is depleted by CO formation. However, as one lowers the metal abundance to [A/H] = -2, carbon is released as conditions for CO association become less favorable. The total amount of free carbon does not increase as occurred in the 4000 K models, but its rate of decrease is slowed, allowing for increased CH formation at [A/H] = -2. This realises the effect described in §III, where the G-band's rate of weakening at this temperature gives the appearance of a feature which will be stronger than neighbouring, purely atomic, absorption features. By [A/H] = -3, CO formation is of no importance and the CH number densities and consequently the molecular G-band component diminish in unison with the atomic number densities and the metal-line strengths. In these oxygen-rich model atmospheres the N(O) - N(C) at a given depth has stabilised at X(O) - X(C), i.e. the difference in the overall abundance of oxygen and carbon.

(iii) Other temperatures

Carbon monoxide is still an influence at T_{eff} = 5500 K in depleting the amount of free carbon at normal abundance, and releasing it as the metal abundance is lowered. The effect here is even more subtle than the compensating result described in §III for the T_{eff} = 5000 K case. By T_{eff} = 6000 K the effect is not apparent as the overall strength of the G-band in metal-weak, [A/H] = -2, dwarf atmospheres is ~1Å, and this feature is no longer observable in the spectrum.

FIG. 6. - Same as for Figure 5, except for the T_{eff} = 5000 K, log g = 4.0 models.

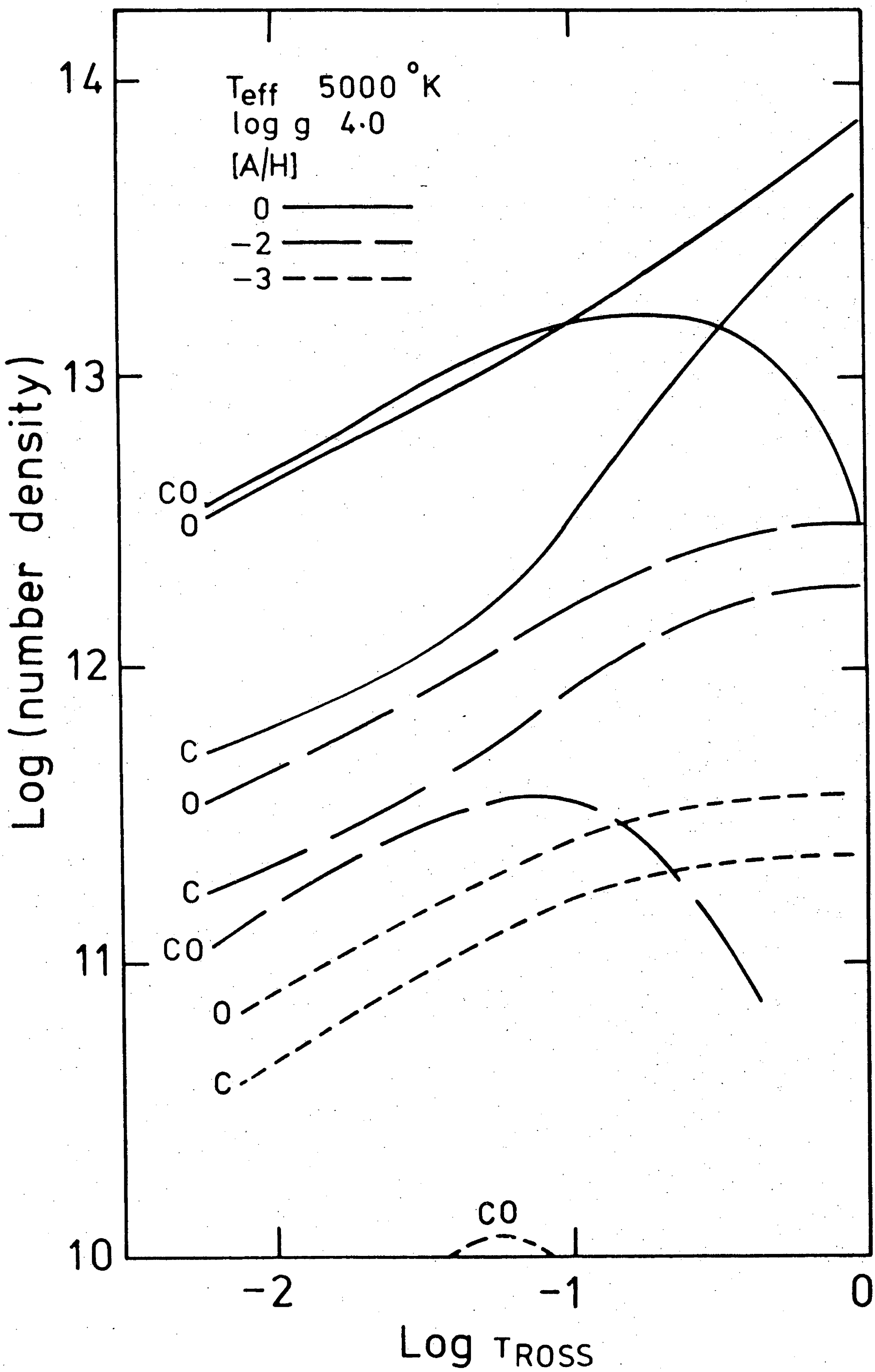

T_{eff} 5000 °K
log g 4·0
[A/H]
0
−2
−3
CO
O
C
O
C
CO
O
C
CO
14
13
12
11
10
Log (number density)
−2
−1
0
Log τ ROSS

At T_{eff} = 4500 K one obtains, as expected, a situation midway between the two temperatures which we have discussed in detail. That is, a greater compensating effect is observed than at 5000 K, but still not the complex reversals apparent at 4000 K.

Finally a few comments about the G-band strengths at T_{eff} = 3500 K. Those computed for the [A/H] = 0 and -2 models are predominantly absorption by strong atomic lines. These lines have broad wings which cause strong depression of the continuum over this small wavelength interval. Thus only the general trend of an increased molecular component, with similar conclusions to those reached in the 4000 K example, can be culled from the data at 3500 K.

(iv) Summary

One can conclude from the above analysis that provided a reasonable temperature estimate is adopted for a star, using a photometric system appropriate to the spectral type, a metal abundance can be derived by using Table 1 from this work for the G-band region and the metal-line strengths tabulated by WBC II. This assumes that the light elements, carbon and oxygen, behave in a similar manner to the heavier elements, in particular calcium and iron. Large deviations between these two determinations would probably indicate anomalous primordial carbon abundances and thus would require closer examination to derive individual abundances for the light elements.

However, for $T_{eff} \lesssim$ 4000 K the metal lines are still a large component (~60%) of the G-band at [A/H] = -2. Thus one's ability to derive reliable abundances at these temperatures using the G-band could become imprecise. This dilemma could be resolved by using another hydride, e.g., MgH, as an abundance indicator in cool, $\lesssim$ 4000 K, subdwarfs. This possibility was also noted by Bidelman and Smethells (1976), who considered

CaH and MgH to behave similarly. We discuss the MgH number densities in the next section.

(b) MgH

To illustrate the behaviour of the MgH molecule, relative to the metals, in our dwarf and subdwarf model atmospheres, we have formed the ratio N(MgH)/N(MgI) at a number of depth points throughout our atmospheres. The results are shown in Figure 7a,b for T_{eff} = 3500 K and 4000 K, respectively. Since both the atomic (Mg *b*) and molecular (MgH) lines occupy the same region of the spectrum, we do not have to consider which continuous opacity source is dominant.

Figure 7 indicates that with decreasing metal abundance the number density of MgH does not decrease as rapidly as the number density of neutral magnesium, and consequently the MgH bands will appear stronger than the atomic lines, in particular, the Mg *b* lines. This will give the "strong MgH" classification noted by Greenstein (1971).

The visibility of MgH also depends on the strength of TiO, which has vibrational bands in this region. A similar situation was discussed by Mould (1976) for TiO bands in the vicinity of molecular bands of another metallic hydride CaH. In the cool metal-deficient model atmospheres, TiO behaves in a similar manner to CO at 4000 K, because both species depend on the partial pressure of two decreasing elements, whereas MgH has one decreasing, Mg, and one increasing, H, component. This increasing component is intrinsically connected with the changing structure of the model atmospheres with metal abundance, and will be discussed in detail in WBC II.

Thus, from the above argument, strong MgH bands in the absence of TiO features would indicate metal deficiency in subdwarf stars, provided this deficiency applied to all elements in the atmosphere of the star. This was also concluded by Eggen and Greenstein in their discussions of the

FIG. 7. - Indicates the strengthening of MgH number densities relative to the number densities of MgI. (a) $T_{eff} = 3500$ K, log g = 5.0, (b) $T_{eff} = 4000$ K, log g = 5.0. The curves, which correspond to varying metal abundance are defined in the same manner as Figure 4.

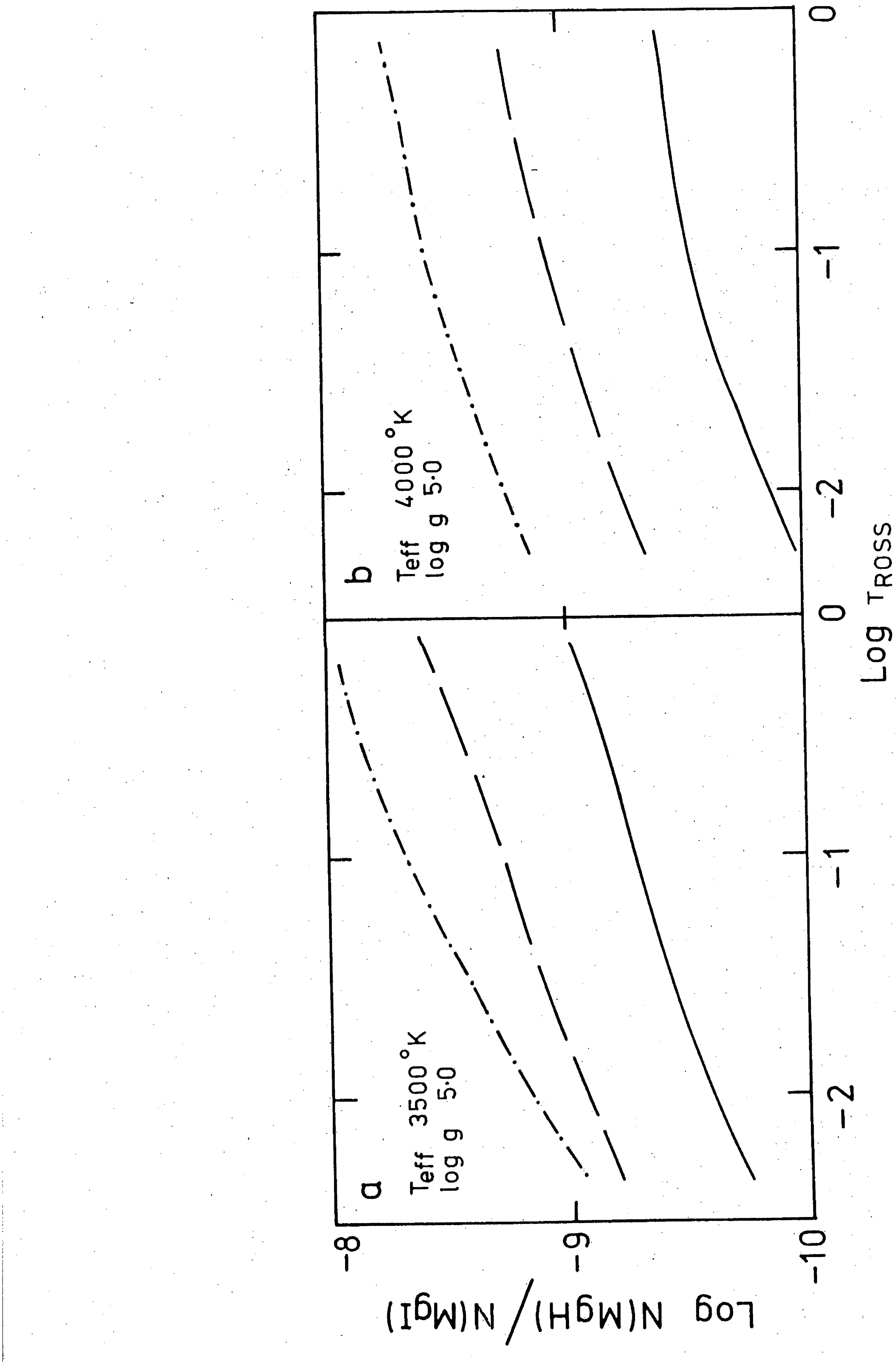
a
Teff 3500°K
log g 5·0
b
Teff 4000°K
log g 5·0
-8
-9
-10
0
-1
-2
Log τROSS
Log N(MgH)/N(MgI)

spectroscopic properties of subluminous stars (Greenstein 1969; Eggen and Greenstein 1965).

V. CONCLUSIONS

We conclude from this research that the G-band region strengthens or at least appears stronger than neighbouring purely atomic-line regions, as one lowers the metal abundance in dwarf model atmospheres with effective temperatures $\lesssim$ 5500 K. This is consistent with the observations of Greenstein (1971) and is due to the rapidly varying abundance of the CH molecule with decreasing metal abundance. Also we have shown that bands of MgH are a similar discriminant in extremely metal-weak stars in the temperature regime, $T_{eff} \lesssim 4000$ K, where the G-band region in metal-deficient models, [A/H] ~ -2, is still dominated by metal lines.

Thus, provided a good temperature estimate is available, we have a discriminant for selecting metal-deficient stars, as well as a method for determining photospheric metal abundances.

Future papers in this series will give observational evidence which supports the above results, and will include data on the metal-line strengths using the same grid of model atmospheres considered in this work.

Acknowledgements

I would like to thank Dr. M. S. Bessell for his help in constructing the grid of flux-constant model atmospheres and also his comments on the manuscript. In addition, I am grateful to Dr. J. R. Mould for providing me with the MgH line list and to Dr. J. L. Greenstein for his extremely useful comments on the manuscript. I also wish to acknowledge the support of an Australian National University Postgraduate Award which enabled access to the UNIVAC 1100/42 computer, operated by the ANU Computer Center.

REFERENCES

Bessell, M. S., Cottrell, P. L., and Wickramasinghe, D. T. 1978, in preparation (WBC II).

Bidelman, W. P., and Smethells, W. G. 1976, in *IAU Symposium No. 72, Abundance Effects in Classification*, ed. B. Hauck, and P. C. Keenan (Dordrecht: Reidel), p. 205.

Cohen, J. G., and Strom, S. E. 1968, *Ap. J.*, 151, 623.

Cottrell, P. L., and Norris, J. 1978, *Ap. J.*, 221, in press (Chapter 2).

Dahn, C. C., Liebert, J., Kron, R. G., Spinrad, H., and Hintzen, P. M. 1977, *Ap. J.*, 216, 757.

Eggen, O. J., and Greenstein, J. L. 1965, *Ap. J.*, 142, 925.

Greenstein, J. L. 1969, in *Low Luminosity Stars*, ed. S. Kumar (New York: Gordon and Breach), p. 281.

———————. 1971, in *IAU Symposium No. 42, White Dwarfs*, ed. W. J. Luyten (Dordrecht: Reidel), p. 46.

Hearnshaw, J. B. 1976, *Astr. Ap.*, 51, 71.

Kurucz, R. L. 1970, *SAO Spec. Rept.*, No. 309.

Lambert, D. L. 1968, *M.N.R.A.S.*, 138, 143.

Minnaert, M., Mulders, G. F. W., and Houtgast, J. 1940, *Photometric Atlas of the Solar Spectrum* (Amsterdam: Schnabel).

Mould, J. R. 1976, *Astr. Ap.*, 48, 443.

Wegner, G. 1975, *M.N.R.A.S.*, 171, 529.

Wickramasinghe, D. T., Bessell, M. S., and Cottrell, P. L. 1977, *Ap. J. (Letters)*, 217, L65 (WBC I).

APPENDIX: NUMBER DENSITIES

MODEL	τ_{ROSS}	N(HI)	N(H_2)	N(H^-)	N(C)	N(O)	N(CO)	N(OH)	N(H_2O)	N(CH)	N(MgH)	N(MgI)
T_{eff}/log g/[A/H]												
4000/5/0	6.5(-3)	1.2(17)	3.7(16)	5.6(8)	1.6(9)	2.4(13)	7.0(13)	1.3(13)	9.5(12)	3.8(7)	8.4(2)	5.9(12)
	1.3(-2)	1.8(17)	6.2(16)	1.1(9)	3.0(9)	3.2(13)	1.1(14)	2.1(13)	1.7(13)	8.8(7)	1.7(3)	9.0(12)
	4.0(-2)	3.1(17)	9.3(16)	3.3(9)	1.5(10)	6.1(13)	1.8(14)	3.3(13)	2.2(13)	4.4(8)	4.1(3)	1.5(13)
	1.2(-1)	5.1(17)	1.1(17)	8.6(9)	8.9(10)	1.1(14)	2.6(14)	4.5(13)	2.0(13)	2.2(9)	7.8(3)	2.1(13)
	2.6(-1)	7.0(17)	1.2(17)	1.7(10)	3.3(11)	1.5(14)	3.3(14)	4.9(13)	1.6(13)	7.2(9)	1.1(4)	2.7(13)
	9.1(-1)	1.1(18)	1.0(17)	4.8(10)	3.9(12)	2.6(14)	4.6(14)	4.5(13)	6.6(12)	6.2(10)	1.7(4)	3.3(13)
4000/5/-2	6.4(-3)	5.4(17)	6.1(17)	4.6(8)	9.8(9)	4.7(11)	6.2(12)	9.7(11)	2.7(12)	9.3(8)	3.0(2)	5.0(11)
	1.4(-2)	8.4(17)	9.6(17)	1.1(9)	2.8(10)	7.5(11)	9.7(12)	1.6(12)	4.1(12)	2.9(9)	6.3(2)	7.7(11)
	3.6(-2)	1.4(18)	1.3(18)	2.9(9)	1.0(11)	1.4(12)	1.4(13)	2.6(12)	5.4(12)	1.0(10)	1.2(3)	1.1(12)
	8.6(-2)	2.0(18)	1.7(18)	6.3(9)	3.0(11)	2.5(12)	1.9(13)	3.9(12)	6.6(12)	2.9(10)	1.9(3)	1.4(12)
	2.7(-1)	3.3(18)	2.3(18)	1.8(10)	1.2(12)	4.9(12)	2.7(13)	6.5(12)	8.3(12)	1.1(11)	3.5(3)	1.8(12)
	8.0(-1)	5.2(18)	3.0(18)	4.4(10)	4.0(12)	9.6(12)	3.5(13)	1.1(13)	1.0(13)	3.6(11)	5.5(3)	2.1(12)
4000/5/-3	7.9(-3)	1.1(18)	2.6(18)	4.8(8)	3.2(10)	5.1(10)	2.2(12)	2.2(11)	1.2(12)	6.2(9)	2.1(2)	1.7(11)
	1.6(-2)	1.7(18)	3.9(18)	1.1(9)	8.0(10)	8.1(10)	3.2(12)	3.5(11)	1.8(12)	1.7(10)	4.0(2)	2.4(11)
	4.3(-2)	2.9(18)	5.6(18)	3.2(9)	3.0(11)	1.9(11)	4.6(12)	6.8(11)	2.7(12)	6.0(10)	7.6(2)	3.3(11)
	1.2(-1)	4.7(18)	7.6(18)	8.4(9)	8.9(11)	4.1(11)	5.9(12)	1.3(12)	4.0(12)	1.7(11)	1.3(3)	4.1(11)
	3.4(-1)	7.4(18)	1.0(19)	2.1(10)	2.3(12)	8.9(11)	7.1(12)	2.4(12)	5.9(12)	4.3(11)	2.0(3)	4.8(11)
	9.5(-1)	1.2(19)	1.3(19)	5.4(10)	5.0(12)	1.9(12)	7.5(12)	4.4(12)	8.6(12)	9.5(11)	3.0(3)	5.4(11)
4000/5/-4	5.4(-3)	1.6(18)	6.2(18)	2.6(8)	4.6(10)	5.3(9)	4.3(11)	3.7(10)	3.4(11)	1.4(10)	6.0(1)	3.2(10)
	1.9(-2)	3.3(18)	1.3(19)	1.1(9)	1.8(11)	1.3(10)	7.8(11)	9.3(10)	8.2(11)	6.7(10)	2.0(2)	6.4(10)
	5.5(-2)	5.7(18)	2.1(19)	3.3(9)	4.7(11)	3.0(10)	9.9(11)	2.0(11)	1.5(12)	1.8(11)	4.0(2)	8.9(10)
	1.3(-1)	8.7(18)	2.7(19)	7.9(9)	9.0(11)	6.4(10)	9.6(11)	3.7(11)	2.2(12)	3.3(11)	5.8(2)	9.9(10)
	3.3(-1)	1.3(19)	3.5(19)	2.1(10)	1.6(12)	1.4(11)	8.2(11)	6.8(11)	3.2(12)	5.6(11)	8.5(2)	1.1(11)
	8.9(-1)	2.0(19)	4.5(19)	5.8(10)	2.4(12)	2.7(11)	6.3(11)	1.2(12)	4.4(12)	8.5(11)	1.3(3)	1.3(11)
4000/5/-5	7.0(-3)	2.8(18)	2.1(19)	2.1(8)	5.0(10)	7.1(8)	7.9(10)	9.5(9)	1.7(11)	3.0(10)	3.0(1)	8.9(9)
	1.9(-2)	5.8(18)	3.6(19)	9.5(8)	1.3(11)	2.3(9)	7.1(10)	2.6(10)	3.5(11)	7.4(10)	6.3(1)	1.2(10)
	4.5(-2)	9.4(18)	4.7(19)	2.9(9)	2.0(11)	5.2(9)	4.9(10)	4.9(10)	5.0(11)	1.1(11)	9.1(1)	1.3(10)
	9.6(-2)	1.3(19)	5.7(19)	6.8(9)	2.7(11)	8.8(9)	3.6(10)	7.3(10)	6.2(11)	1.4(11)	1.3(2)	1.5(10)
	3.1(-1)	2.0(19)	7.4(19)	2.4(10)	3.7(11)	1.7(10)	2.3(10)	1.2(11)	8.1(11)	1.9(11)	2.1(2)	1.8(10)
	8.0(-1)	2.7(19)	8.9(19)	6.2(10)	4.7(11)	2.7(10)	1.6(10)	1.7(11)	9.8(11)	2.4(11)	3.1(2)	2.2(10)
5000/4/0	6.0(-3)	1.2(16)	2.1(13)	2.0(7)	5.2(11)	3.3(12)	3.6(12)	1.1(10)	3.6(7)	1.4(8)	8.5(-1)	
	1.2(-2)	1.7(16)	4.2(13)	4.0(7)	6.6(11)	4.7(12)	5.4(12)	2.2(10)	9.4(7)	2.4(8)	2.0(0)	
	3.3(-2)	3.0(16)	1.0(14)	1.1(8)	1.2(12)	8.2(12)	9.6(12)	5.4(10)	3.1(8)	6.2(8)	6.2(0)	
	9.5(-2)	5.2(16)	1.9(14)	3.1(8)	3.1(12)	1.5(13)	1.5(13)	1.1(11)	6.3(8)	2.1(9)	1.4(1)	
	2.8(-1)	8.1(16)	2.0(14)	8.2(8)	1.3(13)	3.1(13)	1.6(13)	1.6(11)	5.7(8)	7.6(9)	1.8(1)	
	9.4(-1)	1.3(17)	1.1(14)	2.2(9)	4.1(13)	7.0(13)	3.2(12)	1.3(11)	1.4(8)	1.6(10)	7.0(0)	
5000/4/-2	5.9(-3)	7.7(16)	8.5(14)	1.9(7)	1.7(11)	3.4(11)	1.1(11)	7.3(9)	1.4(8)	2.7(8)	7.2(-2)	
	1.2(-2)	1.1(17)	1.8(15)	4.0(7)	2.3(11)	4.9(11)	1.8(11)	1.5(10)	3.9(8)	5.4(8)	1.9(-1)	
	5.0(-2)	2.4(17)	5.3(15)	1.7(8)	5.3(11)	1.1(12)	3.4(11)	4.5(10)	1.7(9)	2.0(9)	8.6(-1)	
	1.1(-1)	3.5(17)	7.3(15)	3.8(8)	9.3(11)	1.7(12)	3.4(11)	6.9(10)	2.3(9)	3.7(9)	1.4(0)	
	3.6(-1)	5.0(17)	5.6(15)	1.5(9)	1.7(12)	2.8(12)	9.2(10)	6.3(10)	1.0(9)	5.2(9)	1.5(0)	
	9.9(-1)	5.4(17)	1.7(15)	8.1(9)	1.9(12)	3.1(12)	4.2(9)	2.0(10)	8.0(7)	2.7(9)	8.6(-1)	
5000/4/-3	7.3(-3)	1.2(17)	1.9(15)	1.9(7)	4.0(10)	6.7(10)	3.7(9)	2.0(9)	5.4(7)	9.5(7)	9.7(-3)	
	1.5(-2)	1.8(17)	4.0(15)	4.0(7)	6.0(10)	1.0(11)	6.8(9)	4.2(9)	1.6(8)	2.0(8)	2.6(-2)	
	5.7(-2)	3.8(17)	1.2(16)	1.8(8)	1.3(11)	2.1(11)	1.2(10)	1.2(10)	6.1(8)	6.7(8)	1.3(-1)	
	1.1(-1)	4.9(17)	1.2(16)	4.7(8)	1.7(11)	2.8(11)	7.0(9)	1.4(10)	5.3(8)	8.7(8)	1.9(-1)	
	3.4(-1)	6.1(17)	7.8(15)	2.0(9)	2.2(11)	3.6(11)	1.2(9)	9.0(9)	1.6(8)	7.9(8)	2.1(-1)	
	7.8(-1)	6.3(17)	3.1(15)	7.5(9)	2.3(11)	3.7(11)	1.1(8)	3.6(9)	2.2(7)	4.6(8)	1.4(-1)	

CHAPTER 6

A MODEL ATMOSPHERE STUDY OF COOL WHITE DWARFS

I. INTRODUCTION

The spectral characteristics of cool white dwarfs have been investigated in several recent papers by Hintzen and Strittmatter (1975) (hereafter HS), Wickramasinghe, Bessell, and Cottrell (1977) (hereafter WBCI), Shipman (1977), and Wehrse (1977). HS constructed metal-line and Hγ profiles from cool ($T_e \gtrsim$ 6000K) white dwarf and subdwarf model atmospheres. From these profiles they concluded that degenerate stars may be confused spectroscopically with subdwarfs. However WBCI, who constructed even cooler models with gravities of 10^4 and 10^8 cm s^{-2}, demonstrated that lines of the Balmer series were a gravity indicator down to an effective temperature, T_e, of ~5000 K. Subdwarfs at this temperature would have many more hydrogen lines than the white dwarfs, with the latter possibly only showing a weak line of Hα on data acquired with current instrumentation. Similar conclusions were reached by Shipman (1977), who constructed pure hydrogen white dwarf model atmospheres in the temperature range 4000 K to 8000 K. Both Shipman and WBCI showed how the convective region expanded in the cool high gravity models, as molecular hydrogen became the dominant species in these atmospheres.

Finally Wehrse (1977), constructed synthetic spectra for a number of H- and He-rich white dwarf model atmospheres in the range 5000 K $\lesssim T_e \lesssim$ 7000 K. Using these spectra he tabulated the visibility characteristics of NaI*D*, MgI*b*, CaI(λ4226A), CaII(*H* and *K*), and Hγ. This provided a broad grid which will enable researchers in this field to derive the metal abundance and the (He/H) ratio from white dwarf spectra, provided some independent method can be used to determine the effective temperature of these stars.

In this chapter the structure of H-rich white dwarf model atmospheres, which I have constructed, will be discussed. These models encompass those used by both WBCI and Cottrell, Bessell, and Wickramasinghe (1977) (hereafter WBCII). This latter paper, which was an analysis of the heavily line-blanketed white dwarf LP701-29 is included in this chapter. This research employed the synthetic spectrum technique, which has been developed by the author and was described in earlier chapters of this thesis (see Chapters 2, 5). Lastly some preliminary He-rich white dwarf models were also converged and their structure and some synthetic spectra are discussed in §III*b* and §IV*b* respectively.

II. MODEL ATMOSPHERES

All the models were constructed using the computer program ATLAS5 (Kurucz 1970), with modifications made by Dr. J. R. Mould. H-rich atmospheres were converged in the temperature range, 3500 K $\leq T_e \leq$ 7000 K, and gravities of 10^8 cm s^{-2}. The metal abundances, [M/TOT], were relative to the total number of atoms, and ranged from normal, [M/TOT] = 0, to 10^{-6} times the solar abundance, [M/TOT] = -6. The He/H ratio was set equal to 0.1. For the He-rich white dwarf models only a limited number of models were computed, at T_e's of 4000 K, 5500 K, and 7000 K, and the same gravities as above. The He/H ratio was 10^5, while the metal abundances, relative to the total abundance of all elements were 10^{-3} and 10^{-5} for the hotter models, and ranged from 10^{-3} to 10^{-6} for the models at 4000 K. In the present calculations no pressure ionisation effects were included. These have been discussed most recently by Böhm *et al.* (1977). The major effect will be to increase the degree of ionisation in the coolest, most metal-deficient models. The implications of my neglect of pressure ionisation will be discussed further in both §III and §IV.

The following continuous opacity sources were included in all the model calculations: absorption by HI, H^-, H_2^+, H_2^-, He^-, CI, MgI, AlI, and SiI, as well as Rayleigh scattering by H, He, and H_2, and electron scattering. Two additional opacities were included which are particularly important in the cool high gravity models constructed in this research. These were the triplet state quasi H_2 molecular opacity (Doyle 1968), and the pressure induced H_2 dipole opacity (Linsky 1969). The latter was discussed by Shipman (1977) where, for his 4000 K model he stated that it was the dominant opacity source in the region where most of the radiation was emitted. The quasi H_2 opacity does not have any effect on the model structure, since its dominant effect is at blue wavelengths (< 3500Å) and thus its importance in the white dwarfs is in determining the strength of the metal lines at short wavelengths, and in the computation of violet continuum colours.

In the equilibrium equations, the following molecules were included: H_2, CO, C_2, CN, and N_2. The models were then converged to flux constancy until the flux errors were less than one and five percent in the radiative and convective regions respectively.

III. MODEL CHARACTERISTICS

The structures and dominant opacity sources of all the white dwarf model atmospheres will be considered in this section. However the H- and He-rich models will be discussed separately.

(a) H-rich White Dwarfs

(i) Model Structure

The temperature and pressure structure of most of the H-rich white dwarf models are shown in Figures 1 to 6, encompassing the temperature range

FIGS. 1.-6. - Model atmospheric structures for the hydrogen-rich white dwarfs with effective temperatures, TEFF, of 7000 K, 6000 K, 5000 K, 4500 K, 4000 K, and 3500 K, respectively. The logarithm of the helium to hydrogen ratio, (HE/H), is -1, and the metal abundance, [M/TOT], which is shown for each curve, is the ratio by number, of the overall metal abundance to the total abundance. [...] refers to the logarithm of this parameter relative to the Sun. The onset of convection in most models is indicated by the pointers. (a) $T(\tau)$, (b) $\log P_g(\tau)$, (c) $\log (P_g/P_e)(\tau)$.

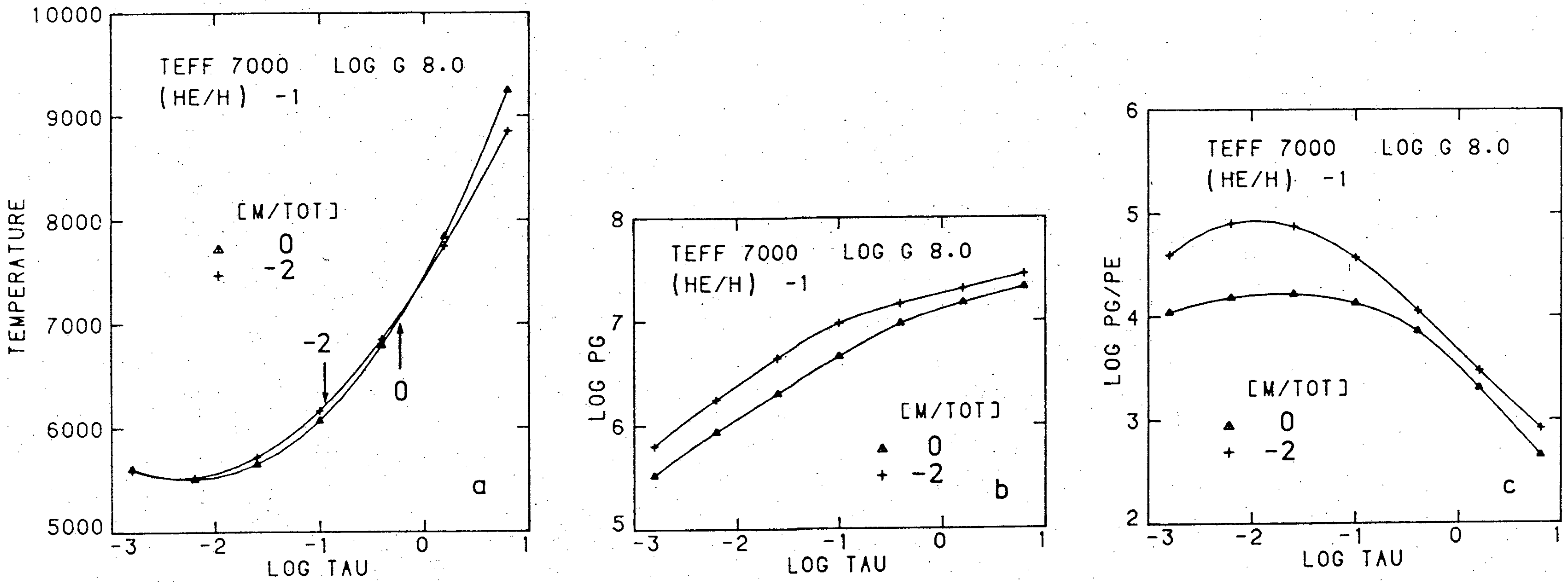
TEFF 7000 LOG G 8.0
(HE/H) -1
[M/TOT]
0
-2
TEMPERATURE
LOG TAU
a
LOG PG
b
LOG PG/PE
c

Figure 1

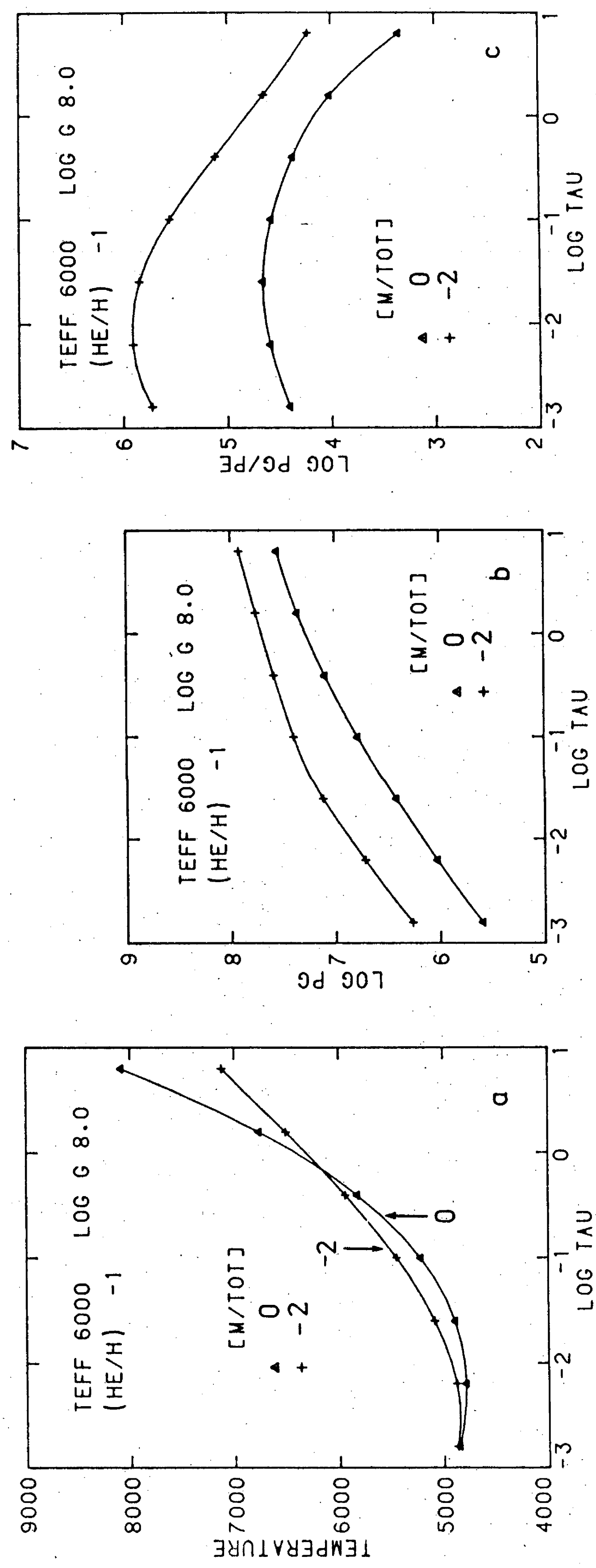

TEFF 6000 LOG G 8.0
(HE/H) -1
[M/TOT]
0
-2
TEMPERATURE
LOG TAU
a
LOG PG
b
LOG PG/PE
c

Figure 2

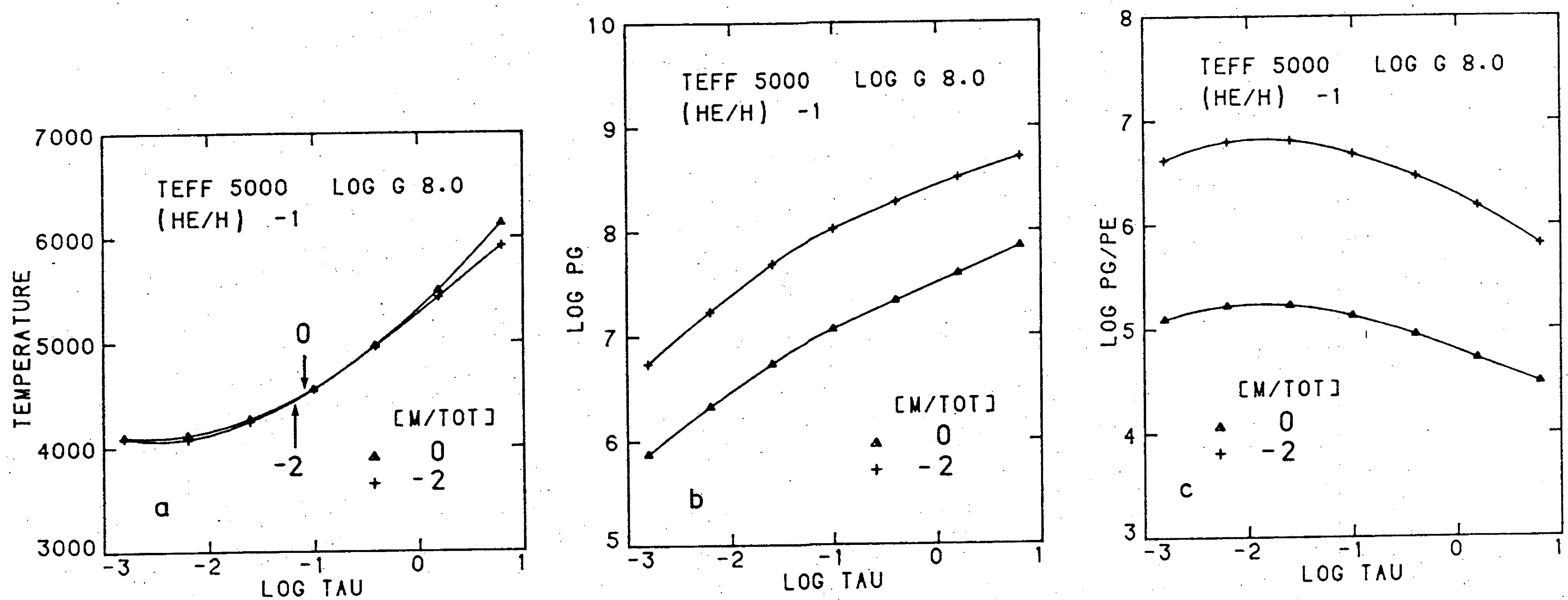

TEFF 5000 LOG G 8.0
(HE/H) -1
TEMPERATURE
7000
6000
5000
4000
3000
0
-2
[M/TOT]
0
-2
a
-3
-2
-1
0
1
LOG TAU
TEFF 5000 LOG G 8.0
(HE/H) -1
LOG PG
10
9
8
7
6
5
[M/TOT]
0
-2
b
-3
-2
-1
0
1
LOG TAU
TEFF 5000 LOG G 8.0
(HE/H) -1
LOG PG/PE
8
7
6
5
4
3
[M/TOT]
0
-2
c
-3
-2
-1
0
1
LOG TAU

Figure 3

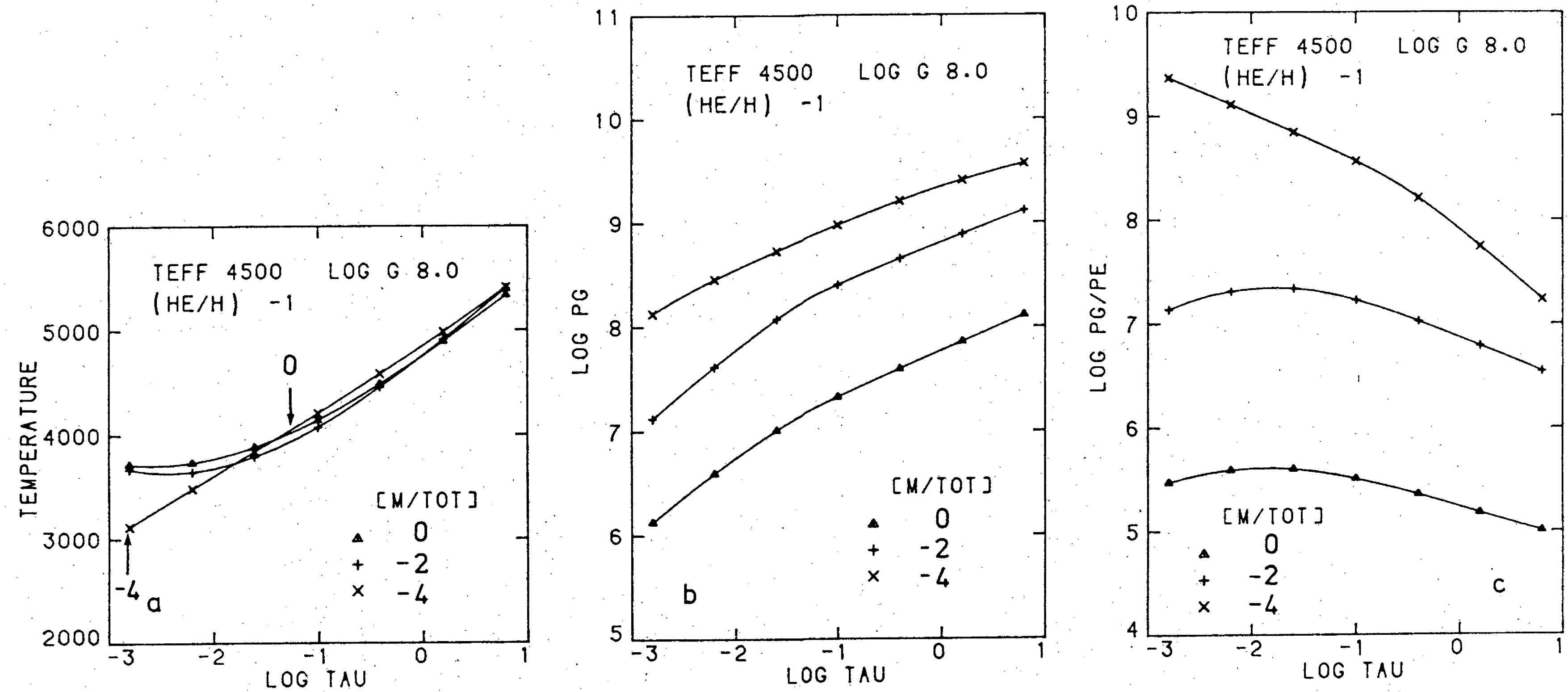
TEFF 4500 LOG G 8.0
(HE/H) -1
TEMPERATURE
LOG TAU
[M/TOT]
0
-2
-4
a
LOG PG
b
LOG PG/PE
c

Figure 4

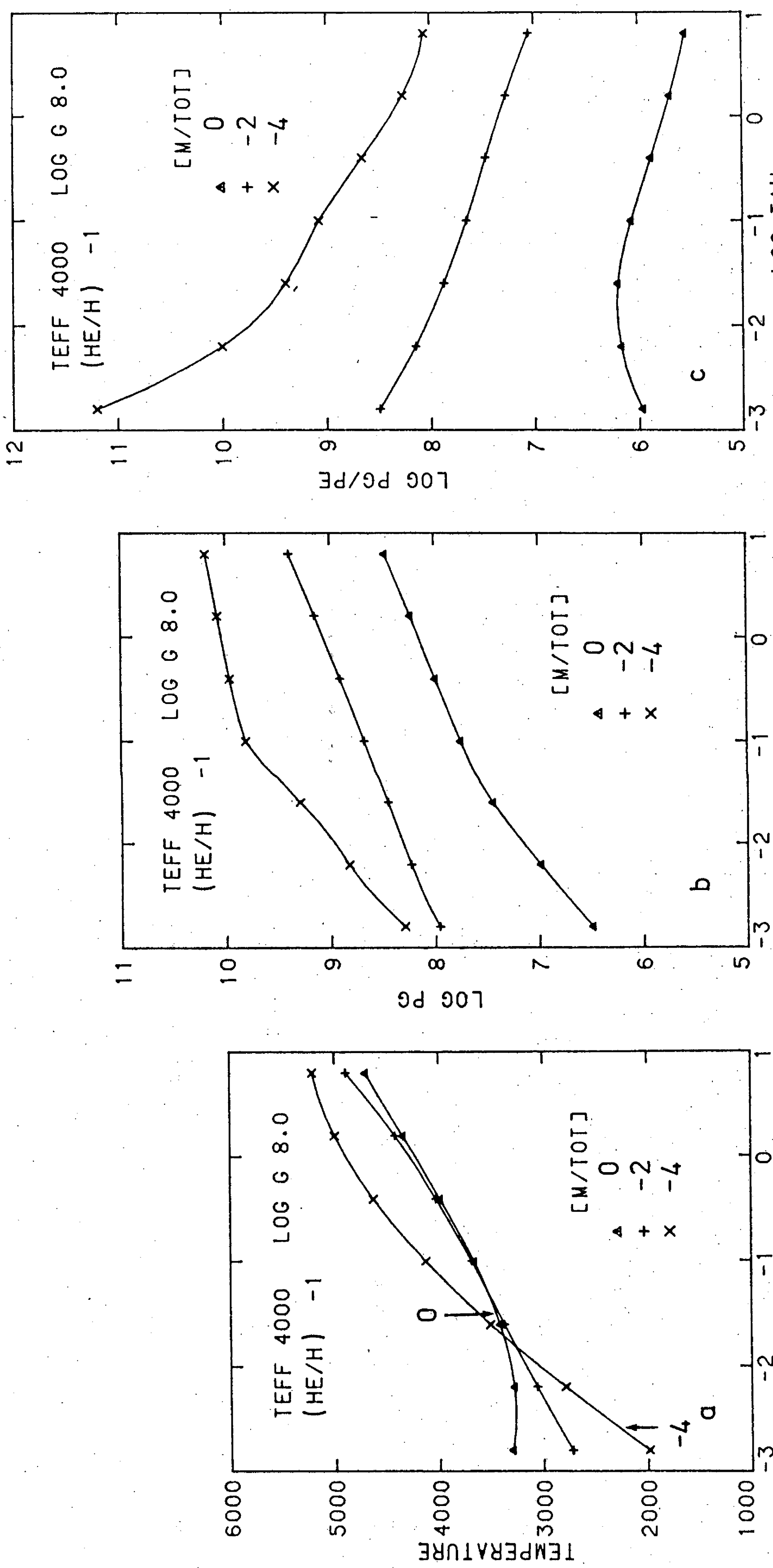
TEFF 4000 LOG G 8.0
(HE/H) -1
[M/TOT]
0
-2
-4
LOG TAU
TEMPERATURE
LOG PG
LOG PG/PE
a
b
c

Figure 5

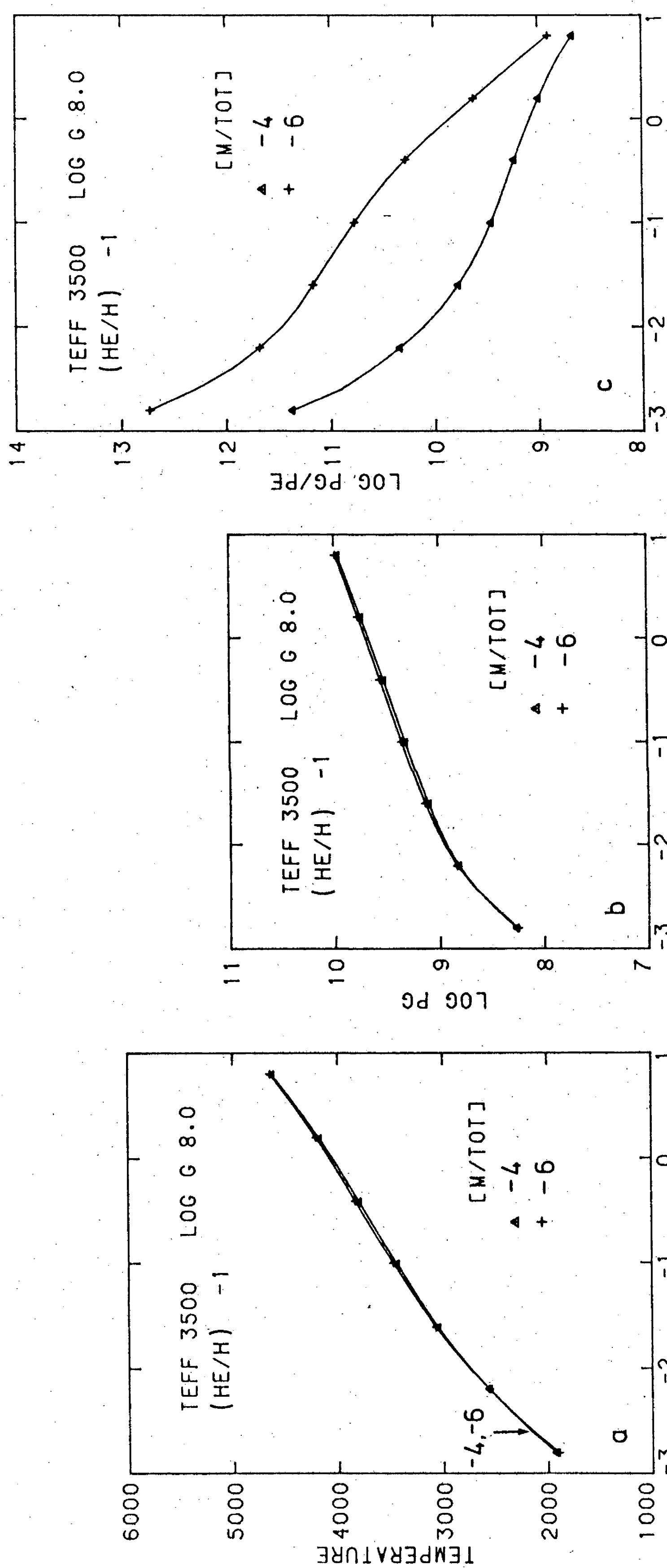
TEFF 3500 LOG G 8.0
(HE/H) -1
[M/TOT]
▲ -4
+ -6
-4,-6
a
TEMPERATURE
LOG TAU
b
LOG PG
c
LOG PG/PE

Figure 6

$3500\ K \lesssim T_e \lesssim 7000\ K$.

Let us consider the $T(\tau)$ relations. These curves become flatter, i.e. the differential temperature between an optical depth τ, of -2.5 and 0 becomes smaller, as T_e is lowered from 7000 K to 5000 K. In addition, as is shown dramatically in Figure 2a, the $T(\tau)$ also becomes flatter as the metal abundance is decreased. Both these can be interpreted as the increasing importance of convection, which transports energy much more efficiently than radiation. This has been discussed by both Wehrse (1975) and WBCI. To determine whether a region is convective, the model atmosphere program ATLAS compares the adiabatic temperature gradient (∇_A) with the actual temperature gradient (∇) of the model. If

$$\nabla_A < \nabla ,$$

the region is considered to be convective. The values of ∇, ∇_A at τ_{ROSS} = 0.01 and 1.0 for most of the models illustrated in Figures 1 to 6, are shown in Table 1. Wehrse (1974) discussed the importance of H_2 formation on ∇_A. Using the temperatures and gas pressures in the above table, and Figure 1 of Wehrse (1974), one sees that ∇_A exhibits a complex variation with both effective temperature and metal abundance. Decreasing [M/TOT] implies an increase in the gas pressure and consequently increased H_2 formation.

This enhanced formation of H_2 produces conditions under which convective energy transport become more favourable. The position of the onset of convection is indicated in Figures 1a to 6a. In fact, the actual temperature gradient in the atmospheres asymptotes towards the adiabatic gradient as both the effective temperature and metal abundance are decreased (see Table 1: ∇, ∇_A for τ_{ROSS} = 1.0), i.e. the efficiency of convection increases in unison with the formation of H_2.

This is also illustrated by Figures 4a and 6a. From the normal abundance T_e = 4500 K model to the T_e = 3500, [M/TOT] = -6 model, the

TABLE 1

TEMPERATURE GRADIENTS

	$\tau = 0.01$				$\tau = 1.0$			
TEFF/log g/[M/TOT]	T	P_g	∇	∇_A	T	P_g	∇	∇_A
7000/8/0	5620	1.4(6)	0.0161	0.330	7700	1.4(7)	0.396	0.349
-2	5630	2.8(6)	0.0156	0.289	7540	1.9(7)	0.382	0.334
6000/8/0	4860	1.7(6)	0.0138	0.197	6450	1.9(7)	0.303	0.269
-2	4900	7.0(6)	0.0023	0.148	6360	5.2(7)	0.235	0.214
5000/8/0	4150	3.4(6)	0.0198	0.111	5300	3.3(7)	0.166	0.155
-2	4120	2.7(7)	0.0117	0.120	5300	2.8(8)	0.169	0.166
4500/8/0	3750	7.9(6)	0.0445	0.109	4800	6.3(7)	0.141	0.135
-2	4000	6.0(7)	0.1920	0.134	4800	6.3(8)	0.166	0.164
-4	3600	4.2(8)	0.1848	0.1838	4860	2.3(9)	0.1914	0.1903
4000/8/0	3275	1.5(7)	0.0011	0.141	4250	1.5(8)	0.144	0.141
-4	3180	6.4(8)	0.2295	0.2291	4470	3.5(9)	0.1824	0.1819
3500/8/-4	2770	8.9(8)	0.2624	0.2616	4050	4.7(9)	0.1998	0.1995
-5	2800	9.5(8)	0.2601	0.2596	4075	5.0(9)	0.1994	0.1992

outer layers, log $\tau < -1.5$ have become much cooler, and the adiabatic gradient in the latter model has been established throughout almost the whole atmosphere. This also explains the lack of change in temperature structure at 3500 K as the metal abundance is changed by a factor of 100. The cause of this temperature gradient is the gradual movement of convection into the outer layers as the atmospheric pressures, P_g (see b's of Figures 1 to 6) increase. The change from radiative to convective equilibrium in the outer layers is shown in Figure 5a, as the metal abundance is lowered from 0 to -4 at an effective temperature of 4000 K.

The ratio of gas to electron pressure, log P_g/P_e illustrates the effect of convection on the ionisation conditions. The models at T_e = 4000 K (Figure 5c) will be used as examples. As the convective region grows with a decrease in the metal abundance, the temperature of the surface layers is lowered relative to the more metal-rich models. This decrease in temperature means a lower degree of ionisation, hence a smaller electron pressure and an upward trend in the P_g/P_e (τ) relation at low optical depths. However, the ionisation conditions in some of the coolest, most metal-deficient models must be treated with a little caution as the P_g of $\sim 10^{10}$ dynes cm^{-2} imply a particle spacing of $\sim 2.5 \times 10^{-8}$ cm. This is only ~5 times the Bohr radius, and thus some pressure ionisation would be expected.

Summarizing, Figures 1 to 6 illustrate the changing conditions in the atmospheres of hydrogen-rich white dwarfs, as both the effective temperature and metal abundance are varied. The general trend in these models as both these parameters decrease, is an increase in convective energy transport as a result of increased H_2 formation. In addition, a decrease in the degree of ionisation in the outer layers of the cooler models ($T_e \lesssim$ 4500K) results, as a consequence of the establishment of convection throughout the whole atmosphere (log τ -3 to +1). Under these conditions, the actual temperature gradient follows the adiabatic gradient.

In the next section, the dominant opacity sources in these hydrogen-rich white dwarf model atmospheres will be considered, and in particular the effect of increased H_2 formation on these opacities.

(ii) Opacity Sources

Using a print option existing within the original code, the ATLAS5 program lists the strength of all the opacity sources as a function of both optical depth and wavelength. Thus the strongest opacity in the region where most of the radiation is emitted can be determined, and the changing fortunes of all opacities can be investigated as both the temperature and metal abundance are varied.

At T_e = 6000 K and 7000 K, H^- is by far the dominant source of continuous opacity in both the normal and 10^{-2} metal abundance models. In the two models at 7000 K, and the metal-deficient 6000 K model, the electrons come from hydrogen, whereas in the normal abundance 6000 K model, the electrons are supplied about equally by hydrogen and the metals, principally Mg, Si, and Fe.

As the atmospheric conditions become cooler, and temperatures are not sufficiently hot for hydrogen to be ionised, other opacity sources, that is apart from H^-, become increasingly important. Also, as the metal abundance is lowered, the electron supply dries up. Thus negative ion opacities, e.g. H^- and He^- decline in favour of molecular opacities, principally involving H_2.

The most important opacity sources at T_e = 5000 K and 4000 K are shown in Figures 7 and 8, respectively. In particular the H_2 dipole opacity (Linsky 1969) determines the atmospheric structure in the H-rich white dwarfs with metal deficiencies greater than 10^3 and T_e's $\leq$ 4000 K. The increasing strength of this opacity with decreasing metal abundance will also have an

FIG. 7. - Dominant opacity sources for the TEFF = 5000 K models at τ_{ROSS} = 1. (a) [M/TOT] = 0, (b) [M/TOT] = -2.

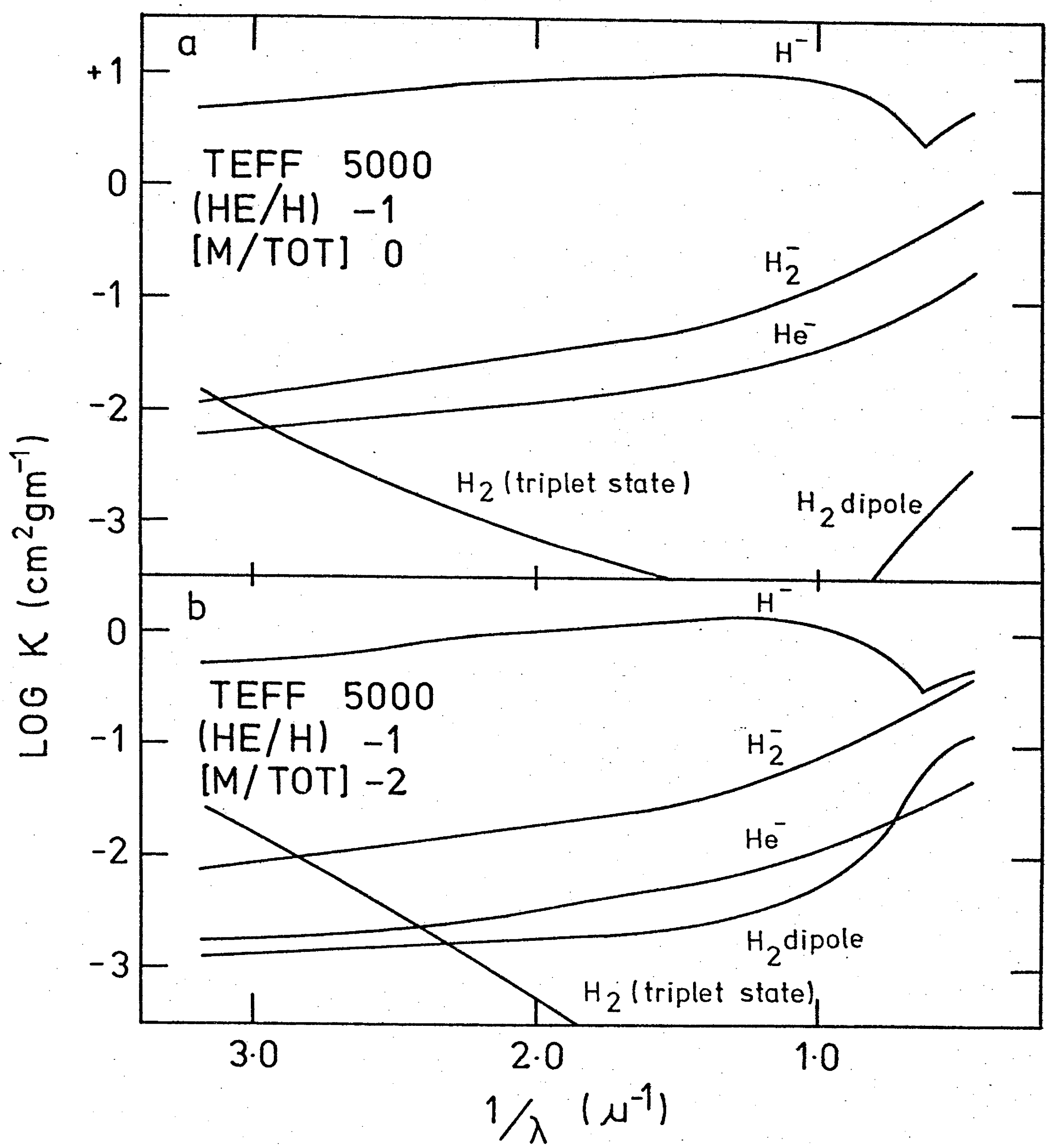
a
TEFF 5000
(HE/H) -1
[M/TOT] 0
H⁻
H₂⁻
He⁻
H₂ (triplet state)
H₂ dipole
b
TEFF 5000
(HE/H) -1
[M/TOT] -2
H⁻
H₂⁻
He⁻
H₂ dipole
H₂ (triplet state)
+1
0
-1
-2
-3
LOG K (cm²gm⁻¹)
3·0
2·0
1·0
1/λ (μ⁻¹)

FIG. 8. - Dominant opacity sources for the TEFF = 4000 K models at τ_{ROSS} = 1. (a) [M/TOT] = 0, (b) [M/TOT] = -3, (c) [M/TOT] = -6.

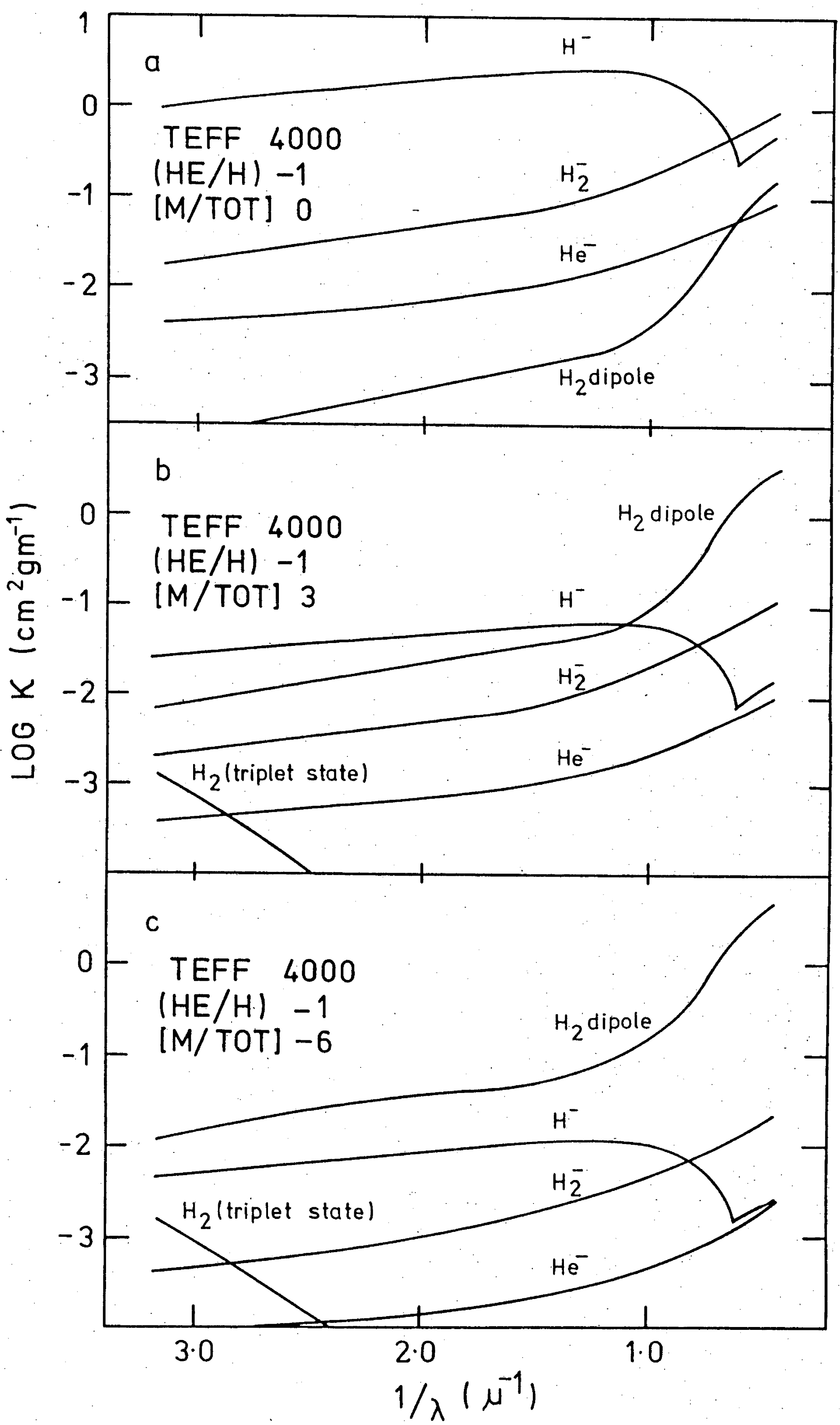
a
H⁻
TEFF 4000
(HE/H) -1
[M/TOT] 0
H_2^-
He⁻
H_2 dipole
b
TEFF 4000
(HE/H) -1
[M/TOT] 3
H_2 dipole
H⁻
H_2^-
He⁻
H_2 (triplet state)
c
TEFF 4000
(HE/H) -1
[M/TOT] -6
H_2 dipole
H⁻
H_2^-
H_2 (triplet state)
He⁻
LOG K $(cm^2 gm^{-1})$
1
0
-1
-2
-3
3·0
2·0
1·0
$1/\lambda\ (\mu^{-1})$

effect on the line strengths, since the *total* continuous opacity remains approximately constant as the metal abundance is lowered from 10^{-3} to 10^{-6} times the solar abundance at T_e = 4000 K (Figure 8b,c).

(b) Helium-rich White Dwarfs

(i) Model Structure

Figures 9 to 11 illustrate the $T(\tau)$, $P_g(\tau)$, and $P_g/P_e(\tau)$ relations for the He-rich white dwarfs, where the He/H number ratio is 10^5. For some of these model atmospheres (indicated by an asterisk in the Figures), which had metal deficiencies greater than 10^3, model convergence was difficult. Small temperature corrections (ΔT's $\simeq$ 5K) had a large effect on the errors (sometimes > 100%), as a flux constant solution was approached. These models are therefore not as reliable as others in the grid. However at 5500 K, good convergence was obtained for both the 10^{-3} and 10^{-5} metal abundance models.

In contrast to the H-rich white dwarf models, the helium models which I converged do not have convective zones which expand into the surface layers as both the temperature and metal abundance are lowered. The position of the onset of convection is indicated in Figures 9a to 11a.

However, Böhm *et al.* (1977) produced model envelopes in which convective energy transport was supported out to $\bar{\tau} \sim 10^{-2}$. More importantly, the convection commences at successively smaller optical depths as the temperature was lowered. The $T(\tau)$ of their T_e = 4000 K, pure-He model is shown in Figure 11a. By comparison, the models which I constructed have structures which do not change dramatically with temperature *or* metal abundance. This can be explained by the absence of any absorption species or ionisation zone which can decrease the adiabatic temperature gradient, and consequently make convection more favourable. For the models which I have constructed, the atmospheric temperatures are not hot enough for significant amounts of helium to be ionized, and the low hydrogen abundance

FIGS. 9.–11. – Model atmospheric structures for the helium-rich white dwarfs with TEFF = 7000 K, 5500 K, and 4000 K, respectively. The (HE/H) ratio is +5, and [M/TOT] is shown for each curve. (a), (b), and (c) are as for Figure 1. The asterisks refer to models for which poor convergence was obtained, and the pointers indicate the onset of convection. In Figure 11a the Böhm *et al.* (1977), 4000 K, He model is shown.

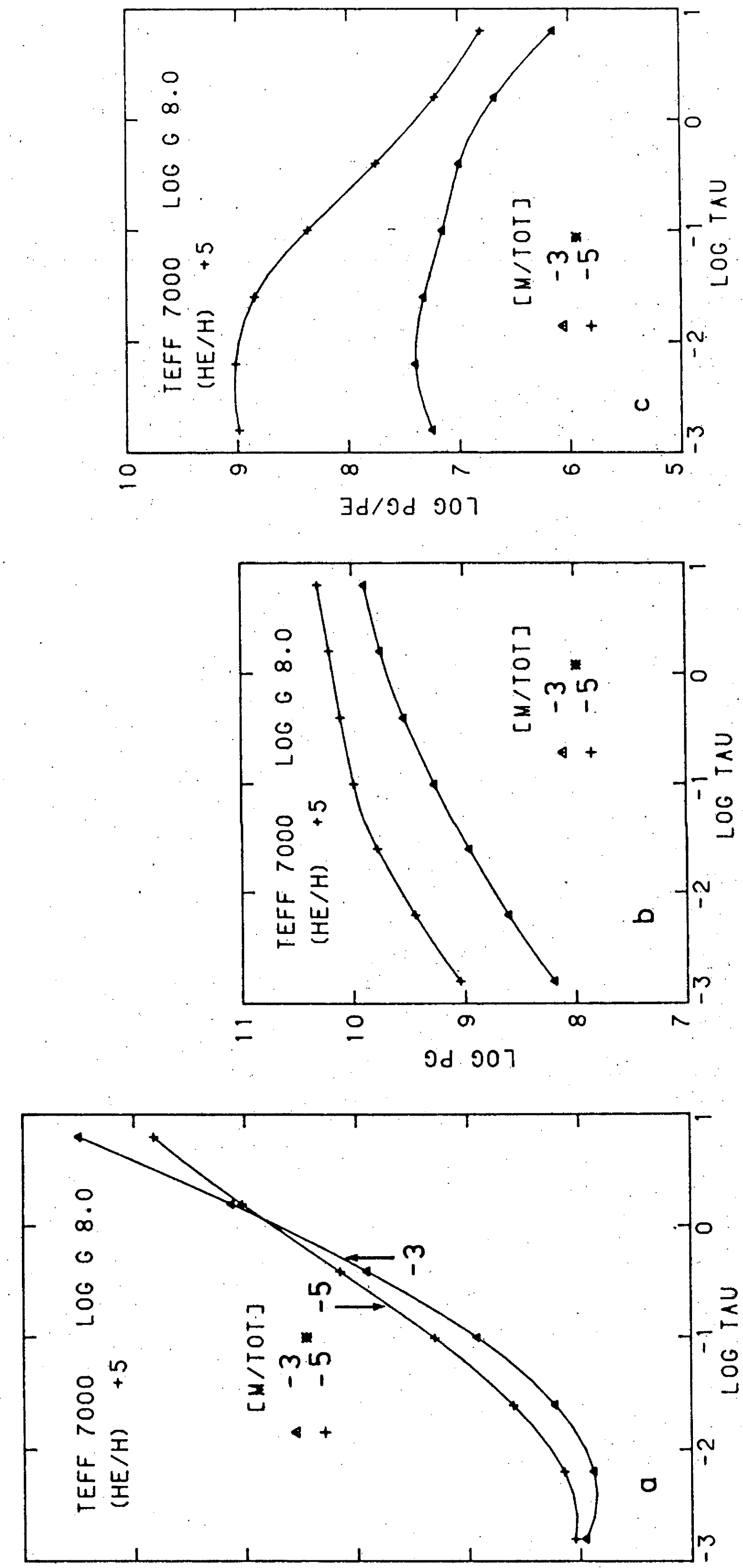
TEFF 7000 LOG G 8.0
(HE/H) +5
[M/TOT]
-3
-5
TEMPERATURE
LOG TAU
a
LOG PG
b
LOG PG/PE
c

Figure 9

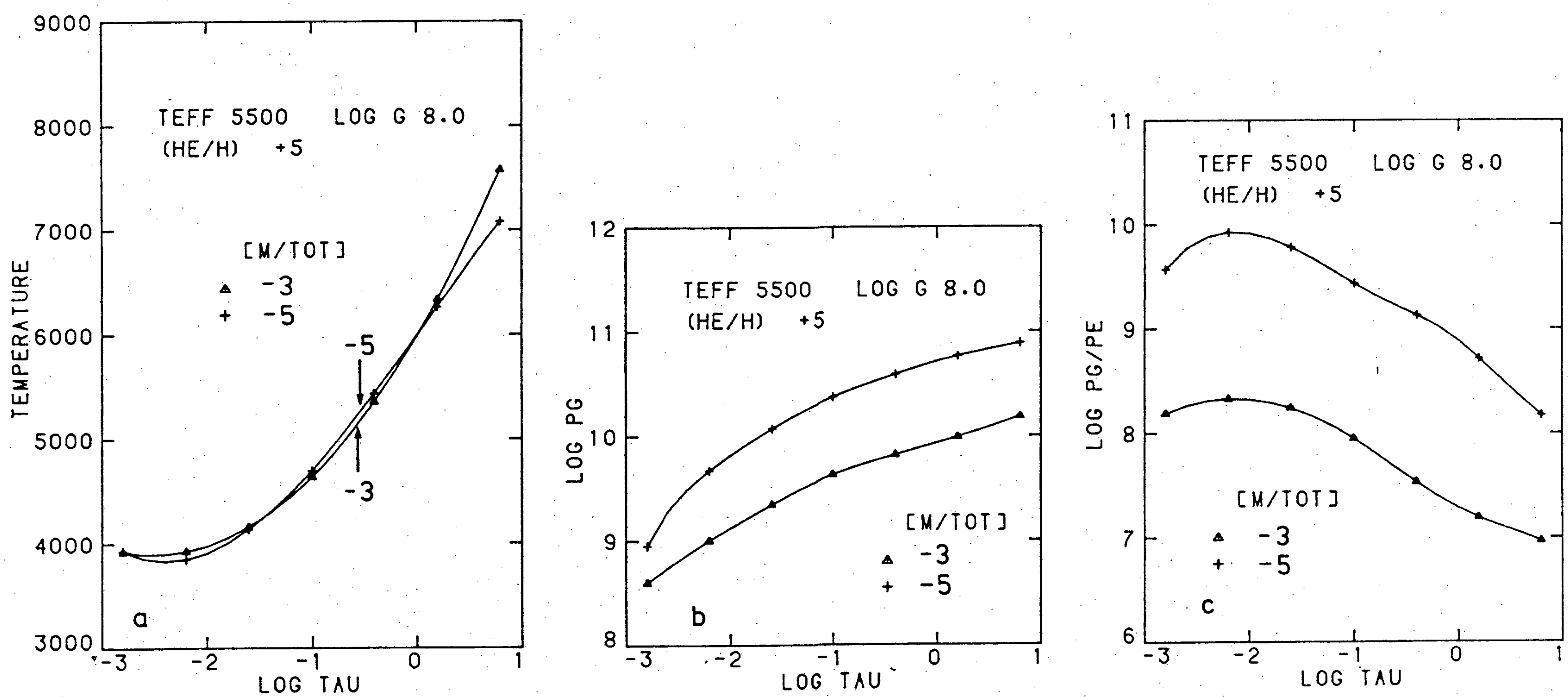
TEFF 5500 LOG G 8.0
(HE/H) +5
[M/TOT]
-3
-5
-5
-3
a
TEMPERATURE
LOG TAU
b
LOG PG
c
LOG PG/PE

Figure 10

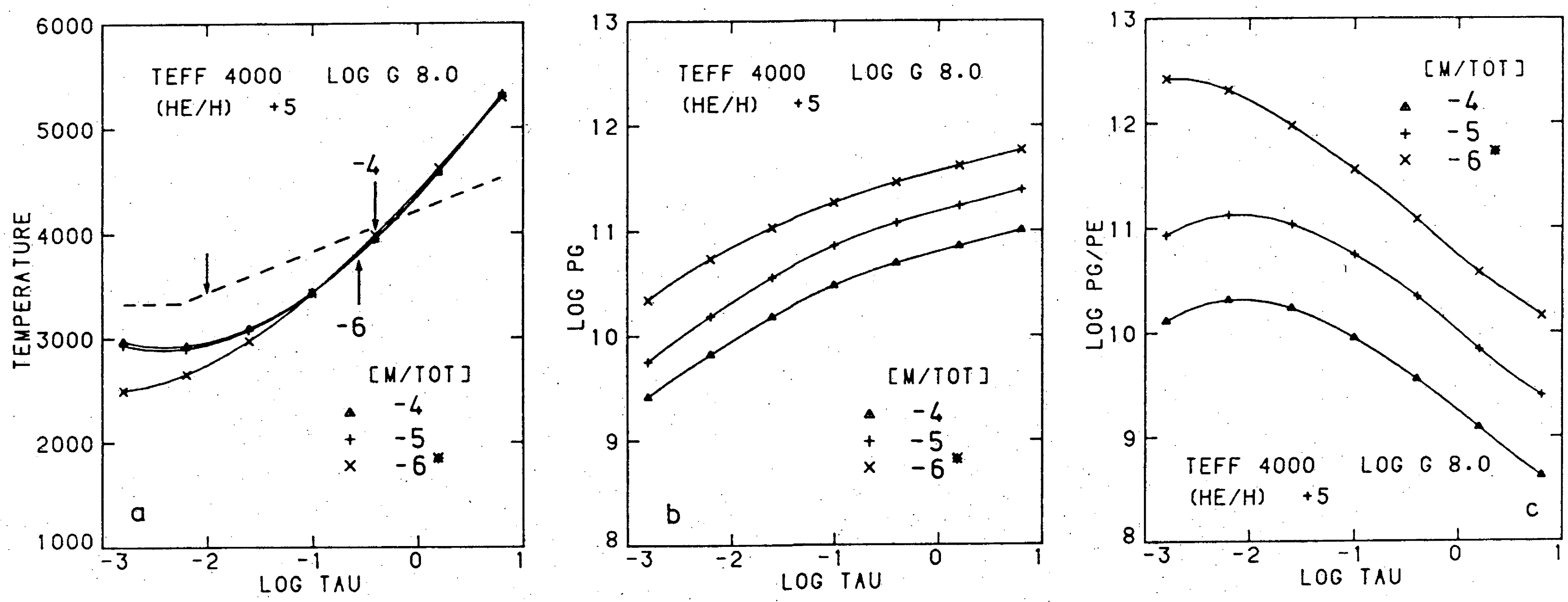
TEFF 4000 LOG G 8.0
(HE/H) +5
[M/TOT]
-4
-5
-6*
-4
-6
a
b
c
TEMPERATURE
LOG PG
LOG PG/PE
LOG TAU

Figure 11

(He/H = 10^5) means that there are not large amounts of ionised or molecular hydrogen. This latter species had the most significant effect on convection in the H-rich white dwarfs. Thus, my neglect of pressure ionisation (included by Böhm *et al.* 1977), could have significant effects on the convective flux, by altering the position of ionisation zones.

Next, let us investigate the pressures in these helium-dominated atmospheres (b's of Figures 9 to 11). As a result of the more transparent He^- opacity, the gas pressures are significantly higher than in the equivalent hydrogen models. A representative value is $\sim 10^{11}$ dynes cm^{-2}, which corresponds to a particle spacing of $\sim 1.3 \times 10^{-8}$ cm. This is similar to the atomic radius of He, 1.8×10^{-8} cm, which is the half distance of closest approach of atomic centres in the crystalline state. Thus according to the model atmospheres constructed in this analysis, the atoms will be packed close together, and under these conditions pressure ionisation would be expected. However this was not considered in the current research. Thus, conclusions concerning the ionisation equilibria in these models will be unrealistic, and the elctron pressures will be too low. In particular, although the very high gas pressures imply strong line broadening, the ratio of neutral to ionised line strengths will not be reliable.

To conclude this section, the dominant opacity sources which determine the structure of the He-rich white dwarf model atmospheres will be discussed.

(ii) Opacity Sources

Inspection of the continuum opacities for all the He-rich models which were computed in this analysis, reveals that He^- is the only significant opacity. More specifically, He^- is the strongest continuum opacity by about 4 orders of magnitude in all but the coolest most metal-deficient model atmospheres. At 4000 K the principal opacity sources are illustrated in

Figure 12. This shows that in the very metal-deficient atmospheres, [M/TOT] < -6, H_2 dipole opacity will be the next most important opacity in the wavelength region where most of the star's energy is being radiated, namely at ~1μ. Thus as the metal abundance is lowered from 10^{-6}, this opacity will determine the atmospheric structure, rather than Rayleigh scattering by helium, which was predicted by Bues and Wehrse (1976). However scattering will be the major contributor to the continuum opacity at wavelengths where most of the metals have strong lines, viz. λλ~3000 to ~5000Å.

The source of electrons for the He^- opacity in these atmospheres changes significantly as both the effective temperature and metal abundance are lowered.

At T_e = 7000 K and [M/TOT] = -3, the electrons come approximately equally from hydrogen and the metals (principally Mg, Si, and Fe). However, hydrogen becomes by far the dominant electron supplier as the metals are reduced to 10^{-5}. The same trend is evident at 5500 K, but the cooler atmospheric conditions mean that it is more difficult for H to be ionised. Thus for the metal-rich (10^{-3}) model, electrons come from the metals, but by [M/TOT] = -5, the metals are sufficiently poor that both hydrogen and the metals are providing the same number of electrons. As the effective temperature is lowered still further to 4000 K, conditions are just too cool for significant amounts of hydrogen to be ionised and thus even in the most metal-deficient model (10^{-6}), the electrons are still provided by the elements Na, Mg, Al, Fe, Si, K, and Ca. Therefore as the metals are reduced, the electron supply declines more rapidly than in the hotter, but similar metal abundance models. This is reflected in the increasing importance of Rayleigh scattering by He and the H_2 dipole opacity at T_e = 4000 K, as the metals are extracted from the atmospheres (see Figure 12).

FIG. 12. - Dominant opacity sources for the He-rich 4000 K models. (a) [M/TOT] = -3, (b) [M/TOT] = -6.

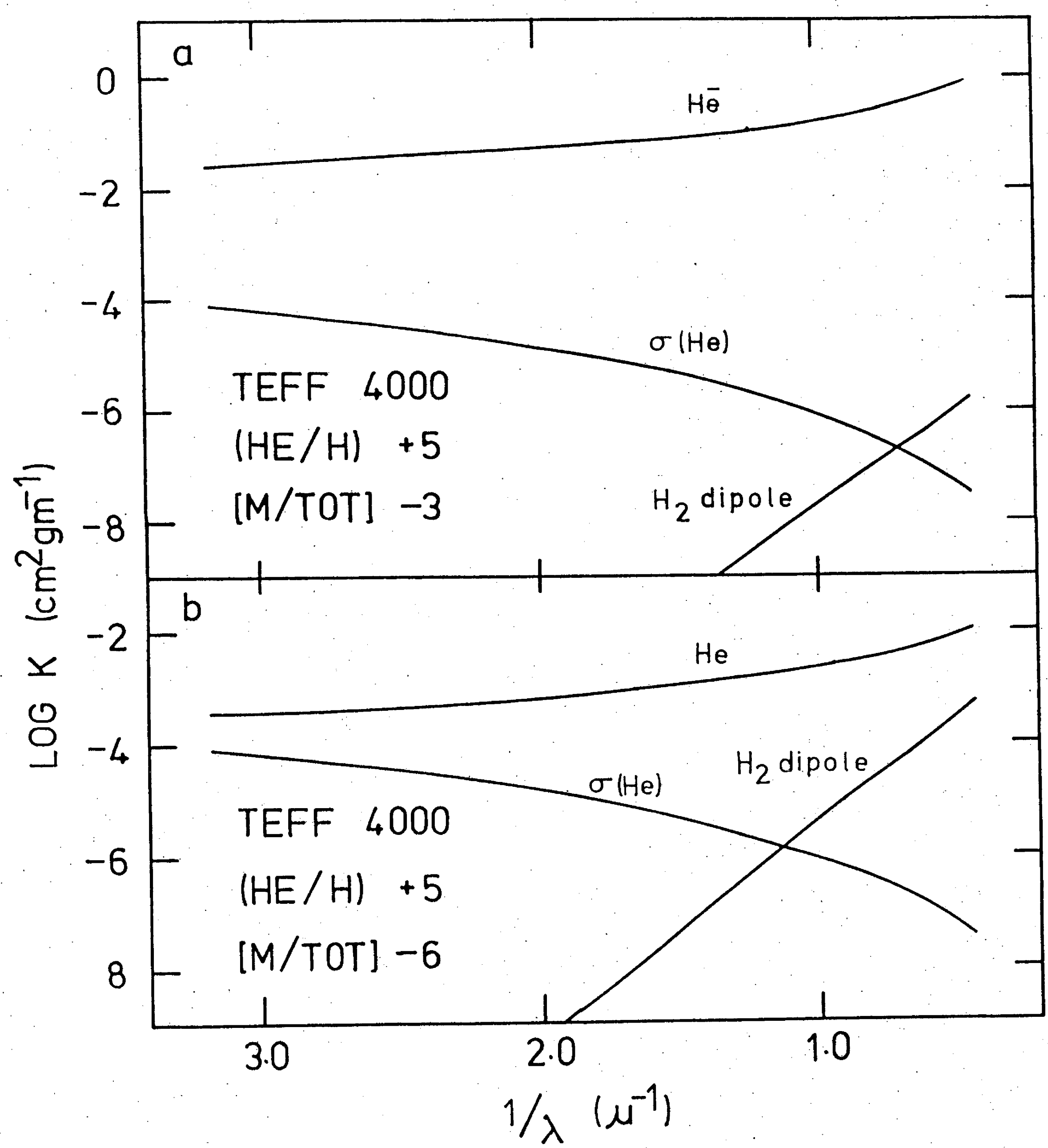
a
0
-2
-4
-6
-8
He⁻
σ (He)
H2 dipole
TEFF 4000
(HE/H) +5
[M/TOT] -3
b
-2
-4
-6
8
He
σ (He)
H2 dipole
TEFF 4000
(HE/H) +5
[M/TOT] -6
LOG K (cm2gm-1)
3.0
2.0
1.0
1/λ (μ-1)

IV. SYNTHETIC SPECTRA

(a) *Spectrum synthesis of the heavily-blanketed white dwarf LP701-29*

(i) *Abstract*

Synthetic spectra are constructed for the white dwarf, LP701-29, assuming a hydrogen-rich atmospheric composition. The observed spectrum is consistent with a metal abundance, [M/TOT] ~ -3.0. The possibility of a helium-rich atmosphere is also discussed.

(ii) *Introduction and observations*

The spectrum synthesis technique has enabled abundance determinations in spectral regions which are too crowded for individual line measurements. This synthesis method has been applied to cool stars with a wide range of luminosities. Generally, cool degenerate spectra can be analysed by constructing individual line profiles (i.e. van Maanen 2, Wegner 1972). Recently, however, two white dwarfs, G165-7 (Hintzen and Tapia 1975; Greenstein 1976) and LP701-29 (Dahn *et al.* 1978) have been discovered which show strong line-blanketing in the blue spectral regions. This strong absorption, which can be identified with low excitation potential metal lines, provides an opportunity to extend the spectrum synthesis analysis to white dwarf spectra.

The former star, G165-7, has been interpreted as a cool He-rich degenerate star (Hintzen and Tapia 1975) from the absence of hydrogen lines at its effective temperature, T_e, of 7000° K (Greenstein 1976). However, for cool, $T_e < 5000^{\circ}$ K, H-rich white dwarfs, both Shipman (1977) and WBCI have shown that the hydrogen lines would not be detectable on observational material obtained with current instrumentation. Thus, H- and He-rich white dwarfs in this temperature regime would not be distinguishable by this criterion. Two estimates of the effective temperature of LP701-29 were made by Dahn *et al.* (1977). They obtained a $T_e \sim 4200^\circ$ K by fitting a black-body curve to their scanner observations, in particular in the region $\lambda\lambda 5500\AA$ to $7500\AA$. However their energy distribution indicated a $T_e < 4000^\circ$ K when compared with the continuum fluxes of Shipman's (1977) zero metal, H-rich model atmosphere with $T_e = 4000^\circ$ K and log g = 8.0. For our abundance analysis we assume a H-rich atmospheric composition and adopt a $T_e = 4000^\circ$ K for LP701-29. We discuss the H-rich assumption and this temperature estimate further in *(iv)*. The effects of a He-rich atmosphere are also considered in this section.

Using log g = 8, appropriate for H-rich white dwarf atmospheres (*cf.* Wehrse 1975) and a $T_e = 4000^\circ$ K, we constructed model atmospheres with varying metal abundance, as described by WBCI. Finally, using a spectrum synthesis technique *(iii)*, we estimate the metal abundance, [M/TOT], for LP701-29, by comparison of this spectrum with the observational data of Dahn *et al.* (1978) (their Figure 3).

(iii) Spectrum synthesis technique

Atomic lines used to construct the representative synthetic spectrum were limited to those lines whose equivalent widths were greater than 150mÅ in the solar atlas (Moore *et al.* 1966). Clearly this procedure for determining the violet-blanketing spectrum relies on the extensive broadening of the strong lines, e.g. CaII, CaI, produced by the extremely high gas pressures (log $P_g \sim$ 8-9) in these model stellar atmospheres, but neglects the contribution of the many weaker lines, both atomic and molecular (e.g. CN). Hence the blanketing effects are, in general, underestimated. The broadening of the lines at these gas pressures is predominantly by van der Waal interactions. The present analysis uses the theory of these encounters as developed by Unsold (1955).

A final line list included approximately 220 lines of Mg, Si, Ca, Ti, Cr, Mn, Fe, and Ni, in the wavelength interval from λλ3400Å to 5400Å, the limits of the high resolution blue spectrum shown by Dahn *et al.* (1978). The gf values for this list were taken from the extensive tabulations of Kurucz and Peytremann (1975).

We then calculated the line opacity, and hence emergent flux, by employing a similar technique to that described by Cottrell and Norris (1978), using a modified version of the ATLAS model atmosphere program (Kurucz 1970). Two significant changes were made.

Firstly, the wavelength sampling interval was increased from 0.05Å to 10Å. Secondly, in computing the emergent flux at any wavelength point, all lines within ±500Å were included. Both these changes resulted from the extremely broad line profiles produced by the high gas pressures existing in the atmospheres of stars with these temperatures and gravities. For example, the wings of the CaI line at λ4226Å sometimes extend several hundred angstroms from the central wavelength.

(iv) Results and discussion

Figure 13a shows two synthetic spectra, constructed from model atmospheres with $T_e = 4000^\circ$ K, log g = 8, and [M/TOT] = -2, -3. The major features, CaI, CaII, and MgI are indicated, with the remaining structure principally due to FeI. In Figure 13b we have superimposed the observation from Dahn *et al.* (1978) upon the synthetic spectrum with [M/TOT] = -3, which is our estimate of the metal abundance in LP701-29.

There are three important discriminants for inferring this abundance from the synthetic spectra. They are (1) the long wavelength wing of the CaI line at λ4226Å, (2) the plateau between λλ4400Å and 4500Å, and (3) the region around the MgI*b* lines at λ~5180Å.

The poor fit in the region λλ4000Å to 4150Å is probably due to our neglect of the weaker lines and has already been mentioned in §(*iii*). In

FIG. 13. - Blanketing spectrum of LP701-29. (a) Two synthetic spectra with parameters TEFF = 4000 K, log g = 8, and [M/TOT] = -2,-3 (upper curve). These spectra are normalised at λ5400Å. The dashed line is the position of the continuum for the unblanketed [M/TOT] = -3 model. (b) Observation (dashed line) compared with a synthetic spectrum having parameters TEFF = 4000 K, log g = 8, [M/TOT] = -3. The observed and synthetic spectra are fitted in the region λ~4950Å. The divergence of the two spectra longward of λ5100Å is an instrumental effect.

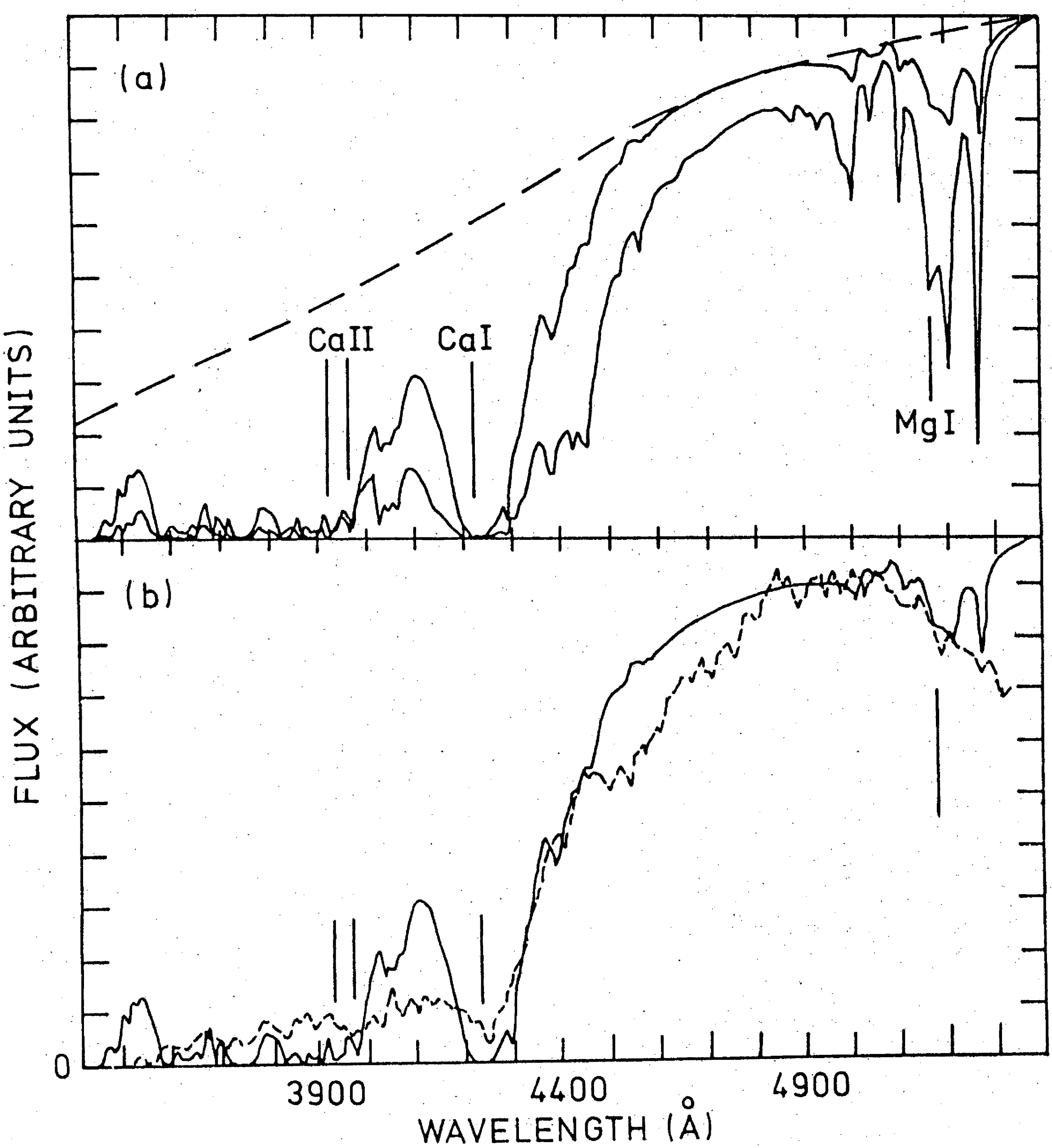
(a)
CaII
CaI
MgI
(b)
FLUX (ARBITRARY UNITS)
0
3900
4400
4900
WAVELENGTH (Å)

addition, the cores of the strong lines are stronger than observed. These cores are formed at low optical depths where the structure of these model atmospheres is not well determined due to our neglect of metal-line blanketing. As well as these anomalies, two additional uncertainties must be mentioned; (1) the pressure broadening theory, (Unsold 1955), used to compute the metal line profiles is uncertain at the high gas pressure ($\log P_g \sim 8$-9) existing in these metal-deficient white dwarfs, and (2) the observational data, with which our synthetic spectra were compared, have not been instrumentally corrected. In general, however, reasonable agreement was found with the observations.

Dahn *et al.* (1978) have suggested that LP701-29 may have a He-rich atmosphere. We have investigated this possibility by computing cool He-rich model atmospheres with gravities, $\log g = 8$. The important opacity sources in these atmospheres are He^- and Rayleigh scattering by He. The latter becomes dominant in very metal deficient ([M/TOT] ~ -7) atmospheres. If we compare the conditions prevailing at a given optical depth of a He-rich atmosphere with those of a H-rich atmosphere at the same metal abundance, in the former we have (a) a lower opacity per gram since both He^- and He Rayleigh scattering are weaker sources of opacity in comparison to H^- and H_2 dipole opacity, and (b) higher gas pressures ($\log P_g \sim 10$-11) and hence greater pressure broadening. Both these imply considerably stronger lines in a helium atmosphere, which in turn would indicate a lower metal abundance in order to fit the observations of Dahn *et al.* (1978). Although this lower [M/TOT] gives weaker lines, the increase in pressure broadening, because of the lower opacity, gives a synthetic spectrum which is significantly different from the observations (see §IV*b* for the synthetic spectra constructed for some of the He-rich models). Additionally, the degree of ionisation will increase with this decrease in metal abundance, as the metals are still the major electron contributors. This will not only weaken the blanketing due to FeI, the principle source of blocking below λ3800Å, but also CaI, λ4226Å, the strongest line observed in the spectrum. Correspondingly, we predict that in a He-rich atmosphere, CaII, H and K, will become the strongest lines in the spectrum. Although we can dismiss a He-rich atmosphere for LP701-29, the gas pressures which we computed for our most metal deficient ([M/TOT] = -6) He models, implied an atomic spacing of ~2Å. Thus the theory invoked in these latter computations may be suspect.

Finally a comment about the effective temperature of LP701-29. Our adopted value of $T_e = 4000^\circ$ K may be in error by $\pm 200^\circ$ K, when one compares the observed fluxes (Dahn *et al.* 1978) with the energy distributions of our model atmospheres. However, this has no effect on our two major conclusions, (a) that LP701-29 is a H-rich white dwarf having (b) a metal abundance, [M/TOT] ~ -3.0. Additional infrared fluxes and cool-blanketed model atmospheres are required in order that a more precise effective temperature be derived for LP701-29.

(v) Conclusions

In the preceding analysis we have attempted to synthesise the spectrum of LP701-29 assuming a hydrogen-rich composition. Reasonable agreement with the observations was obtained for a model with $T_e = 4000^\circ$ K, log g = 8, [M/TOT] = -3.0. Although there are uncertainties involved in the model computations and we do not obtain a detailed fit to the observations, a helium-rich composition does not seem appropriate for this star. Not only would the lines be significantly broader, but the degree of ionisation would be greater. Thus LP701-29 appears to be a cool counterpart of the DA sequence of white dwarfs.

(b) Synthetic spectra of cool He-rich white dwarfs

As confirmation of the hydrogen-rich nature of LP701-29, synthetic spectra were computed for two of the He-rich model atmospheres at $T_e = 4000^{\circ}$ K. They are shown in Figure 14, and they contrast with those shown in Figure 13. In particular, as noted in §IV*a*, the spectra have significantly broader lines than those for the H-rich models. However, one must be cautious in placing too much significance on the synthetic spectra using the He-rich models. Recalling the discussion in §III*b*, the ionisation equilibria may be unrealistic due to the neglect of pressure ionisation in the model atmospheres. Consequently the neutral lines are probably too strong, but the greater pressure broadening of lines in the He-rich spectra distinguishes them from the comparatively sharp lines constructed for the H-rich models.

V. SUMMARY

The atmospheric structures of cool (effective temperature, $T_e \lesssim 7000^{\circ}$ K) H- and He-rich white dwarf model atmospheres have been discussed in detail. The following conclusions were reached: For the models where hydrogen was dominant, molecular hydrogen (H_2) became more important as the temperatures were decreased and the gas pressures increased (the latter resulting from the lowering of the metal abundance). Large amounts of H_2 provided the necessary conditions for increased convective energy transport in the outer layers. Consequently, in very cool ($T_e \lesssim 4000^{\circ}$ K) metal-deficient ($M/TOT < 10^{-3}$) models, the adiabatic temperature gradient was established throughout the whole atmosphere ($-3 < \log \bar{\tau} < 1$). This led to a cooling of the outer layers and therefore a decrease in the electron pressure, and a lowering of the level of ionisation. However, in contrast, the He-rich models had no large surface convective zones, since there were *no* abundant species at these atmospheric temperatures which could lower the

FIG. 14. - Blanketing synthetic spectra for He-rich white dwarfs with TEFF = 4000 K, and [M/TOT] = -3 and -6. The dashed line corresponds to the line-free flux distribution for the [M/TOT] = -3 model. The positions of CaI (4226) and the Na*ID* lines are indicated.

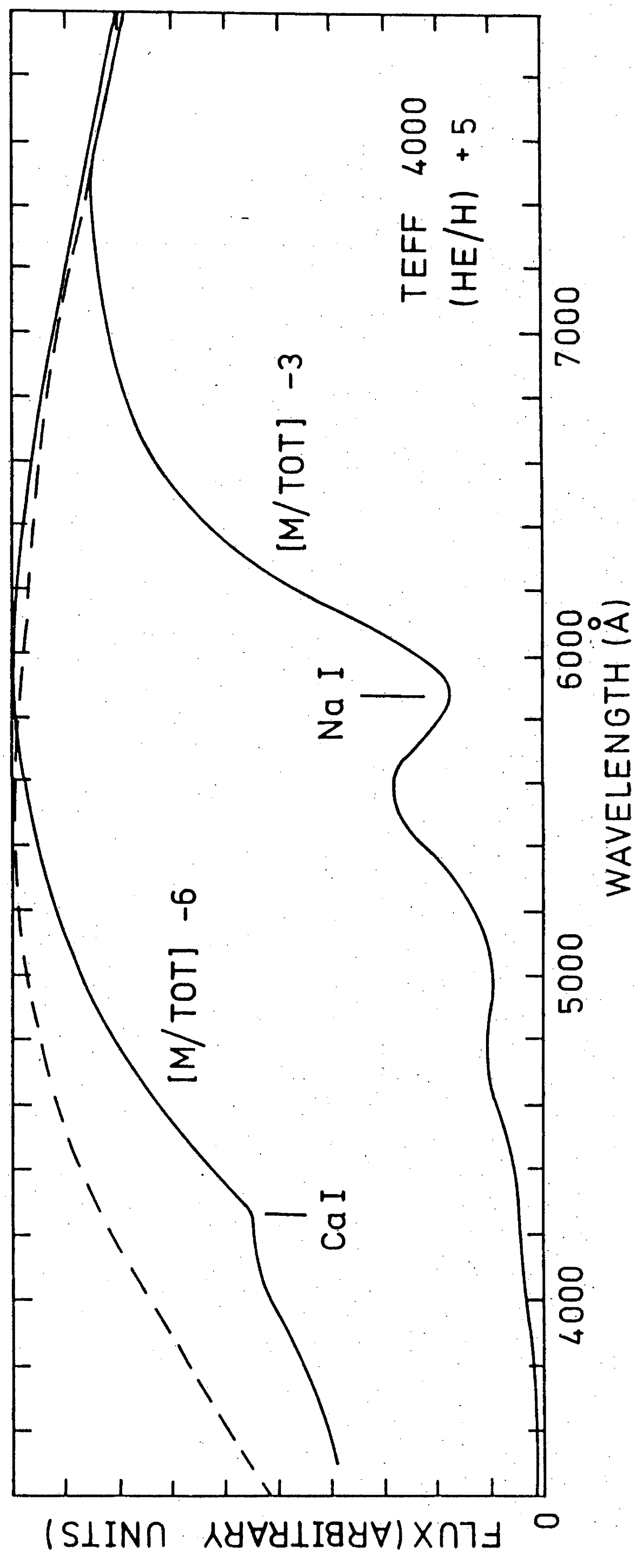
TEFF 4000
(HE/H) +5
[M/TOT] -3
[M/TOT] -6
Na I
Ca I
4000
5000
6000
7000
WAVELENGTH (Å)
0
FLUX (ARBITRARY UNITS)

adiabatic temperature gradient, and enhance conditions for convection.

The main sources of continuum opacity have also been considered for both white dwarf classifications. For H-rich white dwarfs the importance of H^- depended critically on the supply of electrons. As T_e was lowered to 4000° K and the metals to 10^{-3} their solar value, H_2 dipole opacity was dominant in regions where most of the energy was radiated. For helium white dwarf models, He^- was always the dominant opacity.

Finally, synthetic spectra were constructed for both H- and He-rich model atmospheres at $T_e = 4000^\circ$ K, and have been compared with the spectrum of the heavily blanketed white dwarf, LP701-29. From this comparison it was concluded that a hydrogen-dominated composition with a metal abundance 10^{-3} that of the Sun, provided the best fit to the observational data.

REFERENCES

Böhm, K.-H., Carson, T. R., Fontaine, G., and Van Horn, H. M. *Ap. J.*, 217, 521.

Bues, I., and Wehrse, R. 1976, *Astr. Ap.*, 51, 461.

Cottrell, P. L., Bessell, M. S., and Wickramasinghe, D. T. 1977, *Ap. J. (Letters)*, 218, L133 (WBCII).

Cottrell, P. L., and Norris, J. 1978, *Ap. J.*, 221, 893 (Chapter 2).

Dahn, C. C., Hintzen, P. M., Liebert, J. W., Stockman, H. S., and Spinrad, H. 1978, *Ap. J.*, 219, 979.

Doyle, R. O. 1968, *Ap. J.*, 153, 987.

Greenstein, J. L. 1976, *Ap. J. (Letters)*, 207, L119.

————. 1976, *A. J.*, 81, 323.

Hintzen, P. M., and Tapia, S. 1975, *Ap. J. (Letters)*, 199, L31.

Hintzen, P. M., and Strittmatter, P. A. 1975, *Ap. J. (Letters)*, 201, L37.

Kurucz, R. L. 1970, *SAO Spec. Rept.*, No. 309.

Kurucz, R. L., and Peytremann, E. 1975, *SAO Spec. Rept.*, No. 362.

Linsky, J. L. 1969, *Ap. J.*, 156, 989.

Moore, C. E., Minnaert, M. G. J., and Houtgast, J. 1966, *NBS Monog.*, No. 61.

Shipman, H. L. 1977, *Ap. J.*, 213, 138.

Unsold, A. 1955, *Physik der Sternatmosphären*, 2nd ed. (Berlin: Springer-Verlag).

Wegner, G. 1972, *Ap. J.*, 172, 451.

Wehrse, R. 1974, *Astr. Ap.*, 35, 157.

————. 1975, *Astr. Ap.*, 39, 169.

————. 1977, *Mem. Soc. Astr. It.*, 48, 13.

Wickramasinghe, D. T., Bessell, M. S., and Cottrell, P. L. 1977, *Ap. J. (Letters)*, 217, L65 (WBCI).

SUMMARY AND FUTURE WORK

In this thesis the spectrum synthesis technique has been used over a wide range in luminosities, from cool white dwarfs to peculiar giant stars. I will briefly recall the main conclusions of each chapter, indicating where additional research could provide a better understanding of the composition and evolution of our Galaxy, with the possible extension to extragalactic systems. Each of the chapters will be summarised under one of the following headings: giants, dwarfs/subdwarfs, white dwarfs.

(a) Giant stars

Using a curve-of-growth analysis, followed by the spectrum synthesis program, the iron, carbon, nitrogen and oxygen abundances were determined in the weak-G-band star HD 91805. This, and ~30 similar objects were identified by Bidelman and MacConnell (1973) in their objective prism survey. The abundances determined for HD 91805 were

$$[Fe/H] \sim 0.0,\ [C/H] \sim -1.4,\ [N/H] \sim +0.6,\ [O/H] \sim +0.1.$$

DDO photometry of the larger group of weak-G-band stars, including HD 91805 was obtained, and compared with similar photometry of the Hyades group members. Coupling this photometry with a comparison of high dispersion spectra of HD 91805 and HD 28307 (the latter a Hyades cluster member), it was concluded that the weak-G-band objects are probably "clump" stars. At this evolutionary phase helium is being burned in the core following the helium flash at the tip of the red giant branch. The quiescent nature of the core-helium burning phase means that a more turbulent evolutionary phase is required during which the peculiar carbon and nitrogen abundances, indicated above, could be attained. A number of mechanisms were considered: helium-core flash, mass loss, hydrogen-shell instabilities, and the Paczyński mechanism of N/C enrichment by meridional circulation. The latter method, accompanied by some mass loss, gave a suitable explanation to the observed abundances.

Since this work was completed, a paper by Sneden *et al.* (1978) was published which analysed another weak-G-band star, HR 6766. These authors determined CNO abundances, a $^{12}C/^{13}C$ ratio and a lithium abundance. The CNO abundances deviated little from values obtained in the present work. Sneden *et al.*'s (1978) derived abundances were:

$$[M/H] \sim -0.15; \quad [C/H] \sim -1.49; \quad [N/H] \sim +0.23; \quad [O/H] \sim -0.38;$$

$$^{12}C/^{13}C \sim 4 \text{ and } \log N(Li) \sim +0.75.$$

They considered two scenarios to interpret their observations.

(i) A higher temperature at the base of the convective envelope, which can allow the CNO cycle to process the outer layers. The enhanced lithium abundance provides constraints on the time scales of the convective mixing, since lithium would be readily destroyed at the temperatures necessary for the CNO cycle.

(ii) An inhomogeneous main sequence star which has an extremely carbon-poor envelope, but normal abundances in the interior. The latter seems somewhat artificial since inhomogeneous models have been hard to construct theoretically, and thus the idea of hot bottom atmospheres seems the most plausible of their two scenarios. However the Paczyński mechanism, proposed by the work presented in this thesis, also adequately interprets the work of Sneden *et al.* (1978).

The carbon-rich Cepheid V553 Centauri, was analysed both spectroscopically and photometrically, and by using similar techniques to those employed in the analysis of HD 91805. The following abundances were derived for V553 Centauri:

$$[Fe/H] \sim -0.1, \; [C/Fe] \sim +0.8, \; [N/Fe] \sim +0.5.$$

For the carbon enrichment to have been produced during the star's evolution, V553 Centauri must have evolved past the helium-core flash stage, since carbon is only produced via the triple-α process. Additional processing of carbon to nitrogen (via the CNO cycle) is required to produce the observed enhanced nitrogen abundance. Finally, as a consequence of the near-solar iron abundance (which by inspection of the synthetic spectra appears to apply equally well to the other heavy elements), V553 Centauri is possibly a loop Cepheid, and could be the progeny of the strong-lined RR Lyrae stars. For this object to be looping into the instability strip at its comparatively low luminosity of ~2, it must have undergone substantial mass loss on the giant branch.

The last group of giant stars examined in this thesis were also selected from the extensive tabulations of Bidelman and MacConnell (1973). These were the extremely weak-metal stars, for which carbon and nitrogen abundances were obtained by constructing synthetic spectra of the G-band, the $\Delta v = 0$ blue CN bands, and the NH features around $\lambda \sim 3360$Å. Included in this analysis were two previously studied extremely metal-poor stars, HD 122563 and HD 165195. The following correlation was obtained:

$$[C/N] = 0.5(\log g) - 1.3,$$

indicating a decrease in carbon to nitrogen ratio as the gravity is reduced. In addition, the nitrogen to metal abundance showed a slight positive luminosity effect. Thus as the stars evolve to higher luminosities (lower gravities), there is an enrichment of nitrogen and a depletion of carbon. Since many of the objects appear to have luminosities lower than that required for helium-shell flashing, these peculiar abundances are possibly produced during evolution on the first giant branch. Therefore, these extremely metal-poor objects have probably mixed CNO processed material into their outer layers. The work of Dearborn, Lambert, and Tomkin (1975) and Dearborn, Eggleton, and Schramm (1976), where the $^{12}C/^{13}C$ ratio was shown to decrease with increasing luminosity, appears similar to the results obtained in the present research. Thus, following Dearborn *et al.* (1976), the combination of mass loss and hydrogen-shell instabilities on the first giant branch can produce low $^{12}C/^{13}C$, as well as enhanced N, and low C/N ratios. An extension of the present work would be to determine C/N and $^{12}C/^{13}C$ ratios in a larger sample of metal-poor stars, thus providing further evidence for the hypothesis that CNO cycle material has been mixed into the surface layers. An indication of the phase of this mixing could also be culled from more extensive data.

(b) Dwarfs/subdwarfs

For this luminosity class, a grid of model atmospheres was constructed in the temperature range from 3500 K to 6000 K. Synthetic G-bands and MgH bands near λλ~4300Å and ~5200Å respectively, were computed and revealed two significant results.

(i) The G-band region is a metal abundance discriminant for stars with $T_{eff} \lesssim 5500$ K. In fact, at $T_{eff} = 4000$ K, the model with [A/H] = -4 has a stronger G-band than the [A/H] = 0 model.

(ii) MgH bands are an abundance discriminant for dwarf/subdwarf stars with $T_{eff} \lesssim 4000$ K.

Both of these results provide an explanation for the "CH strong" and "MgH strong" classifications of Greenstein (1971). The strengthening of these molecular bands has been investigated by a detailed examination of the molecular equilibria. In particular, the amount of free carbon available for CH formation is determined by the behaviour of CO, OH, and H_2O in these model atmospheres. At normal abundance, CO forms readily, but as the metal abundance is lowered this species declines in importance relative to OH and H_2O. This decline in CO releases carbon which is then available for CH formation. The above discriminants could both be used in objective prism surveys to isolate extremely metal-deficient dwarfs, which can then be analysed in more detail to unveil new information about the early evolution of the Galaxy.

(c) Cool white dwarfs

The spectrum synthesis technique was applied to degenerate stars by matching the synthetic blanketing spectrum of a T_{eff} = 4000 K, log g = 8.0, [M/H] = -3, H-rich model atmosphere, with the observed spectrum of the white dwarf LP701-29, which has been published by Dahn *et al.* (1978). Thus, the DA sequence of white dwarfs appears to extend at least to this temperature.

A large portion of this chapter was devoted to the description of the white dwarf model atmospheres (both hydrogen-and helium-rich), which were constructed in the temperature range, 3500 K $\lesssim T_{eff} \lesssim$ 7000 K. The following major results were obtained: for the H-rich models,

(i) molecular hydrogen (H_2) became increasingly important as both the temperature and metal abundance were decreased.

(ii) Large amounts of H_2 provided the necessary conditions for increased convective energy transport in the outer layers.

(iii) Increased convection near the surface meant that in the coolest most metal-deficient models, the adiabatic gradient was established throughout the atmosphere. This gradient produced a cooling of outer layers and therefore a decrease in the electron pressure, and a lowering of the level of ionisation.

In contrast, for the He-rich white dwarf models there were no large convective zones, since there was no abundant species which could lower the adiabatic temperature gradient. The sources of continuum opacity were also considered in both classifications of white dwarfs. H^- is the dominant opacity in all but the coolest, most metal-deficient models, where the H_2 dipole opacity becomes dominant at wavelengths where most of the energy is radiated. He^- is always the dominant opacity in the He-rich models.

In some of the cool He-rich model atmospheres the gas pressures were extremely high. Under these circumstances pressure ionisation should be considered. Thus to extend this area of research, it is proposed to include pressure ionisation effects, which should produce more realistic helium models.

REFERENCES

Bidelman, W. P., and MacConnell, D. J. 1973, *A. J.*, 78, 687.

Dahn, C. C., Hinzten, P. M., Liebert, J. W., Stockman, H. S., and Spinrad, H. 1978, *Ap. J.*, 219, 979.

Dearborn, D. S. P., Lambert, D. L., and Tomkin, J. 1975, *Ap. J.*, 200, 675.

Dearborn, D. S. P., Eggleton, P. P., and Schramm, D. N. 1976, *Ap. J.*, 203, 455.

Greenstein, J. L. 1971, in *IAU Symposium No. 42, White Dwarfs*, ed. W. J. Luyten (Dordrecht: Reidel), p. 46.

Sneden, C., Lambert, D. L., Tomkin, J., and Peterson, R. C. 1978, *Ap. J.*, 222, 585.